University of Pardubice

Faculty of Chemical Technology

Department of Physical Chemistry

Crystallization Behavior of Far-Infrared Chalcogenide Glasses

DOCTORAL THESIS

Author: Ing. Daniela Brandová

Supervisor: prof. Ing. Jiří Málek, DrSc.

Supervisor specialist: Ing. Roman Svoboda, Ph.D.

2019

I hereby declare:

This thesis was prepared independently. All the literary sources and the information I used in the thesis are listed in the bibliography. I got familiar with the fact that the rights and obligations arising from the Act. No. 121/2000 Coll., Copyright Act, apply to my thesis, especially with the fact that the University of Pardubice has the right to enter into a license agreement for use of this thesis as a school work pursuant to § 60, Section 1 of the Copyright Act, and the fact that should this thesis be used by me or should a license be granted for the use to another entity, the University of Pardubice is authorized to claim a reasonable contribution from me to cover the costs incurred during making of the thesis, according to the circumstances up to the actual amount thereof. I am aware that my thesis will be accessible to the public in the University Library and via the Digital Library of the University of Pardubice in agreement with the article 47b of the Act. No. 111/1998 Coll., on Higher Education Institutions, and on the Amendment and Supplement to some other Acts (the Higher Education Act), as subsequently amended, and with the University Pardubice's directive no. 9/2012.

In Pardubice on

I would like to thank my supervisor prof. Ing. Jiří Málek, DrSc. for the possibility of my Ph.D. study under his guidance. I appreciate his help and professional advice.

I am very grateful to Ing. Roman Svoboda, Ph.D. for his patience, awesome and endless help, support and professional advice during my Ph.D. study.

My appreciation also belongs to my colleagues for their support, friendship and scientific help.

Annotation

This doctoral thesis presents a detailed characterization of thermal and structural properties of the selected tellurium-based chalcogenide glasses. These glassy materials belong among very promising but only rarely explored materials, potentially suitable for the far-infrared optics and glass-ceramics applications. The thermal behavior of investigated glassy systems is characterized by means of differential scanning calorimetry (DSC) and thermomechanical analysis (TMA; selected systems). In the presented doctoral thesis a systematic approach to the description of complex crystallization (and relaxation) kinetics by means of the commonly used and state-of-art methodologies and models is adopted in order to achieve full description of the observed phenomena and provide the possibility of accurate kinetic predictions. The observed complexity of crystallization processes of all investigated systems is solved by means of two approaches, i.e. the mathematic deconvolution and kinetic deconvolution of the crystallization DSC data. The advantages and disadvantages of both tested methods are discussed. In addition, the observed thermal behavior of studied systems is correlated with the structural information provided by XRD analysis, Raman spectroscopy and infrared (IR) microscopy, so that the effects of the present structural units can be better understood. Thermal stability of the prepared glasses is thoroughly analyzed, offering an insight into the problematic associated with inconsistent evaluations of glass-stability criteria. Combination of the calorimetric and thermo-mechanical data allows precise and reliable determination of the true glass temperature workability window. Since thermal stability and workability are the key factors for application of the far-infrared chalcogenide glasses (and most glassy materials in general), the suggested methodology of glass-stability evaluations may be of high value for both the material scientists and application specialists. The presented doctoral thesis is composed of 16 papers. The theoretical overview of main solved topics (glass formation, crystallization, theory of kinetic analysis, etc.) is presented first. The summary of main achievements and conclusions of this thesis can be found at the end of this thesis.

Keywords: *crystallization kinetics; chalcogenide glass; glass stability; DSC; TMA; XRD; Raman spectroscopy; infrared microscopy*

Annotation in Czech

Předkládaná dizertační práce představuje detailní studii termických a strukturních vlastností vybraných teluridových chalkogenidových skel. Tyto skelné materiály patří mezi slibné ale pouze výjimečně zkoumané materiály, jež mohou potenciálně představovat materiály vhodné pro optické aplikace operující ve vzdálené oblasti infračerveného spektra a sklokeramiku. Termické chování studovaných systémů je charakterizováno pomocí diferenční skenovací kalorimetrie (DSC) a termomechanické analýzy (TMA; vybrané systémy). V předložené dizertační práci je osvojen systematický přístup k popisu komplexní krystalizační (a relaxační) kinetiky prostřednictvím běžně užívaných i nejmodernějších metodologií a modelů za účelem dosažení úplného popisu pozorovaných jevů a poskytnutí možnosti přesných kinetických predikcí. Pozorovaná komplexita krystalizačního procesu všech zkoumaných systémů je řešena s využitím dvou přístupů, a to matematické a kinetické dekonvoluce krystalizačních DSC dat. Výhody a nevýhody obou metod jsou diskutovány. Kromě toho je termické chování studovaných systémů korelováno se strukturní informací získané z rentgenové difrakční analýzy, Ramanovy spektroskopie a infračervené mikroskopie, tudíž je možné lépe porozumět působení přítomných strukturních jednotek. Tepelná stabilita připravených skel je důkladně analyzována a nabízí vhled do problematiky spojené s nekonzistentním zhodnocením kritérií stability. Kombinace kalorimetrických a termomechanických dat umožňuje přesné a spolehlivé určení skutečného teplotního okna pro zpracování skla. Vzhledem k tomu, že tepelná stabilita a zpracovatelnost jsou klíčovými faktory pro optické aplikace chalkogenidových skel (a obecně většiny skelných materiálů) operujících ve vzdálené oblasti infračerveného spektra, tudíž navržený postup vyhodnocování tepelné stability skel může mít vysokou hodnotu jak pro materiálový výzkum, tak i pro odborníky se zaměřením na aplikovatelnost daných materiálů.

Předložená dizertační práce se skládá z 16 článků, jimž předchází teoretický přehled hlavních řešených témat (tvorba skla, krystalizace, teorie kinetické analýzy, atd.). Souhrn hlavních cílů a závěrů práce lze nalézt na konci této dizertační práce.

Klíčová slova: *kinetika krystalizace; chalkogenidové sklo; skelná stabilita; DSC; TMA; XRD; Ramanova spektroskopie; infračervená mikroskopie*

LIST OF PAPERS

Paper I

Thermal behavior of $Ge_{20}Se_yTe_{80-y}$ infrared glasses (for y up to 8 at. %)

R. Svoboda, D. Brandová, J. Málek

J. All. Compd. **680** (2018) 427-435.

Paper II

Se-doped $GeTe_4$ glasses for far-infrared optical fibers

R. Svoboda, D. Brandová, M. Chromčíková, M. Setnička, J. Chovanec, A. Černá, M. Liška, J. Málek

J. All. Compd. **695** (2017) 2434-2443.

Paper III

Non-isothermal crystallization kinetics of $GeTe_4$ infrared glass

R. Svoboda, D. Brandová, J. Málek

J. Therm. Anal. Calorim. **123** (2016) 195–204.

Paper IV

Influence of particle size on crystallization and relaxation behavior of $Ge_{20}Se_4Te_{76}$ glass for infrared optics

D. Brandová, R. Svoboda, J. Málek

J. Non-Cryst. Solids **433** (2016) 75-81.

Paper V

Combined dilatometric and calorimetric study of kinetic processes occurring in $Ge_{20}Te_{76}Se_4$ infrared bulk glass

R. Svoboda, D. Brandová, J. Málek

J. Non-Cryst. Solids **432** (Part B) (2016) 493-498.

Paper VI

The effect of Se ↔ Te substitution on crystallisation micro-mechanisms evincing in $GeTe_4$ glass

R. Svoboda, D. Brandová, L. Beneš, J. Málek

J. Therm. Anal. Calorim. **123** (2016) 205-219.

Paper VII

Crystallization behavior of $(GeTe_4)_x(GaTe_3)_{100-x}$ glasses for far-infrared optics applications

R. Svoboda, D. Brandová

J. All. Compd. **770** (2019) 564-571.

Paper VIII

Thermokinetic behavior of Ga-doped $GeTe_4$ glasses

Roman Svoboda, D. Brandová, M. Chromčíková, M. Liška

J. Non-Cryst. Solids, in press.

Paper IX

The effect of powder coarseness on crystallization kinetics of $Ge_{11}Ga_{11}Te_{78}$ infrared glass

R. Svoboda, D. Brandová

J. Therm. Anal. Calorim. **129** (2017) 593-599.

Paper X

Correlation of structural, thermo-kinetic and thermo-mechanical properties of the $Ge_{11}Ga_{11}Te_{78}$ glass

R. Svoboda, D. Stříteský, Z. Zmrhalová, D. Brandová, J. Málek

J. Non-Cryst. Solids **445-446** (2016) 7-14.

Paper XI

Thermal behavior of $Ge_{20}Te_{80-y}I_y$ chalcogenide glasses (for y up to 15 at.%)

D. Brandová, R. Svoboda

J. Am. Ceram. Soc., submitted.

Paper XII

Thermo-kinetic behavior of $Ge_{20}Te_{75}I_5$ glass for infrared optics

D. Brandová, R. Svoboda

Phil. Mag., in press.

Paper XIII

Thermo-structural characterization of $(As_2Se_3)_{100-x}$-$(As_2Te_3)_x$ glasses for infrared optics

D. Brandová, R. Svoboda

J. Am. Ceram. Soc. **102** (2019) 382-396.

Paper XIV

Thermal characterization of $(As_2Se_3)_{0.5}$-$(As_2Te_3)_{0.5}$ infrared glass

D. Brandová, R. Svoboda, M. Liška, J. Málek

J. Non-Cryst. Solids **475** (2017) 121-128.

Paper XV

Crystallization kinetics of glassy materials: the ultimate kinetic complexity?

D. Brandová, R. Svoboda, Z. Olmrová Zmrhalová, J. Chovanec, R. Bulánek, J. Romanová

J. Therm. Anal. Calorim. **134** (2018) 825-834.

Paper XVI

Crystal growth from mechanically induced defects. A phenomenon observed for glassy materials.

R. Svoboda, D. Brandová

J. Therm. Anal. Calorim. **127** (2017) 799–808.

Table of contents

SYMBOLS

A	preexponential factor of universal DSC kinetic equation (crystallization kinetics)
A_{TNM}	preexponential factor of TNM model (relaxation kinetics)
a_0	parameter of Fraser-Suzuki function corresponding to the amplitude of deconvoluted curve
a_1	parameter of Fraser-Suzuki function corresponding to the position of deconvoluted curve
a_2	parameter of Fraser-Suzuki function corresponding to the half-width of deconvoluted curve
a_3	parameter of Fraser-Suzuki function corresponding to the asymmetry of deconvoluted curve
c_p	isobaric heat capacity
d_{aver}	average particle size
E_A	apparent activation energy of crystallization
$F(t)$	relaxation function of given property
$First_j$	index of the first point of given curve (MKA)
$f(\alpha)$	kinetic model
$f'(\alpha)$	differential form of kinetic model
H	enthalpy
j	index of given measurement (MKA)
K_H	Hruby criterion
K_{LL}	Lu and Liu criterion
K_{LX}	Long criterion
K_{SP}	Saad and Poulain criterion
K_W	Weinberg criterion
K_{ZW}	Zhang criterion
$K(T)$	temperature-dependent rate constant
$Last_j$	index of last point of the given curve (MKA)
$l_{onset,DSC}$	sample height at $T_{onset,\ DSC}$
l_{max}	maximum sample height during the TMA crystallization measurement
l_{min}	minimum sample height during the TMA crystallization measurement
M	kinetic exponent of autocatalytic (Šesták-Berggren) model

m	kinetic exponent of Johnson-Mehl-Avrami model
N	kinetic exponent of autocatalytic (Šesták-Berggren) model
n	number of measurements (MKA)
n_r	refractive index
p	property
p_0	index representing the initial state of glass
p_∞	index representing the equilibrium state of glass
q^+	heating rate
q^-	cooling rate
R	universal gas constant
RSS	sum of squared residua (MKA)
t	time
T	temperature
T_c	crystallization temperature
T_f	fictive temperature
$T_{flow,\ TMA}$	temperature corresponding to the first sample height decrease
T_g	glass-transition temperature
T_{ic}	initial crystallization temperature (TMA)
T_m	melting temperature
$T_{onset,\ DSC}$	temperature corresponding to the true crystallization onset
T_p	temperature of the maximum of crystallization peak
T_0	temperature corresponding to the initial state of glass
T_α	temperature corresponding to the chosen value of conversion
V	volume
w_j	weighting factor for curve j (MKA)
x	non-linearity parameter
$Y_{cal,j;k}$	calculated value of the point k of the curve j
$Y_{exp,\ j;k}$	experimental value of the point k of the curve j
α	conversion
α_{exp}	coefficient of thermal expansion
$\alpha_{max,\ y}$	conversion corresponding to the maximum of y(α) function
$\alpha_{max,\ z}$	conversion corresponding to the maximum of z(α) function
β	non-exponentiality factor
β_c	compressibility

ΔH	enthalpy change
Δh^*	apparent activation energy of structural relaxation
ΔT	temperature difference between T_c and T_g
ΔT_{DSC}	temperature difference between sample and reference temperature in DSC
Φ	heat flow
Φ^{red}	so-called reduced heat flow
$\Phi(T)$	measured temperature dependence of heat flow
$\Phi_g(T)$	temperature dependence of heat flow extrapolated for the glassy region
$\Phi_l(T)$	temperature dependence of heat flow extrapolated for the undercooled liquid region
Φ_α	heat flow corresponding to the chosen value of conversion

ABBREVIATIONS

AC(M,N)	autocatalytic (Šesták-Beggren) model
DSC	differential scanning calorimetry
DTA	differential thermal analysis
D1-3	diffusion model
D4	Ginstling-Brounhstein model
FS	Fraser-Suzuki function
GS	glass stability
IR	infrared
JMA(m)	Johnson-Mehl-Avrami model
KAHR	Kovacs-Aklonis-Hutchinson-Ramos model
KAS	Kissinger-Akahira-Sunose method
MKA	multivariate kinetic analysis
RO(n)	reaction-order model
RSC	Robertson-Simha-Curro model
R2	contracting area model
R3	contracting volume model
TMA	thermo-mechanical analysis
TNM	Tool-Narayanaswamy-Moynihan model
w.w.	workability window
XRD	X-ray diffraction

1 GLASS

Glass belongs to a group of materials with non-crystalline structure. From the macroscopic point of view, these materials are considered as solid matters, but the atomic arrangements correspond rather to the arrangements in the melt/liquid – the glass is a stiffened melt/liquid with a rigid structure. This non-equilibrium state can be achieved by a sufficiently fast cooling of a melt/liquid. The acquired system is therefore metastable and the high energy/kinetic barriers prevent the material from the transition to the equilibrium state.

The history of glass itself comes up to thousands of years B.C. The earliest man-made glass objects are dated around 3500 B.C. and were found in Egypt and Mesopotamia, but as far as the place of the first finding, the disputes have been still dragged. The glass production has undergone a revolutionary change around 100 B.C., when the glass-blowing has been discovered by the glassmakers of Syria. It can be assumed that the discovery of glass took place at about the same time, in various civilizations, all over the world. Before glass became really useable, a lot of time has passed. Nowadays the development of glass technology has been continuing and has not been limited to the silicate glasses, but the non-oxide glasses (such as fluoride, borate or chalcogenide glasses) play an important role in many applications from various fields. [1-3]

In particular, the chalcogenide glasses belong to the technologically important and interesting materials due to their unique properties (e.g. high transmittance in the infrared region of the electromagnetic spectrum, semiconducting properties, high refractive index – higher than SiO_2-based glass, etc.), thus these materials are widely used as large capacity data-storage media (CDs, DVDs, BlueRay Discs or non-volatile PCRAMs), elements for infrared optics (fibers, lenses, etc.), optoelectronics, memory switches or various electronic thresholds. [4,5]

1.1 Glass formation

The reversible transition, when the undercooled liquid (during further cooling) passes into a thermodynamically non-equilibrium glassy state, is called the glass transition. A liquid above its melting point represents the initial state; when the cooling begins, most materials start to solidify, crystallization occurs and these processes are connected with discontinuous change of volume, enthalpy, Gibbs energy, etc. This can be avoided by a sufficiently rapid cooling of the melt/liquid, when the material does not have enough time for the nucleation and subsequent crystal growth, leaves the liquid state and changes to a mechanically rigid system – the glass. The viscosity of the system within the cooling process gradually increases until the value equals approx. 10^{12} Pa.s – at this moment the glass is formed. Nonetheless, the glassy structure still remains disordered and keeps the liquid-like structure. This process is characterized by continuous change of the volume, enthalpy, Gibbs energy, while the discontinuity in the second derivative of Gibbs energy occurs, i.e. in the temperature dependence of heat capacity c_p, coefficient of thermal expansion α_{exp}, compressibility β_c. The Gibbs energy values representing the system in glassy state are higher than values corresponding to the crystalline state.

In Fig. 1, the temperature dependence of given property (enthalpy, volume) in the glass transition area is displayed. As can be seen, above the melting point only the melt occurs. As the temperature of melt gradually decreases, at the melting point the crystalline phase arises. This phenomenon is accompanied by a mentioned discontinuous change of given property (enthalpy, volume, etc.). However, if the cooling is fast enough, firstly the undercooled liquid emerges and then during the additional cooling, the glass is formed. This phenomenon on temperature dependence of given property is demonstrated as a departure from the equilibrium with the decrease of property-temperature dependence slope. The temperature corresponding to this departure is referred to as a glass transition temperature T_g. The glass transition temperature is a very important parameter determining the properties and behavior of the resulting glass. Above this temperature, the system behaves like a melt, becomes more formable; under this temperature the system behaves like a solid with a rigid structure. The glass transition temperature is not a thermodynamic quantity. This means that this value is influenced, for example, by the method of glass preparation (cooling rate q^-). At higher cooling rate, the curve corresponding to the glassy state on the temperature dependence of the given property deviates earlier, i.e. at a higher temperature, compared to

a slower cooling rate. The red-labeled curve in Fig. 1 corresponds to the process, when the glass is heated by applied heating rate (q^+), above the T_g, the structure of glass is more loosened, and at the crystallization temperature T_c the crystallization occurs and the crystalline network is formed. With the increasing temperature the melting of crystalline structure occurs, which is characterized by a melting temperature T_m. [5-8]

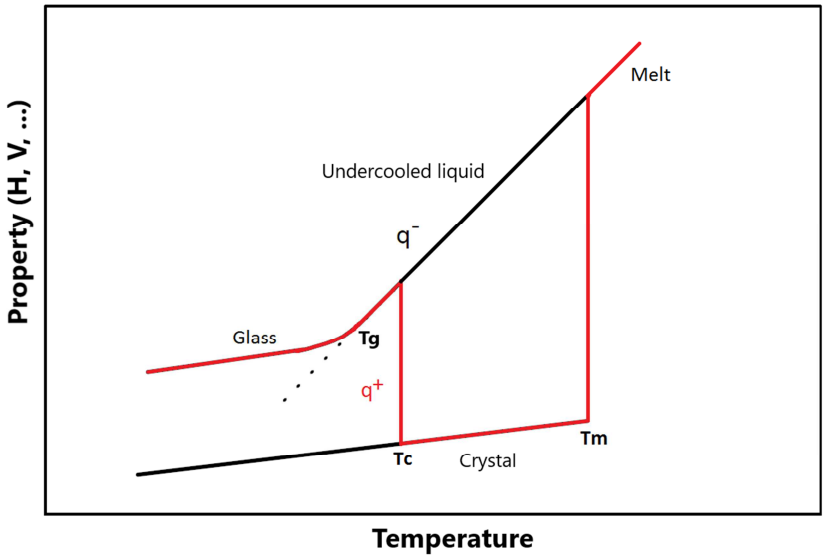

Figure 1: The temperature dependence of given property (H, V, …) in the glass transition area; corresponding temperatures are displayed; q^- represents the cooling rate, q^+ represents the heating rate; the red curve indicates the path for heating of the glass.

1.1.1 Structural relaxation in glasses

In regard to the above-mentioned facts, the glass transition is not a thermodynamically controlled process due to its dependence on actual experimental conditions. Therefore it means that the glass transition process is kinetically controlled. If the undercooled liquid is sufficiently cooled and the glass is formed, the non-equilibrium glassy state endeavors to reach the equilibrium. This process is known as a structural relaxation and is associated with slow molecular rearrangement. In a consequence of the structural relaxation processes, the glassy structure becomes more and more compact. The state to which the glassy structure relaxes is the state of the undercooled liquid (extrapolated to a given temperature range),

which represents the “equilibrium state” when the glasses and glass-forming processes are under consideration. Here, the system is in the so-called kinetic equilibrium, i.e. the high energy/kinetic barriers hinder the further decrease and transformation to the crystalline state. Certainly, these structural changes lead to several changes in physical properties, for example optical transmittance or density. The capability of prediction or monitoring these changes plays an important role for the potential glass technology. The classification of relaxation process is based on the property, which is monitored. The two most common properties are the volume and enthalpy. [6-10]

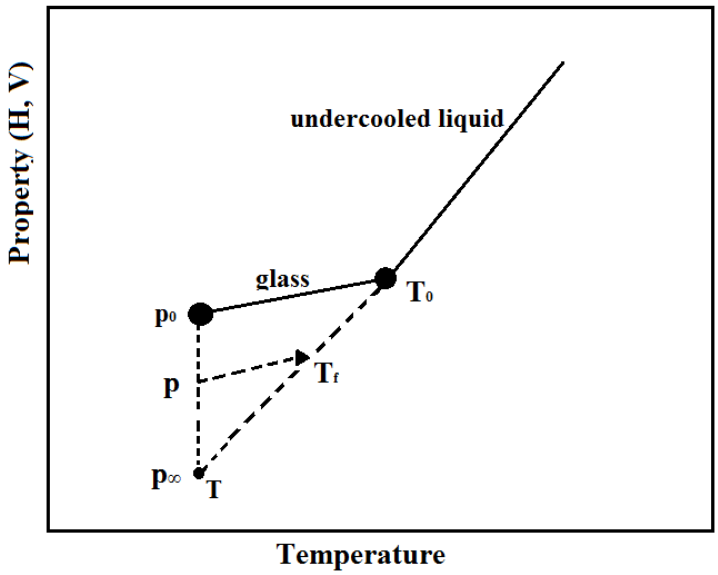

Figure 2: The temperature dependence of relaxing given property (H, V, …) in the glass transition area; T_0, p_0 corresponds to an initial state of the formed glass; p_∞ corresponds to the equilibrium state of glassy material.

Fig. 2 illustrates the change of given property (enthalpy, volume) of a formed glass in the metastable equilibrium within the relaxation process. The solid line indicates a change of property due to applied cooling until the glass is formed and reaches the temperature T. If the glassy material undergoes the annealing at this reached temperature, the relaxation goes on, the glassy structure changes and tries to get closer towards equilibrium. A symbol "T_f" denotes the fictive temperature [11] and with using this parameter the structure of relaxing glassy material can be characterized. The fictive temperature T_f defines the temperature of undercooled liquid with the same structure as the relaxing glass acquires. [10,12]

The two common ways exist to examine the relaxation process - the dilatometric and the calorimetric measurements of structural relaxation. The volume relaxation experiments can be realized by using the mercury dilatometer and the vast study on amorphous polymers using this method was accomplished by Kovacs [13]. Unfortunately, this method is rather limited due to e.g. its volume change sensitivity, size and fragility of dilatometer, the possible reaction of certain amorphous glasses with mercury. Another dilatometric method used for the examination of relaxation process can be the method of thermomechanical analysis (TMA). These experiments proceed from the plain dependence of glass transition temperature on cooling rate and their series with various applied cooling rates. [79,82] Next, for the enthalpy relaxation experiments the calorimetric methods may be used (such as DSC). The great advantage of DSC method is the complete information about whole thermal history of the sample, with no data loss. Also, the sensitivity of this method is better in contrast to the mercury dilatometry method due to the much lower thermal gradients within and outside of the DSC sample. [14,15]

1.2 Crystallization

The crystallization process belongs among the first-order phase transitions (according to Ehrenfest), and is characterized by a discontinuous change in temperature dependence of volume, enthalpy, entropy, etc. The atomic reorganization into a periodical crystal structure goes on, the Gibbs energy value decreases to the minimum and the crystalline system reaches the thermodynamically equilibrium state. The crystalline system may be obtained by a slow cooling of a melt, when the melt material has enough time (within the cooling) to create a periodically organized system – a crystal; or the another way to acquire the crystalline products is the so-called cold crystallization including a heating of the amorphous/glassy material to its crystallization temperature. [5,7]

The crystallization could be described by two subsequent processes – the nucleation and the crystal growth. Firstly, the new-phase nuclei are created, the amount and size of nuclei steadily increases simultaneously. This process is called nucleation and may proceed with two different mechanisms – homogeneous or heterogeneous nucleation. In the first case, the nuclei emerge randomly throughout the volume of melt, solid or crystal; in the second case, the nuclei originate at energy-efficient/preferred locations (such as defects, inclusions,

dislocations, additive atoms), which function as crystallization centers; the magnitude of the energy barrier is in most cases several orders less than in case of homogenous nucleation. [5,7,9,10,16]

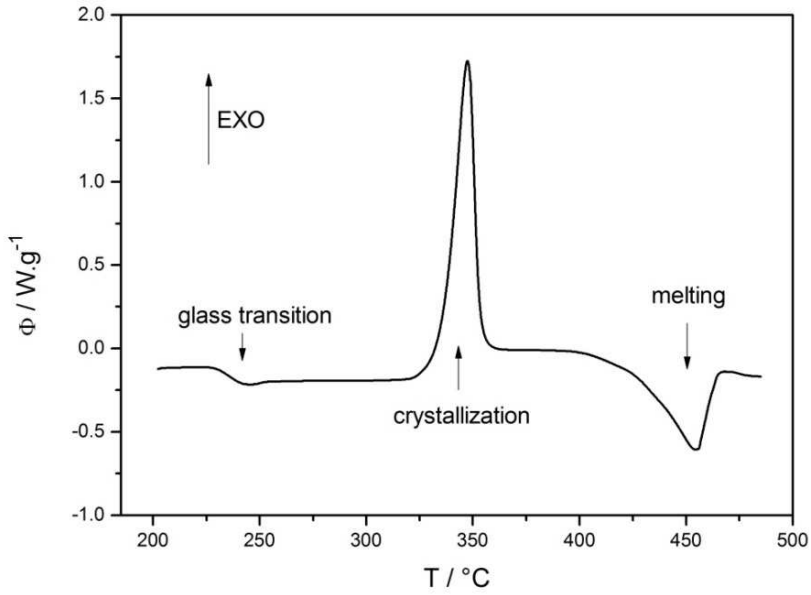

Figure 3: The example of DSC curve observed for non-isothermal measurement; the corresponding thermal effects are denoted.

Secondly, the crystal growth follows and includes two important processes – the mass transport to and through the newly-emerged phase interface. The studies focused on a description of crystal growth may be performed with utilization of two approaches – the direct microscopic observation with using the microscopic methods (optical, electron microscopy) and three basic phenomenological models (normal growth, screw dislocation growth, two-dimensional surface nucleated growth models [19,20]); or the usage of indirect macroscopic observation of crystallization. This method is based on thermal analysis, which can be realized by means of differential thermal analysis (DTA), differential scanning calorimetry (DSC) and also by means of thermomechanical analysis (TMA) – more on this option will be discussed in Chapter 3. [5-10,16-18]

1.3 The prediction of glass stability (the glass-stability criteria)

The glass-stability (GS) criteria are widely used parameters in scientific practice to characterize and predict the behavior of amorphous/glassy materials. Further, with their knowledge, it can be estimated whether the required substance is capable of forming a stable glass or not. The noticeable effort has been dedicated to the search of the most suitable GS criteria in regard to the potential real-life applications of the given glassy material.

The glass-forming criterion introduced by Zachariansen [21] represents the oldest way to assess the ability to form a glass. This criterion works on the assumption of the structural preconditions of studied systems. However, there is a certain limitation. It is necessary to know the structure of the emerging glass, which is not always possible, primarily in case of the newly studied systems.

The thermodynamic approach to glass-stability evaluations is based on e.g. the bond energy determinations, the differences in the electronegativity of constituent elements, the relations between the characteristic temperatures - glass transition temperature T_g, crystallization temperature T_c (onset vs. maximum of the signal) and melting temperature T_m and their ratios. [5,22] The last mentioned GS criteria based on relations between the characteristic temperatures have an advantage in their relative simplicity (due to their evaluation) and good functionality in series of chemically resembling glasses. The most common used GS criteria include the criteria defined by Hruby K_H [23], Saad and Poulain K_{SP} [24], Weinberg K_W [25], Lu and Liu K_{LL} [26], Long K_{LX} [27], and Zhang K_{ZW} [28]. With using these criteria, it is possible to determine the ability of the material to form glass and its subsequent stability. As the most suitable criterion (for chalcogenide materials) was found the Hruby criterion (see Ref. [29]) that manifested the lowest normalized variability with the experimental conditions in contrary to K_W, K_{LL}, K_{LX} and K_{ZW}. As was mentioned, these criteria function in series of structurally similar glasses, but the great disadvantage of their usage exists, the large influence of experimental conditions (such as a sample form, heating rate, the way of determination of each characteristic temperature, i.e. onset vs. signal maximum) is obvious. Nonetheless, the difference between the glass transition temperature T_g and the crystallization temperature T_c has still remained crucial. The wider the difference $T_c - T_g$, the more stable the glass is. In scientific practice the so-called ΔT criterion ($\Delta T = T_c - T_g$) [30-32] is used to consider the thermal stability of the given glassy system. In addition, a new approach has been recently suggested [33] containing the combination of crystallization

temperature value (obtained from DSC crystallization measurements) and the information about glass-softening and viscous flow effects (obtained from TMA crystallization measurements), which becomes more apparent and important in the crucial temperature region between the glass transition temperature and crystallization. More on these issues will be discussed in Chapter 5.3.

The last (but not least) way to characterize the glass ability or stability represents the kinetic models. This alternative approach (with regard to thermodynamic approach) takes into account the fact, that each material is able to form a glass, if the adequate cooling rate is applied. The initial point of considering the glass ability or stability represents the construction of T-T-T (Temperature-Time-Transformation) curves. Unfortunately, a huge amount of information is required and not all of the needed parameters are often available. That is a great limitation of applicability the kinetic models. [5,22]

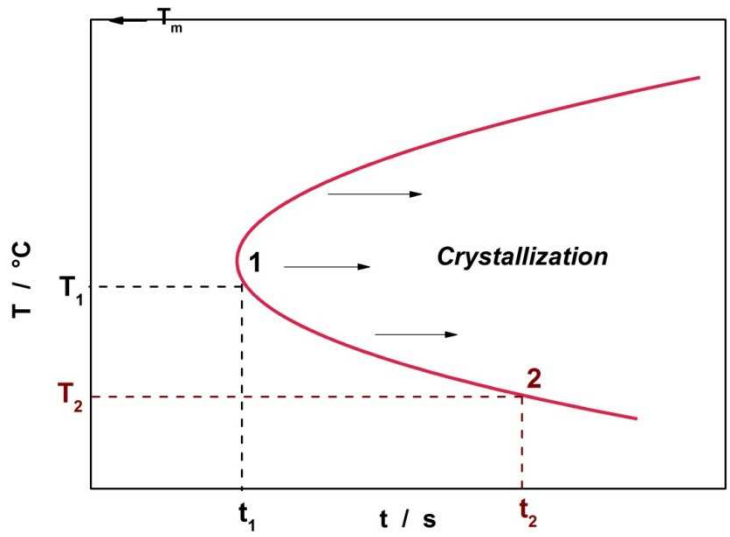

Figure 4: The illustration of T-T-T curve; the temperature and the corresponding time needed to the crystallization of given portion of glass are depicted.

2 TELLURIUM-BASED CHALCOGENIDE GLASSES

Chalcogenide glasses belong to a section of inorganic amorphous materials having chalcogens as main matrix elements. The chalcogens are the elements from the 16th group of the periodic system of elements (except oxygen), i.e. sulfur, selenium, tellurium. Polonium also ranks among chalcogens, but its strong radioactivity hinders the usage in this application area.

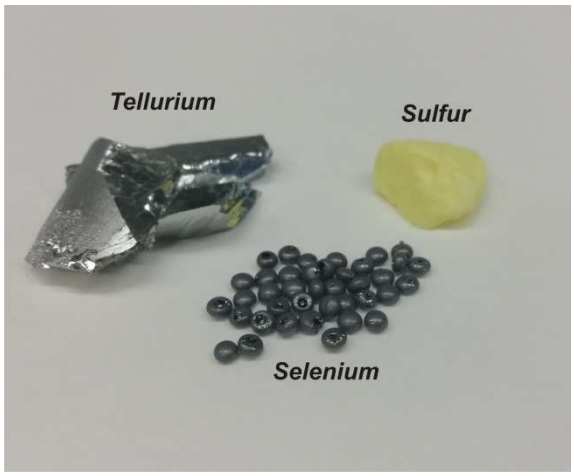

Figure 5: Chalcogens - tellurium, sulfur, selenium

One of the promising chalcogenide materials are the tellurium-based glasses. These systems are well-known for their excellent transmittance in the infrared (IR) region. The transmittance window can range from 2 up to 28 μm; it depends on the exact composition. This feature can be successfully utilized in various hi-tech IR applications including biosensors with usage in medicine or environmental sphere [34], CO_2 detectors fighting the global warming [35], space optics detecting the biological life markers (such as absorption bands of CO_2, O_3, H_2O) on exoplanets [36-38]. The great disadvantage of telluride glasses is their high tendency towards crystallization, which results in complications in the further processing of the glassy material. Each of all processing steps must then be strictly controlled to prevent the possible crystallization. Nowadays, the great emphasis is placed to the search of the material with appropriate thermal, optical and compositional properties. The main goal is then to achieve the highest thermal stability of telluride glasses, while the best optical properties will be kept. Therefore, the doping of telluride matrix with stabilizing components (e.g. selenium, gallium or iodine) proceeds. Currently, these materials

undergo in-depth testing, because the detailed studies of the thermal properties of these materials have yet been missing; except the basic parameters such as the characteristic temperatures (T_g, T_c, T_m). As is apparent, it is necessary to carry out an overall detailed study involving the thermal characterization of materials (determination of the GS criteria), the development of the kinetic processes associated with the glass formation and the crystallization (across the compositional lines of the studied glasses), the structural arrangement of glassy and crystallization products and the influence of various experimental conditions, which may affect the applicability of glassy materials for practical usage. The subsequent knowledge of ongoing kinetic processes, thermal properties and structural arrangement may serve to predict the behavior of the material for arbitrary conditions that can be used in finding the new hi-tech materials, technology for the glass-preparation or usage of these glasses in commercial applications. [30-32,34-42]

2.1 Doped Ge-Te glasses

The aforesaid problem associated with relatively high tendency towards crystallization of tellurium-based glasses can be solved by stabilizing the fully telluride matrix using some added elements. Nowadays, main advance is being built around the $GeTe_4$ matrix, which is further doped by stabilizing elements - Se, Ga or I. Each of these elements plays a different role in a resulting glassy structure. These operations improve then the qualities of given glassy material for its later processing, e.g. the fiber-drawing or molding.

2.1.1 Ge-Se-Te system

The doping of Ge-Te matrix by adding a slight amount of selenium shows certain benefits in contrary to the other two competing systems (Ge-Ga-Te and Ge-I-Te). In case of Ga-doped systems, the studied glasses have more inclined towards crystallization than the Se-doped glasses, this fact plays a crucial role in a potential glass-processing (e.g. fiber-drawing). The preparation of Ge-I-Te glasses is more difficult due to the considerable volatility of iodine. So the glasses based on Ge-Se-Te composition stand for the promising materials operating in the far-IR region. A small addition of selenium to the telluride matrix functions as a stabilizer of resulting glassy system, while the transmittance is influenced only weakly. The main goal of studies dealing with the glasses with possible utilization in the area

of IR applications has been an improvement of thermal stability while keeping the transmittance window as wide as possible. [32,35,37,42-45] Therefore, as was reported in Refs. [32,35,42], the percentage amount of added Se content must be kept under 5 at. % due to its influence on the final width of transmittance window.

The glass-forming ability of the Ge-Se-Te system is discussed in Refs. [42,46,47] including the supported information with regard to the phase diagrams. It was found that the ternary Ge-Se-Te system contains the two glass-forming regions represented by Se-rich and Ge- or Te-rich glasses. In Fig. 6A, the illustration of Ge-Se-Te ternary diagram including the two mentioned glass-forming regions is displayed. In Fig. 6B, the obtained phase diagram corresponding to Ge-Se-Te system is demonstrated. These results originate from the systematic study of about hundred samples with different compositions along the Ge-Se-Te system. The samples were prepared by a classical melt-quench technique with quenching in air and their thermal behavior was explored by means of DTA. [46,47]

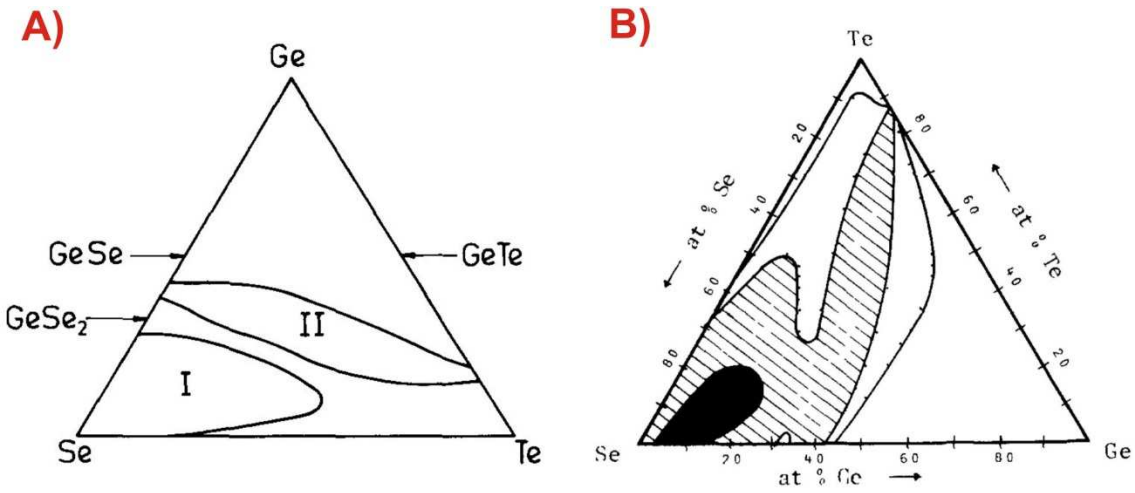

Figure 6: Ternary phase diagrams corresponding to the Ge-Se-Te system;

A) Ge-Se-Te phase diagram with marked two glass-forming regions [46]: I. The first region of glass-forming (Se-rich glasses)

II. The second region of glass-forming (Ge- and Te-rich glasses).

B) Phase diagram of Ge-Se-Te system with marked four glass-forming regions [47]: the colour-filled area - glasses without recrystallization

i. **the dashed area - glasses with recrystallization**
ii. **the dotted area - partially crystalline**
iii. **the hemmed area - crystalline.**

Several calorimetric studies of the Ge-Te systems doped with various representations of selenium were performed using DSC. [32,35,42,44,48] The mutual feature of these studies (regarding the potential IR applications of the investigated glasses) was an attempt to find the glass composition with optimum thermal and stability properties, i.e. extending the highest difference between the temperatures corresponding to the glass transition T_g and crystallization T_c, which determines the processability of glassy material. The paper [35] deals with the thermal study of $Ge_{20}Se_xTe_{80-x}$ (x = 1 - 5 and 10 at. %) systems (including the $Ge_{20}Te_{80}$ system). It was found that the most suitable compositions in regard to future IR applications are the compositions containing 3 - 5 at. % of selenium, which represent the systems with the highest ΔT values around 106 - 112 °C, while for the pure $Ge_{20}Te_{80}$ glass the ΔT value equals ~ 79 °C (due to a metallic nature of tellurium). The glassy composition with 10 at. % of Se is probably near to the non-mixing zone and on that account its thermal stability decreases. The suitability of selected compositions for the possible processing of glassy material to obtain the optical devices has been confirmed by the next supported studies based on measurements of IR transmission spectra, where the width of IR transmission window has not been affected by a substitution of tellurium compound by low percentage amount of selenium. The other studies [32,42,44] work with similar compositions of Ge-Se-Te systems, with more or less changing representation of Ge-content (from 15 to 21 at. %), while the amount of selenium has been kept under 5 at. % due to the holding the best thermal stability without compromising the width of IR transmittance window.

Table 1: The ΔT values of selected compositions of Ge-Se-Te system; Se content kept at 3 at. %; for illustration the information about ΔT value of non-doped $Ge_{20}Te_{80}$ system added.

Composition	ΔT (°C)
$Ge_{20}Te_{80}$ [42]	79
$Ge_{15}Se_3Te_{82}$ [42]	90
$Ge_{20}Se_3Te_{77}$ [32,42]	119 or 106
$Ge_{21}Se_3Te_{76}$ [32,42]	115 or 123

The further experiments with these glassy systems, such as measurements of IR transmission spectra or fiber-drawing experiments without any apparent crystallization confirmed that the best choice with regard to thermal stability and optical properties for future

IR applications is the composition with 3 at. % of selenium. [32,35,42,44,48] The ΔT values of selected compositions are listed in Table 1.

2.1.2 Ge-Ga-Te system

The chalcogenide germanium-tellurium glasses doped by a slight amount of gallium introduce another possible way to get the materials with potential utilization as IR optical devices. The poor glass stability of Ge-Te system is solved by incorporating the Ga content in the resulting structure. In comparison to the Ge-Se-Te system, the Ge-Ga-Te system is more susceptible towards crystallization (within the shaping process), but the transparency capability is significantly higher than in case of Se-doped systems, where the presence of selenium narrows the transmittance window of resulting IR glass. [30,37,43,45,49-51] It was demonstrated (see Ref. [30]) that Ga-doped systems are able to extend the transmittance window up to 28 μm.

In Fig. 7, the scheme of Ge-Ga-Te ternary phase diagram is illustrated. As can be seen, the region in which the glassy matters in this system can be obtained is quite small and is centered along the pseudo-binary line $GeTe_4$-$GaTe_3$. This statement has been supported by the investigations of some glass-forming studies on tellurium-based glasses. [30,45,49,51]

This glassy system belongs to the relatively new-discovered group of chalcogenide glasses, therefore not so many studies concerned with thermal behavior have been carried out. The interesting systematic research of Ge-Ga-Te system has been introduced in Ref. [30] - 13 glassy compositions along the pseudo-binary line $GeTe_4$-$GaTe_3$ were investigated. With regard to the thermal stability, the DSC experiments were performed and on the basis of characteristic temperatures (such as T_g, T_c, T_m) the values of ΔT criterion were estimated. The highest ΔT values were obtained for the $Ge_{15}Ga_{10}Te_{75}$ (ΔT = 113 °C) and for the $Ge_{10}Ga_{15}Te_{75}$ (ΔT = 100 °C) glassy compositions, which determine these reported compositions as the thermally stable leaders in this Ga-doped system. In consequence, the optical properties of the studied compositions were tested by means of IR transmission spectra measurements. It was found that the transparency ranges from 1.99 up to 28 μm with the maximum transmission of about 55 %.

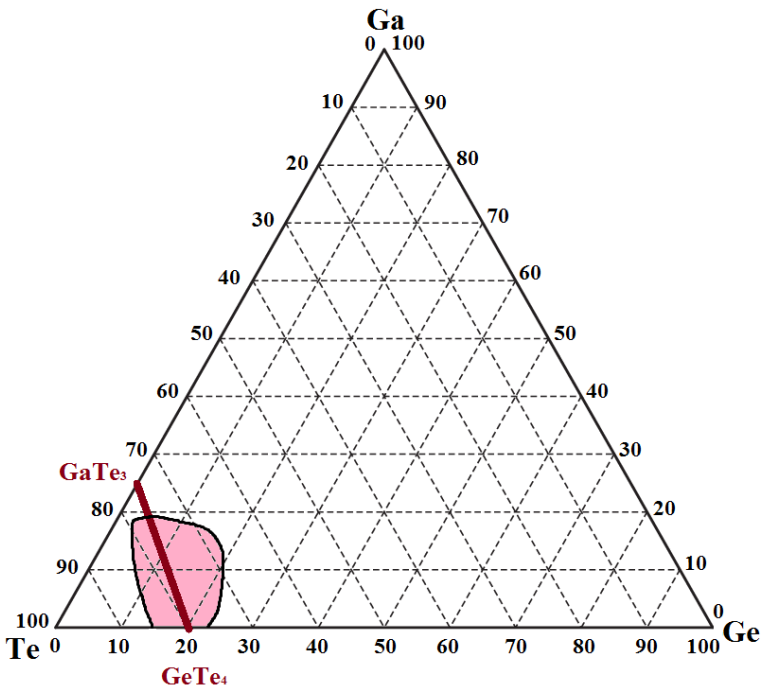

Figure 7: The schema of ternary phase diagram corresponding to the Ge-Ga-Te system;

i. the red line represents the pseudo-binary line $GeTe_4$-$GaTe_3$,

ii. the colour-filled area stands for the glass-forming region.

Another study focused on thermal behavior of Ge-Ga-Te system [51], namely the $(GeTe_4)_{1-x}Ga_x$ and $(GeTe_5)_{1-x}Ga_x$ (x = 0; 5; 10; 15 at. %) compositions, discusses the improving impact of Ga on the thermal behavior of Ga-doped Ge-Te matrix. In this work, the ΔT values of studied glassy compositions are evaluated. The required value of ΔT criterion representing the thermally stable glasses (estimated as $\Delta T \geq 100$ °C) was not reached in any studied composition.

2.1.3 Ge-I-Te system

The alternative way to stabilize the Ge-Te matrix against devitrification represents the doping of tellurium matrix with iodine. The volatility of iodine may make the glass synthesis a little bit more difficult, but the features of resulting glassy material are interesting due to the thermal stability and large transmittance window in far-IR region of prepared glass. The iodine plays a role of terminating atom of the three-dimensional network, the iodine

atoms are not bridging and also have propensity to trapping the electrons from Te. These properties of iodine in glassy matrix prevent the material from crystallization. [45,49,52-56]

The scheme of glass-forming region in case of Ge-I-Te system is illustrated in Fig. 8. As can be seen, the glass-forming area is very confined (similar to the Ge-Ga-Te system). This conclusion emerges from few glass-formation studies [45,54,55], which were performed by means of DTA and DSC. One of the first DTA studies of glass-formation ability documented the glass compositions up to 12 at. % of iodine [54], the follow-up DTA study [55] is concerned with five compositions also up to 12 at. % of iodine and various representations of gallium content (from 13 to 21 at. %). The further exploration of the Ge-I-Te system was carried out by the DSC study of 26 glassy compositions [56]. The glass-forming area ranges around the $GeTe_4$ composition. [54-56]

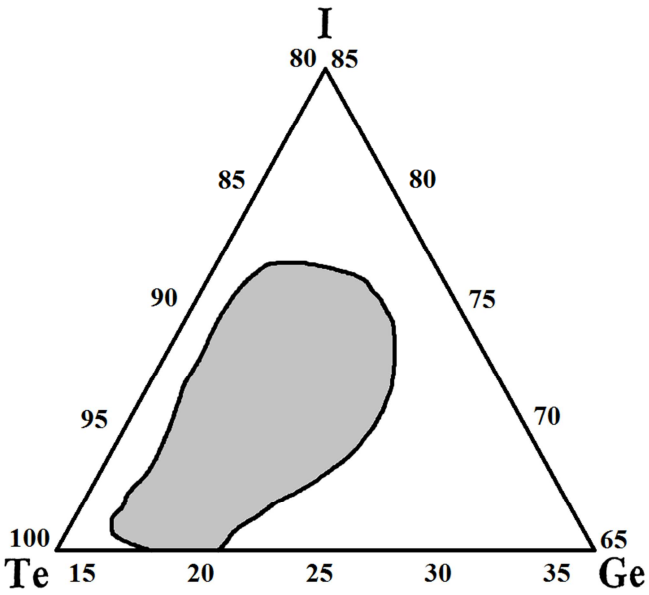

Figure 8: The schema of ternary phase diagram corresponding to the Ge-I-Te system; the color-filled area stands for the glass-forming region.

With regard to the thermal behavior of the ternary Ge-I-Te system, not many studies are available [54-56]. In Ref. [56] the information about calorimetric properties (such as characteristic temperature and ΔT values) of five iodine-doped Ge-Te systems can be found. It was estimated that the glassy composition with 7 at. % of iodine is the most thermally stable glassy system due to its high difference between the glass transition temperature and crystallization temperature, which equals to 124 °C. In contrary to the Ge-Ga-Te system

the difference in ΔT values is more than 100 °C. The suitability of the $Ge_{20}I_7Te_{73}$ system for the potential far-IR applications was verified also by the transmission spectra measurements, where the wide transmittance range (from 2 to 22 μm) was estimated. [56]

Naturally, the values of other physical properties of doped Ge-Te systems are available in literature, for example the values of refractive index, electrical resistivity or bond strength. [30,32,44,50,56,57] Several studies [30,32,44,50,56] reported the refractive index value equals ~ 3.3 for Te-rich glasses (the lower value of n ~ 2.5 for Se-rich glasses). With respect to a semi-conductor behavior of chalcogenide glasses, in case of doped Ge-Te systems this property was also confirmed by the resistivity and electrical conductivity measurements [30,32].

2.2 As-Se-Te system

The As-Se-Te system belongs to the other (besides the $GeTe_4$ glasses) known tellurium-based materials with potential utilization in far-IR optical application area. This ternary system profits from the advantages arising from the combination of As-Se and As-Te binary systems. The binary As-Se system ranks among the well-known very good glass-formers and has been extensively tested for decades. The studies focused on thermal, relaxation, crystallization and viscosity behavior of As_2Se_3 glass are available, e.g. in Refs. [58-63]. The vast systematic study [58] has been pursued on crystallization kinetics, viscosity behavior, thermal expansion coefficient of As_2Se_3 system with using various methods, e.g. DSC, the parallel-plate viscometer, microscopic methods (optical, scanning and transmission microscopy), etc.

The As_2Se_3-As_2Te_3 system pertains to the comparatively newly emerged group of IR tellurium-based glassy materials, where the fully-tellurium As_2Te_3 matrix is supplied by certain amount of As_2Se_3. This allows combining the advantage of tellurium glass (such as a large transmittance window in far-IR region of electromagnetic spectrum) and the advantage of selenium glass, which is known as a dependable glass-former. Thus, the As_2Se_3 part functions as a stabilizing factor for further improvement of the thermal stability against crystallization of the resulting glass. This system is therefore assumed to be an alternative to the Ge-Te glasses. [31,34,38,40,43-45,49]

As is apparent, the glassy matters in the pseudo-binary As_2Se_3-As_2Te_3 system can be created almost in the whole compositional range; the glass-forming region of As-Se-Te system is depicted in Fig. 9. [49,64]

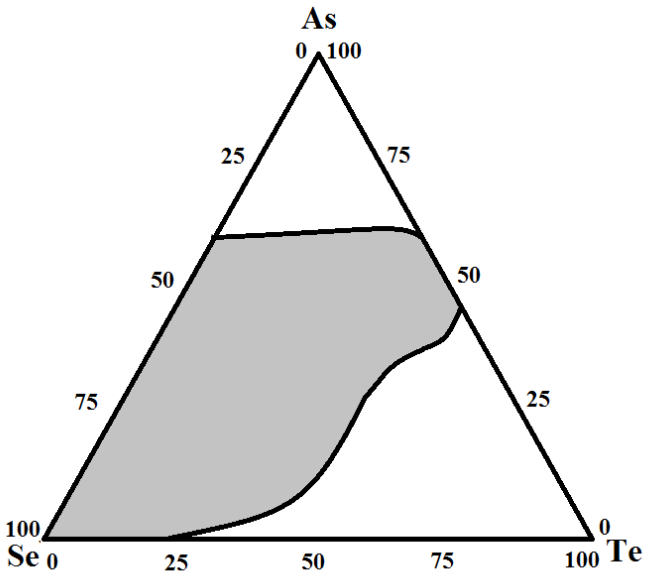

Figure 9: The scheme of ternary phase diagram corresponding to the As-Se-Te system; the color-filled area stands for the glass-forming region.

Several studies, e.g. Refs. [31,34,38,40,43-45,49,64-69], focused on the As-Se-Te system from the structural or thermal points of view exist, but they do not deal with the tellurium-based As-Se-Te glassy matrix. As a stable glassy composition was found to be the $As_3Te_2Se_5$ [65,66] glass, which is positioned in the middle of the glassy area. This system was investigated in terms of T_g measurements, dependence of viscosity on temperature (usable in process of the fiber diameter modification) and transmission spectra measurements. The transmittance window in IR optical region ranging from 2 to 18 μm was estimated. [49,70-72] As is obvious, the detailed studies concerned with thermal behavior of these Te-based glassy systems is absent.

3 MACROSCOPIC MEASURING METHODS OF CRYSTALLIZATION

The scientific research attaches importance to the study of crystallization processes occurring in glassy materials as a consequence of wide-ranging usage of these materials. If the crystallization kinetics is well-known, the predictions of the preparation conditions, potential real-life applicability and so on can be done, which enable a better control of the experimental conditions and properties of resulting glassy material.

The crystallization processes in various materials may be monitored by two basic methods, namely by the direct (microscopic) and indirect (thermal analysis) observations. The usage of indirect macroscopic procedures includes the methods of thermal analysis (e. g. DTA, DSC, TMA) and is a favorite and widespread way how to obtain the valuable data about crystallization process, which are further used for e.g. an evaluation of crystallization kinetics.

3.1 Differential scanning calorimetry (DSC)

Differential scanning calorimetry belongs to a group of thermal-analysis methods used in particular to study of thermal manifestations of physical processes occurring in the materials (e. g. phase transitions, chemical reactions, decomposition processes). These thermal processes can be studied in dependence on temperature or time during a defined temperature program. [5,73-80]

Many phase changes in materials are accompanied either by the heat release (exothermic reaction) or by the heat consumption (endothermic reaction). This type of process is called a first-order phase transition and is detected as a peak in the DSC experiment. The second-order transitions are not associated with release or consumption of the heat, but the thermal capacity of the material changes, which can be seen in the DSC record as a sudden step-change of the baseline. Thus, the principle of DSC is a measuring of the heat amount, which is needed to increase the sample temperature and the reference as a function of temperature. As a reference material some inert matter, such as alumina, may be used, but

nowadays an empty aluminum crucible is usually used. According to the detecting method of the calorimetric signal, the differential scanning calorimeters are divided into two groups, namely the heat flux and power compensation types of DSCs. In the case of the heat flux DSC instrument, the temperature difference between the sample and the reference ΔT_{DSC} is measured in dependence of the sample temperature. This signal is then converted and registered as a heat flow (Φ):

$$\Phi = \frac{dH}{dT} \tag{1}$$

where H is an enthalpy, T is a temperature. In Fig. 10, the temperature dependence of enthalpy (A) and the derivated temperature dependence of enthalpy (B), which corresponds to the temperature dependence of isobaric heat capacity c_p and is proportional to the DSC record, are displayed.

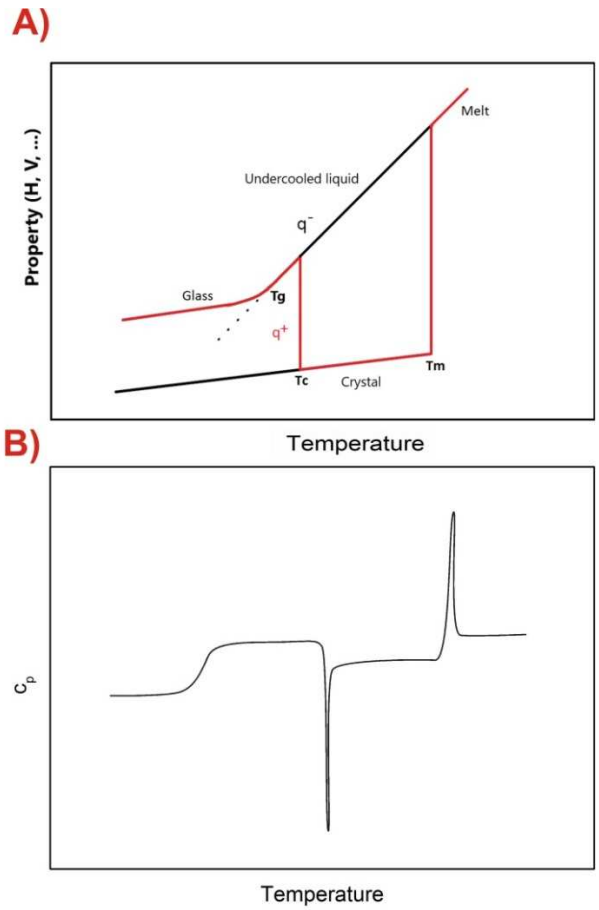

Figure 10: **A) The temperature dependence of given property (H, V, …) in the glass transition area; the red curve indicates the path for heating of the glass. B) Schematic derivation of sketched red-labeled heating curve from graph A - the obtained temperature dependence of c_p.**

The power compensation DSC calorimeters work on a principle of compensation of each temperature change between the sample and the reference temperatures by means of an electric heating-up. Here, this is the heat flow that was needed to the compensation of the temperature difference as a function of temperature or time. [73-80]

The actual process rate is directly proportional to the measured heat flow. The constant of proportionality is then the overall enthalpy change ΔH (for the calibrated devices). The kinetic equation is then determined as:

$$\Phi = \Delta H \cdot \left(\frac{d\alpha}{dt}\right) \tag{2}$$

where α stands for a degree of conversion and t is a time. In the case of non-isothermal DSC measurements, the Equation (2) changes its form to the Equation (3):

$$\Phi = \Delta H \cdot \left(\frac{d\alpha}{dT}\right) \cdot \left(\frac{dT}{dt}\right) \tag{3}$$

If the kinetic analysis is required, a kinetic dataset needs to be prepared. The kinetic dataset contains points and each of these points is characterized by the values of temperature (T), heat flow related to the sample weight (Φ, $W.g^{-1}$) and degree of conversion (α) (see the Equation (4)). [76-79]

$$\alpha_j = \frac{1}{\Delta H} \cdot \int_{T_0}^{T_j} \Phi \cdot dT \tag{4}$$

Note that all measurements performed within the framework of the present doctoral thesis were performed using the TA Instruments DSC Q2000, with the T-zero technology, which accounts for the so-called heat inertia effects [83]. Hence the simplified base DSC equation (Eq. 3) could be employed for all relevant evaluations of the DSC data.

3.2 Thermomechanical analysis (TMA)

Thermomechanical analysis is based on the measurement of the sample deformation under defined loading as a function of temperature (or time), while the measured sample is subjected to a controlled temperature regime. The deformation of given sample is registered by the change in the height of the sample, then the certain glass properties such as length expansion, glass transition temperature, viscosity of undercooled liquid, crystallization temperature or melting point can be determined. It is also possible to observe the penetration of the needle into a compact sample that allows the softening temperature of the sample to be evaluated. For films or fibers, this method enables to pursue the applied force changes at a constant length (relaxation). Thus the TMA is the universal thermal-analysis method that allows the observation of crystallization process, as well as the softening and melting processes, volume and linear expansion. The study of crystallization by means of TMA is based on the viscosity behavior of glass-forming undercooled liquids. The behavior of crystallization curve is illustrated in Fig. 11A, which exhibits a typical behavior during the non-isothermal measurement, the height change of the sample is monitored in relation to the temperature.

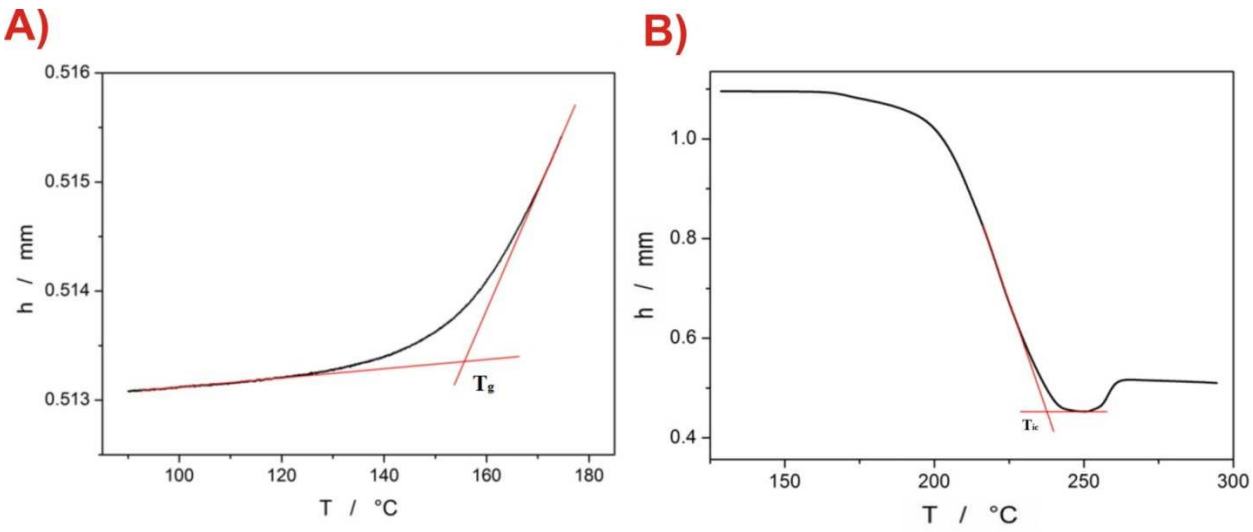

Figure 11: A) The example of the TMA curve and the evaluation of T_g is depicted.
B) The example of the TMA curve and the evaluation of T_{ic} is demonstrated.

The glass transition temperature T_g presents itself as a departure from the curve representing the glassy state to the state of the undercooled liquid. The glass-softening and viscous flow effects play an important role in potential processing of glassy materials (such as

moulding, fiber drawing, etc.) and with the knowledge of these phenomena the conditions within fabrication of glassy products (lenses, fibers, etc.) can be properly controlled. [77-82]

As the temperature rises, the viscosity of the material decreases causing the spread of sample, which is connected with the sample height decrease. The viscosity decreases to an initial crystallization temperature (T_{ic}), when the crystals begin to form in the undercooled liquid. The crystallization of the sample causes an apparent increase of viscosity, due to the crystal formation and their growth, the sample ceases flow and thus the decrease of its height stops. The evaluation of the initial crystallization temperature T_{ic} is suggested. [77-82]

4 THEORY OF KINETIC ANALYSIS

This thesis is primarily focused on the study of crystallization kinetics of tellurium-based chalcogenide glasses with following appraising of the processability of investigated glassy materials. The knowledge of crystallization process kinetics is important for the preparation and further processing of glassy materials due to possibility of monitoring the individual steps, experimental conditions of glass processing and the opportunity to predict the glassy material's behavior under various optional experimental conditions. In this thesis, also the structural relaxation kinetics will be described (rather as a side-note) with respect to the completion of predictions of the glass stability, crystallization and structural processes occurring in the studied chalcogenide systems.

4.1 The procedures of crystallization kinetics assessments

The crystallization kinetics is commonly studied by means of DSC. The kinetic analysis of DSC data is based on the search of the most suitable kinetic model that facilitates an appropriate description of a given kinetic process. If the separation of thermal and rate component of the kinetic equation is possible, the relation characterizing the actual process rate is estimated as:

$$\frac{d\alpha}{dt} = K(T) \cdot f(\alpha) \tag{5}$$

where $\frac{d\alpha}{dt}$ stands for reaction/transformation rate, K(T) is a rate constant (depends on temperature) and f(α) denotes an expression of suitable kinetic model (α is a conversion). The rate constant can be expressed by using the known Arrhenius equation:

$$K(T) = A \cdot e^{-\frac{E_A}{RT}} \tag{6}$$

where A is a preexponential factor, E_A is an apparent activation energy of the studied process, R is an universal gas constant, T is a temperature. The kinetic analysis of DSC data is realized

by means of the DSC universal kinetic equation (see Eq. (7)), which has arisen by the conjunction of above-mentioned equations (2), (5), (6). Thus, the DSC universal kinetic equation is determined as:

$$\Phi = \Delta H \cdot A \cdot e^{-\frac{E_A}{RT}} \cdot f(\alpha) \tag{7}$$

The common kinetic models, which can serve as a description of crystallization kinetics of data provided by DSC, are for example the nucleation-growth Johnson-Mehl-Avrami (JMA(m)), autocatalytic Šesták-Berggren (AC(M,N)), reaction order (RO(n)), diffusion (D1-3), Ginstling-Brounshtein (D4), contracting area (R2) or contracting volume (R3) models. The kinetic models represent a theoretical (mathematical) characterization of studied processes, which experimentally occur in given materials. The Table 2 offers the summary of chosen kinetic models, their labeling and corresponding forms of f(α) functions. [76,77,79,84,85]

Table 2: Kinetic models

Model	Symbol	f(α)
Johnson-Mehl-Avrami	**JMA(m)**	$\boldsymbol{m(1-\alpha)[-\ln(1-\alpha)]^{1-\frac{1}{m}}}$
Autocatalytic Šesták-Berggren	**AC(M,N)**	$\boldsymbol{\alpha^M(1-\alpha)^N}$
Reaction order	**RO(n)**	$\boldsymbol{(1-\alpha)^n}$
1-D diffusion	**D1**	$\boldsymbol{\frac{1}{2\alpha}}$
2-D diffusion	**D2**	$\boldsymbol{-[1/\ln(1-\alpha)]}$
3-D diffusion (Jander)	**D3**	$\boldsymbol{\left[3(1-\alpha)^{\frac{2}{3}}\right] / \left[2(1-(1-\alpha)^{\frac{1}{3}})\right]}$
Ginstling-Brounshtein	**D4**	$\boldsymbol{3/\left[2((1-\alpha)^{-\frac{1}{3}}-1)\right]}$
Contracting area	**R2**	$\boldsymbol{2(1-\alpha)^{\frac{1}{2}}}$
Contracting volume	**R3**	$\boldsymbol{3(1-\alpha)^{\frac{2}{3}}}$

4.1.1 The activation energy determination

The first step of kinetic analysis of experimental DSC crystallization data represents the determination of the activation energy of crystallization. [76,85,86,90] The knowledge of this parameter is necessary, as it can then be used for the evaluation of the basic kinetic model and the crystallization processes in studied material can be appropriately described. Nowadays, there are several methods developed for this purpose, firstly the Kissinger [87] method, further the Friedman [88] and Kissinger-Akahira-Sunose (KAS) [89] methods.

The Kissinger method is simple and is based on the temperature shift of the DSC signal maximum, which is associated with different applied heating rates. The usage of this method therefore consists in case of non-isothermal measurements. The Equation (8) depicts the principle of Kissinger method, where q^+ stands for heating rate and T_p is the temperature corresponding to the maximum of the crystallization peak. The value of the activation energy is derived from the slope of the linear dependence $ln\left(\frac{q^+}{T_p^2}\right)$ vs. $\frac{10^3}{T_p}$.

$$ln\left(\frac{q^+}{T_p^2}\right) = const. - \frac{E_A}{RT_p} \tag{8}$$

Some limitations of usage this method for evaluation the activation energy of crystallization exist. For example, the Kissinger method provides only the E_A single value (representing the dominant crystallization process), which can make the difficulties in an assessment of complex processes, which contain more than one crystallization process. [76,85-87,90]

The Friedman and KAS methods belong to a group of isoconversional methods. These procedures are based on the assumption that the reaction rate in the constant conversion range is only temperature dependent. The degree of conversion remains constant, so the reaction or phase transformations do not vary with changing heating rate. Thus, the values of E_A are estimated as an average of E_A values determined for chosen degrees of conversion. This procedure leads to the minimization of the influence of experimental conditions. These methods are usable for non-isothermal and also for isothermal measurements. [85,88-90]

The Friedman method is a differential isoconversional method of E_A evaluation and is expressed by the Equation (9):

$$\ln(\Phi_\alpha) = const. - \frac{E_A}{RT_\alpha} \tag{9}$$

where Φ_α, T_α are a heat flow and temperature corresponding to the chosen values of conversion; the interval of α values is defined as $0.3 \leq \alpha \leq 0.7$. In this α value interval the values are stabilized and are not affected by the inaccuracies associated with the ascending and descending part of the crystallization peak. The origin of imprecisions in determination of E_A using the Friedman method may be the dependence of both parameters (heat flow and temperature) on the degree of conversion. Further the value of α is estimated on basis of Equation (4), where the value of ΔH can be influenced by several factors. With the increasing applied heating rate, hence the temperature, at which the phase transition takes place, increases, the specific heat value associated with this process also increases. Furthermore, the effect of heat dissipation at lower applied heating rates influences the ΔH value and also indirectly the α value, which is most likely related to the construction of DSC cell itself, when the sensor registers only a part of the developed heat, which may slightly differ for the smaller heat flows in comparison with the case for which the DSC cell has been calibrated. [85,86]

The integral isoconversional methods are based on the application of the isoconversional principles to the equations in the integral form. The modified KAS method is expressed by means of the Equation (10):

$$ln\left(\frac{q^+}{T_\alpha^{1.92}}\right) = const. - 1.0008\frac{E_A}{RT_\alpha} \quad (10)$$

Starink [88] has showed, that some changes in KAS equation parameters lead to a better accuracy of the E_α values. [85,86,89]

4.1.2 The kinetic model and kinetic parameters determination

The second step of kinetic analysis of DSC crystallization data is the search of a suitable kinetic model, which is able to describe the studied crystallization kinetics. This can be achieved by using algorithms based on the characteristic functions y(α) and z(α) [76,84,85] derived by using a simple transformation of experimental DSC data. In case of isothermal measurements, these functions can be expressed as:

$$y(\alpha) = \Phi \tag{11a}$$

$$z(\alpha) = \Phi \cdot t \tag{11b}$$

If the DSC crystallization data were obtained at non-isothermal conditions, the functions y(α) and z(α) are determined as:

$$y(\alpha) = \Phi \cdot e^{\frac{E_A}{RT}} \tag{12a}$$

$$z(\alpha) = \Phi \cdot T^2 \tag{12b}$$

The values of y(α) and z(α) functions are usually subjected to normalization procedure in the interval <0,1>. It helps to an easier data interpretation and the influence of different experimental conditions can be eliminated. Thanks to the transformation of experimental data using characteristic y(α) and z(α) functions, the determination of convenient kinetic model is easier in regard to the actual kinetic processes. The maximum of z(α) function equals to the degree of conversion $\alpha_{max,\ z}$ and corresponds to the maximum process rate, further does not depend on the activation energy value, in contrary to the maximum of y(α) function ($\alpha_{max,y}$), which is strongly affected by the value of the activation energy. The certain kinetic model (suitable to DSC data) can be estimated using the values of the degree of conversion corresponding to the maxima of the characteristic y(α) and z(α) functions and from the resulting shape of their dependency on the degree of conversion. This statement is supported by the fact that the maximum of z(α) function does not depend on the value of the activation energy. [76,84-86,90-92]

In general practice, the most common kinetic models used for the description of crystallization kinetics are the nucleation-growth JMA (m) [93-95] and autocatalytic AC(M,N) [95] models.

If the value of the degree of conversion corresponds to the maxima of the z(α) function and ranges from 0.62 to 0.64 (the theoretical value of $\alpha_{max,\ z}$ equals to 0.632) the

crystallization kinetics can be described by the JMA (m) model. Mathematically, the JMA (m) model can be expressed using this Equation (13):

$$f(\alpha) = m(1-\alpha)[-\ln(1-\alpha)]^{1-\frac{1}{m}} \tag{13}$$

where m stands for the kinetic exponent of JMA (m) model reflecting the respective nucleation-growth mechanisms. [85,86,93-95]

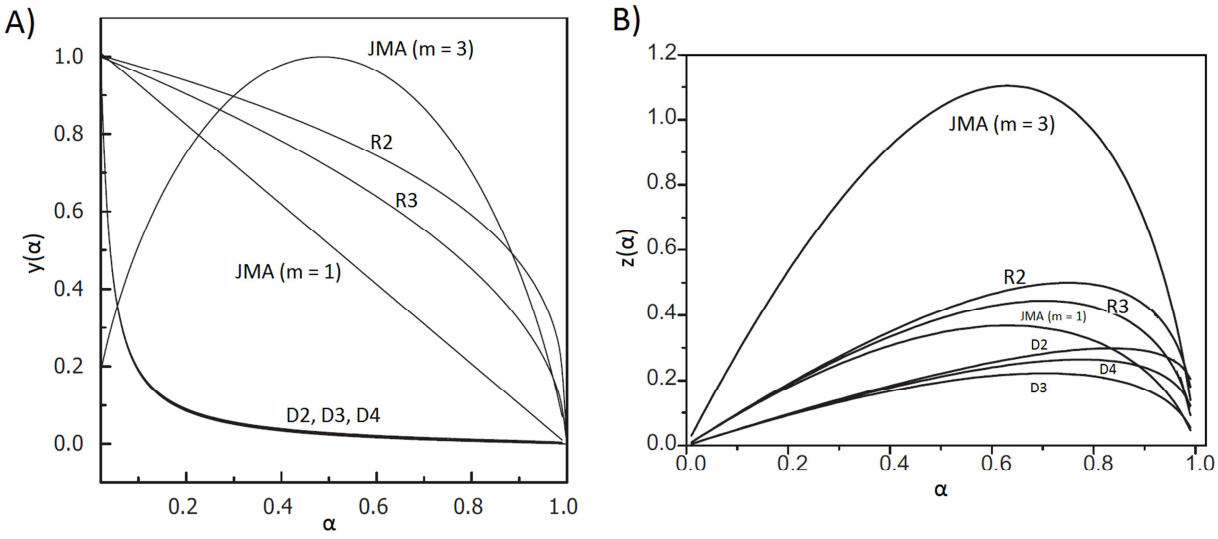

Figure 12: A), B) Schema of y(α) and z(α) plots corresponding to chosen depicted kinetic models.

The JMA (m) model is a one-parameter kinetic model and the value of kinetic parameter m can be determined from the following Equation (14) [97]:

$$m = \frac{1}{1+\ln(1-\alpha_{max,y})} \tag{14}$$

The function y(α) has to provide the maximum value ranging in the interval $0 < \alpha_{max,\,y} < \alpha_{max,\,z}$ with respect to fulfil the condition of m > 1. Another alternative way to determine the value of the parameter m represents the determination from the linear dependence $ln[-ln(1-\alpha)]$ vs. lnt or $ln\frac{1}{T}$. [85,86,93-95,97]

The autocatalytic AC(M,N) model represents the alternative way for description of crystallization kinetics, if the JMA (m) model cannot be used. This semi-empirical kinetic

model has two parameters and the parameters have no physical meaning, nevertheless this model is widely used not only due to its higher flexibility to experimental data. The AC(M,N) model is mathematically expressed as:

$$f(\alpha) = \alpha^M (1-\alpha)^N \tag{15}$$

The kinetic parameters M and N can be determined by means of two consecutive evaluations; firstly the value of $\frac{M}{N}$ ratio used to be assigned (see the Equation (16)) and secondly the value of parameter N can be estimated with using the Equation (17), where the N parameter value is determined from the value of the slope of the below depicted dependence. [85,86,96,98]

$$\frac{M}{N} = \frac{\alpha_{max,y}}{1-\alpha_{max,y}} \tag{16}$$

$$ln\left[\Phi \cdot e^{\frac{E_A}{RT}}\right] = ln(\Delta H \cdot A) + N \cdot ln\left[\alpha^{\frac{M}{N}}(1-\alpha)\right] \tag{17}$$

4.1.3 The preexponential factor determination

The value of the preexponential factor A can be estimated with the knowledge of above-mentioned kinetic parameters, i.e. the activation energy value and the kinetic model and its parameters. If the crystallization kinetics is described by means of autocatalytic AC(M,N) model, the preexponential factor can be evaluated by using the above-quoted Equation (17). Another way how to obtain the A value represents the Equation (18):

$$A = -\frac{q^+ . \frac{E_A}{RT}}{T \cdot f'(\alpha_{max,z})} \cdot e^{\frac{E_A}{RT}} \tag{18}$$

where $f'(\alpha_{max,z})$ stands for the differential form of kinetic model f(α). [85,86]

4.2 Kinetic deconvolution - Multivariate kinetic analysis (MKA)

The multivariate kinetic analysis (MKA) represents a group of model-fitting methods and many ways of model fitting exist. In general practice, the linear or non-linear regression methods can be used. The linear model-fitting methods are based on the linear regression, which means that the conversion and rearrangement of the rate equation to a linear form need to be assigned. The main problem connected with rate equations linearization can arise due to the magnification of the sensitivity of kinetic parameters to points with "small value" and then the distortion of these parameters can deviate from the most important section of the investigated reaction/transformation. In comparison to the usage of linear model-fitting methods, the non-linear techniques can offer a better reliability, an easier optimization of reaction rates, the degrees of conversion or both together; and moreover the non-linear methods are able to include the sets of differential equations of numerical integration. These model-fitting techniques are based on the assumption of the minimization of the difference between the data, which were obtained from experimental measurements, and the calculated data. [85,99-102] The famous method of non-linear fitting techniques represents the method of least squares evaluating the data difference as the residual sum of squares (RSS) [103]:

$$RSS = \sum_{j=1}^{n} \sum_{k=First\ j}^{Last\ j} w_{j,k} \left(Y_{exp_{j,k}} - Y_{cal_{j,k}} \right)^2 \quad (19)$$

$$w_j = \frac{1}{|[d\alpha/dt]_{max}|_j + |[d\alpha/dt]_{min}|_j} \quad (20)$$

where RSS is a sum of squared residua, n is a number of measurements, j is an index of the given measurement, $First_j$ is an index of the first point of the given curve, $Last_j$ is an index of the last point of the given curve, $Y_{exp,\ j,k}$ is an experimental value of the point k of curve j, $Y_{cal\ j,k}$ is a calculated value of the point k of curve j, w_j is a weighting factor for curve j. The series of several measurements performed at different heating rates are the initial datasets, then the full-scale non-linear optimization by means of MKA proceeds and the search of the minimum of RSS by the variations of the kinetic parameters values for the individual reaction steps processes. The standard kinetic models and their mutual dependences (e.g. the parallel, consecutive, competing, reversible, independent etc. models) are usually examined and based on the best value of the correlation coefficient the suitable kinetic model can be determined. [99-103]

4.3 Mathematic deconvolution – Fraser-Suzuki function

Before the development of methodologies for employing the kinetic analysis equations into the complex non-linear optimization algorithms, the mathematic deconvolution was used to approximate the complex kinetics. In case of complex crystallization behavior (scenario where the crystallization peaks overlap), the beginning and the end of each single peak cannot be easily determined. The point is that the set of experimental data are separated to particular components. For this purpose, several mathematical functions exist and can be used, e.g. the Gauss [104], Lorentz [105], Weibull [106] and Fraser-Suzuki (FS) [107-110] functions. The last mentioned Fraser-Suzuki function has a great advantage consisting in it being thoroughly tested in the past – the tests confirmed that (contrary to all the other above-mentioned possibilities) the FS function can describe all kinetics readily occurring for the solid-state reactions. [107-110] The FS functions can be expressed via the Equation (21):

$$y = a_0 \cdot exp\left[-ln2\left[\frac{\ln\left(1+2a_3\cdot\frac{x-a_1}{a_2}\right)}{a_3}\right]^2\right] \qquad (21)$$

where a_0, a_1, a_2, a_3 are parameters of FS function corresponding to an amplitude, position, half-width and asymmetry of curve. The PC software PeakFit (Systat Software Inc.) is instrumental in the processing of experimental data by means of this deconvolution procedure. [107-110]

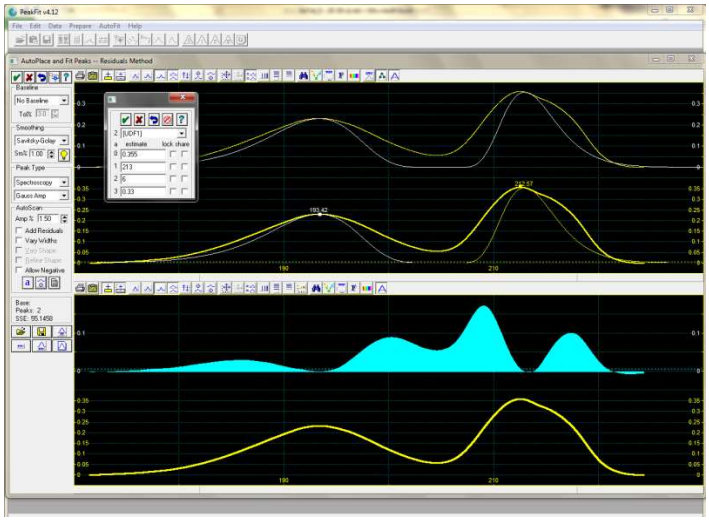

Figure 13: The illustration of deconvolution (FS) procedure with using the PC software program PeakFit 4.2.

The Fig. 13 illustrates the processing of experimental DSC crystallization data within the deconvolution procedure using the PC software program PeakFit 4.2 (Systat Software Inc.) and in the Fig. 14 the example of deconvoluted DSC curve as a result from deconvolution procedure can be seen.

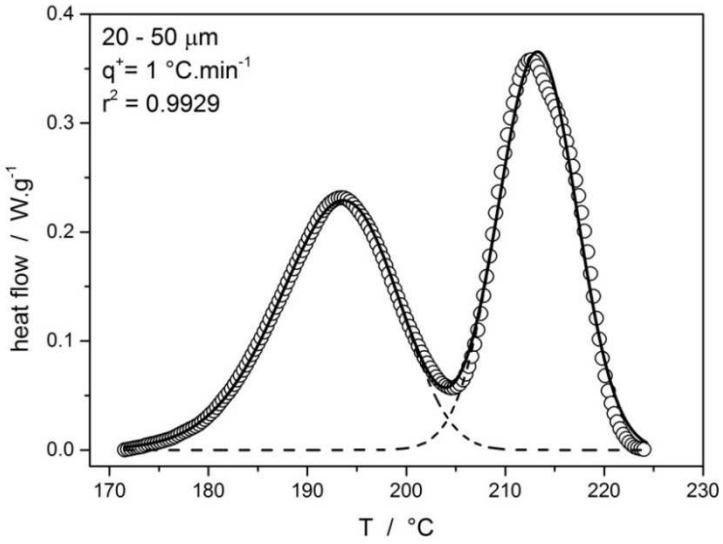

Figure 14: The example of experimental DSC curve after the deconvolution procedure; circles - the experimental data, solid line - the overall fit of the experimental signal, two dashed lines - the two deconvoluted crystallization mechanisms.

4.4 The structural relaxation kinetics

As was mentioned in Chapter 1.1.1, the glass transition is dependent on actual experimental conditions and therefore the glass transition processes are kinetically-controlled. The non-equilibrium glassy state tries to reach the equilibrium state and relaxes to the state of the undercooled liquid, which stands for the most achievable equilibrium state - the system is located in the so-called kinetic equilibrium (the high energy/kinetic barriers prevent the further decrease and transformation to the crystalline state) [6-13]. For the description of these relaxation processes several kinetic models are available. Nowadays, the most common kinetic model determined for this purpose is the Tool-Narayanaswamy-Moynihan (TNM) [11,111,112] model. This phenomenological kinetic model is characterized by four parameters: the apparent activation energy Δh^* of the structural relaxation, the non-linearity parameter x, the non-exponentiality parameter β and the preexponential factor A_{TNM}, which serve to interpret the main relaxation features, such as hysteresis, non-linearity and non-exponentiality. The TNM model can be expressed by following Equation (22) and the next acting parameter - the fictive temperature T_f stands for the temperature of undercooled liquid with the same structure as the relaxing glass achieves and the structure of relaxing glassy material can be characterized by means of this parameter:

$$\tau = A_{TNM}\left[\frac{x\cdot\Delta h^*}{RT} + \frac{(1-x)\cdot\Delta h^*}{RT_f}\right] \tag{22}$$

The parameter x representing the non-linearity of structural relaxation determines the intensity of structure and temperature influence on relaxation process. The distribution of relaxation times is formulated by means of the Equation (23) and with using this stretched exponential function F(t) the TNM model can be implemented.

$$F(t) = exp\left[-\left(\int_0^t \frac{dt}{\tau(T,T_f)}\right)^{\beta}\right] \tag{23}$$

where F(t) is the relaxation function of given property with β value being in the interval $0 < \beta \leq 1$. The non-exponentiality factor β represents the inverse proportionality to the width of distribution relaxation times. [11,111-113] The validity of this TNM model has been

extensively explored during years, see examples in Refs. [114-118], where the good eligibility of this model with regard to the description of structural relaxation processes was confirmed.

In regard to DSC data, the so-called reduced heat flow Φ^{red} (see Equation (24)) was proposed as a substitution of the relaxation function F(t) due to the requirement of the normalization of DSC data in the glass transition region, because the difference between the temperature dependences of heat capacity in the glassy and undercooled liquid regions occurs.

$$\Phi^{red} = \frac{\Phi(T) - \Phi_g(T)}{\Phi_l(T) - \Phi_g(T)} \tag{24}$$

where $\Phi(T)$ are the measured DSC data, $\Phi_g(T)$ and $\Phi_l(T)$ are the temperature dependences extrapolated from the glassy and undercooled liquid regions. [119]

Naturally, other kinetic models solving the structural relaxation kinetics are available, see for example Refs. [120-124]. The alternative to TNM model can be the model called KAHR introduced by Kovacs, Aklonis, Hutchinson and Ramos [120]. This KAHR model is also phenomenological with parameters, which are similar to parameters of TNM model. The next used model to description of relaxation kinetics is RSC model, which was investigated by Robertson, Simha and Curro [121] and this model is based on molecular theory of relaxation kinetics occurring in glassy materials.

5 SUMMARY OF PAPERS

As is well known, the chalcogenide materials have been studied during the past decades and have been found as valuable materials with broad utilization in many areas of technical, industrial, medical, environmental or scientific interests. The large capacity data-storage media (CDs, DVDs, BlueRay Discs or non-volatile PCRAMs), elements for infrared optics (fibers, lenses, etc.), optoelectronics, memory switches or various electronic thresholds can serve as the examples of the usage of these materials.

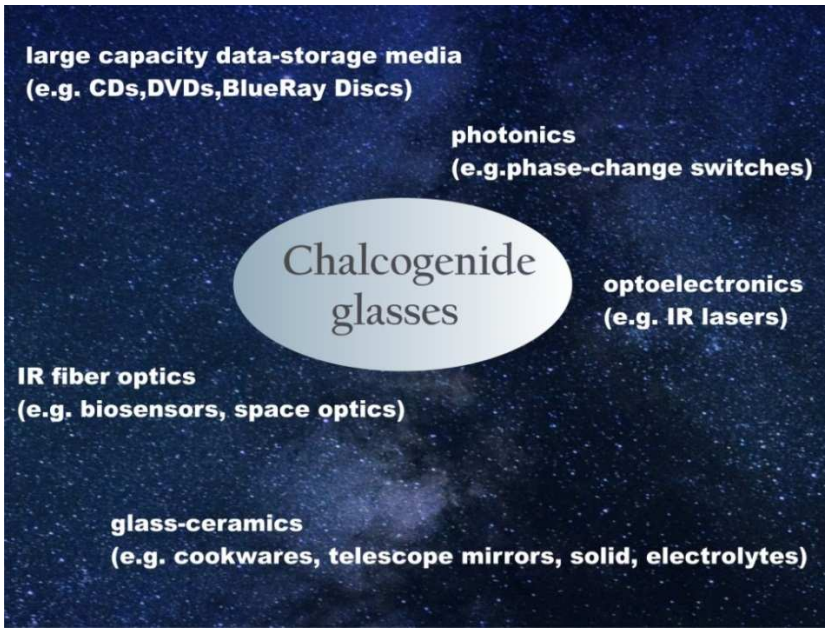

Figure 15: An illustration of broad utilization of chalcogenide glasses.

Nowadays, the special interest is focused on a development of optical chalcogenide materials operating in the far-infrared region of electromagnetic spectrum and the emphasis is put on their following applicability as devices designated for space optics, environmental and medical biosensors, etc. One family of materials, which comply these assumptions, is the tellurium-based chalcogenide glasses. [1-5,30-42]

This doctoral thesis primarily pursues the detailed systematic study and characterization of crystallization behavior of tellurium-based chalcogenide glassy systems with respect to the kinetic processes and their kinetic description by means of commonly used kinetic models, the structural arrangements occurring in studied systems, and the appraisal

of potential real-life applicability of these materials. Also the structural relaxation kinetics has to be described (rather as a side-note) due to the need of the completion of crystallization results for the next predictions of processability and stability of studied materials.

The crystallization process of tellurium-based glasses often shows a certain degree of complexity, which means that the individual crystallization peaks overlap, the beginning and the end of each single peak cannot be easily determined and the crystallization kinetic analysis cannot be properly performed. This issue is commonly solved by means of deconvolution procedure. It means that the set of experimental data are separated to particular components via the various methods of deconvolution. In this thesis, the two ways of deconvolution procedure were used, namely the kinetic deconvolution with usage of multivariate kinetic analysis (which belongs to the group of model-fitting methods) and the mathematic deconvolution, which is based on several mathematical functions, in case of this thesis, the Fraser-Suzuki function was used in particular with following kinetic analysis of individual crystallization processes.

The last area of interest of this doctoral thesis holds the potential practical usage of studied chalcogenide tellurium-based glassy systems. This issue is considered by means of glass stability criteria, which are the useful tools for this purpose. The typical commonly used glass-stability criteria (such as Hruby [23] criterion or the difference between the crystallization and glass transition temperatures) mostly provide a good information about material's glass-stability, but rather qualitative. [29-32] Regarding this limitation, the newly developed criteria for the evaluation of glass stability are suggested [33], described and tested. These new-developed criteria come out from the possibility of the combination of results provided by DSC and TMA; due to the missing information from DSC about glass-softening processes, viscous flow effects and so on. These methods, with which the presented thesis works, belong to the thermo-analytic methods, which are based on an indirect observation of e.g. crystallization processes by means of certain macroscopic property (heat flow and sample deformation in case of the presented thesis) [73-82]. The opportunity to combine the results from DSC and TMA offers a certain benefit with regard to the assessment of glass stability of glassy materials.

More on above-mentioned facts, main goals and conclusions of this doctoral thesis will be discussed in following chapter divided into three sections (basic thermal behavior of the investigated systems, theory and practice of complex crystallization kinetics, and glass stability). All studies presented in this thesis are published as the articles in impacted international journals.

5.1 PAPER DISCUSSION - Part I

The primary aim of the presented doctoral thesis is the characterization of crystallization behavior occurring in the tellurium-based chalcogenide glasses and the description of ongoing crystallization kinetic processes with respect to the determination of the thermal properties of the given studied systems. This is necessary for the characterization and usage of amorphous chalcogenides, the knowledge of ongoing processes allows the predictions of the behavior of examined glasses under any conditions, also their stability can be evaluated and the search of new promising hi - tech materials is facilitated.

As has been specified earlier, this thesis deals with the thermal, kinetic and structural characterization of tellurium-based chalcogenides glasses. It was mentioned in Chapter 2 that the Te-based glasses show a strong tendency towards crystallization. This problem may be solved e.g. by adding of various dopants into the tellurium matrix due to the stabilization of glassy system against devitrification [30-32, 34-42]. The dopants used for the following studies in case of Ge-Te glasses were selenium, gallium and iodine; these dopants were added into Ge-Te matrix in various amounts along the investigated compositional lines due to the effort to uncover the most suitable composition in regard to potential practical usage. The next studied system, the As_2Se_3-As_2Te_3 glass, belongs also to Te-based glasses and was explored with various representations of As_2Te_3 part along the investigated compositional line. Thus, the systematic detailed study of thermal behavior of $Ge_{20}Se_xTe_{80-x}$ (x = 2; 4; 6; 8 %), $Ge_{21}Se_xTe_{79-x}$ (x = 2; 4; 6; 8 %), $(GeTe_4)_x(GaTe_3)_{100-x}$ (x = 40; 50; 60; 67; 75; 86; 100 %), $Ge_{20}I_xTe_{80-x}$ (x = 2; 5; 8; 12; 15 %) and $(As_2Se_3)_{100-x}(As_2Te_3)_x$ (x = 0; 17; 34; 50; 67; 84; 100 %) chalcogenide systems was performed by means of DSC (primarily and for the kinetic analysis purposes), the experiments were carried out under non-isothermal conditions, which means that the monitored property (heat flow) was observed in dependence on temperature, and various sample forms (powders, bulks) were examined with regard to the predicative potential of the realized kinetic calculations.

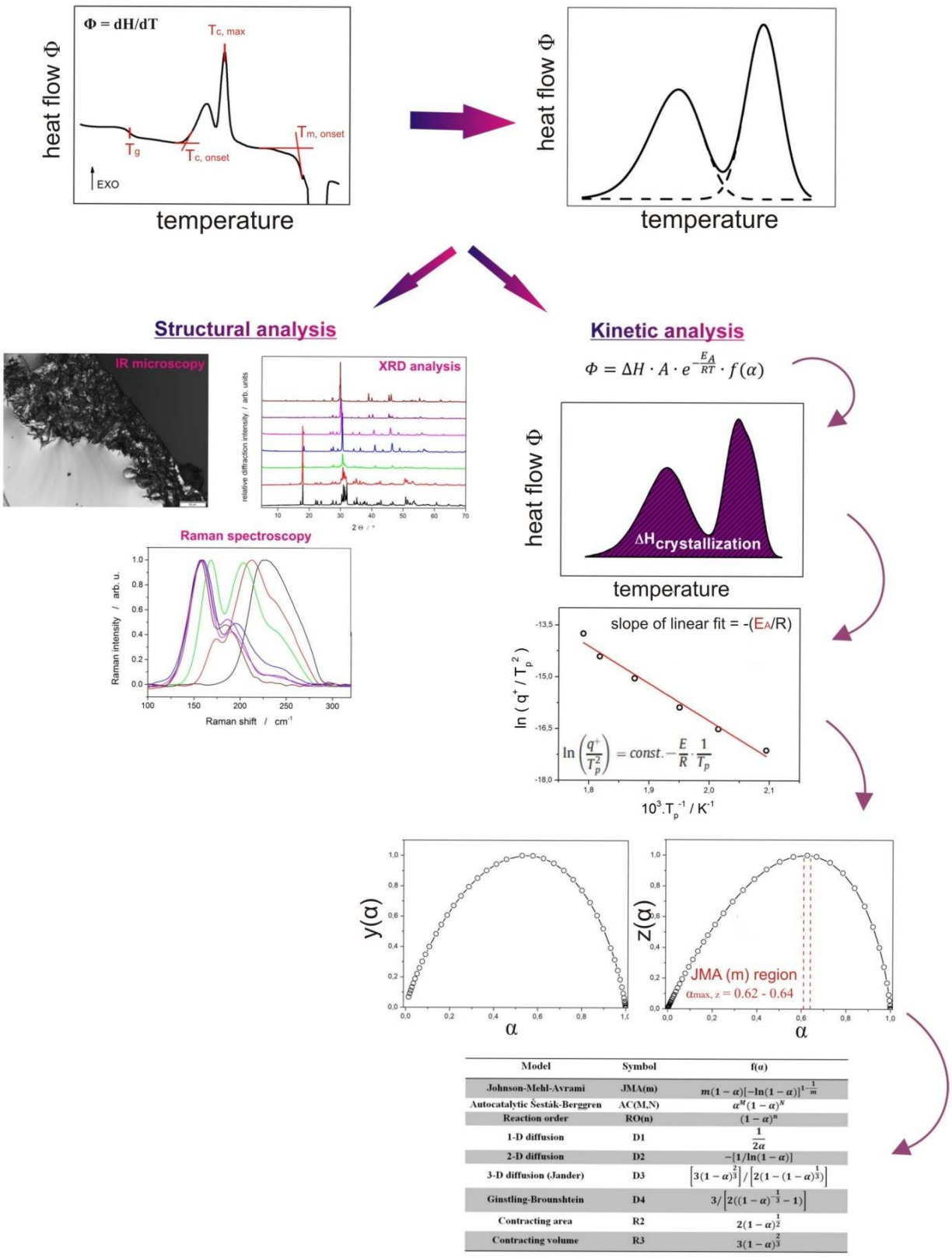

Model	Symbol	f(α)
Johnson-Mehl-Avrami	JMA(m)	$m(1-\alpha)[-\ln(1-\alpha)]^{1-\frac{1}{m}}$
Autocatalytic Šesták-Berggren	AC(M,N)	$\alpha^M(1-\alpha)^N$
Reaction order	RO(n)	$(1-\alpha)^n$
1-D diffusion	D1	$\frac{1}{2\alpha}$
2-D diffusion	D2	$-[1/\ln(1-\alpha)]$
3-D diffusion (Jander)	D3	$\left[3(1-\alpha)^{\frac{2}{3}}\right] / \left[2(1-(1-\alpha)^{\frac{1}{3}})\right]$
Ginstling-Brounshtein	D4	$3/\left[2((1-\alpha)^{-\frac{1}{3}}-1)\right]$
Contracting area	R2	$2(1-\alpha)^{\frac{1}{2}}$
Contracting volume	R3	$3(1-\alpha)^{\frac{2}{3}}$

Figure 16: The illustration of procedures used to characterization of thermokinetic behavior of investigated chalcogenide systems.

The characterization of thermal behavior of investigated glassy systems may be done with usage of the simple scheme illustrated in Fig. 16. Firstly, the raw DSC curves are needed to be investigated with respect to a presence or an absence of expected thermal effects (e.g. glass transition, crystallization, melting), the nature of crystallization effect (e.g. single-peak/multiple-peak behavior) and its behavior under various experimental conditions (e.g. sample form, applied heating rate). Thereafter, the structural analysis of obtained crystallization products needs to be done due to their structural characterization (e.g. XRD, IR microscopy, Raman spectroscopy) and this step can help to identify the ongoing processes in the studied materials. Afterwards, the kinetic analysis is carried out and the complete information about the given system is acquired with the combined knowledge about thermal, structural and kinetic properties.

5.1.1 Ge-Se-Te system

As the first researched material for this thesis objective the selenium-doped $GeTe_4$ glass was selected, the thermal behavior of which was investigated along two selected compositional lines, namely the $Ge_{20}Se_xTe_{80-x}$ (x = 2; 4; 6; 8 %) (**Paper I**) and $Ge_{21}Se_xTe_{79-x}$ (x = 2; 4; 6; 8 %) (**Paper II**) glassy compositions. The amount of added selenium had to be held under 10 at. % due to its influence on the final width of transmittance window. In addition, the glassy composition with 10 at. % of Se is probably near to the non-mixing zone and on that account its thermal stability decreases [32,35,37,42-45].

In Fig. 17, the obtained DSC curves representing the $Ge_{21}Se_xTe_{79-x}$ (x = 2; 4; 6; 8 %) compositions are displayed. As is apparent, the crystallization behavior of the studied systems is greatly influenced by the added amount of selenium into Ge-Te matrix, which is reflected in the separation of the primal surface tellurium precipitation from the subsequent volume-located GeTe and GeTe(Se) (phase contains all three elements) crystal growth (see the results from XRD analysis – Table 3). Also, the new phase (monoclinic $GeSe_2$) emerges under certain conditions, which are close to the equilibrium conditions (such as very low q^+, large bulk-to-surface ratio); and as was found, this new phase substitutes the rhombohedral GeTe. The evolution of the crystallization peaks with increasing amount of Se indicates that the selenium functions as an inhibitor of crystallization process shifting the crystallization to higher temperatures (in comparison with the pure $Ge_{21}Te_{79}$).

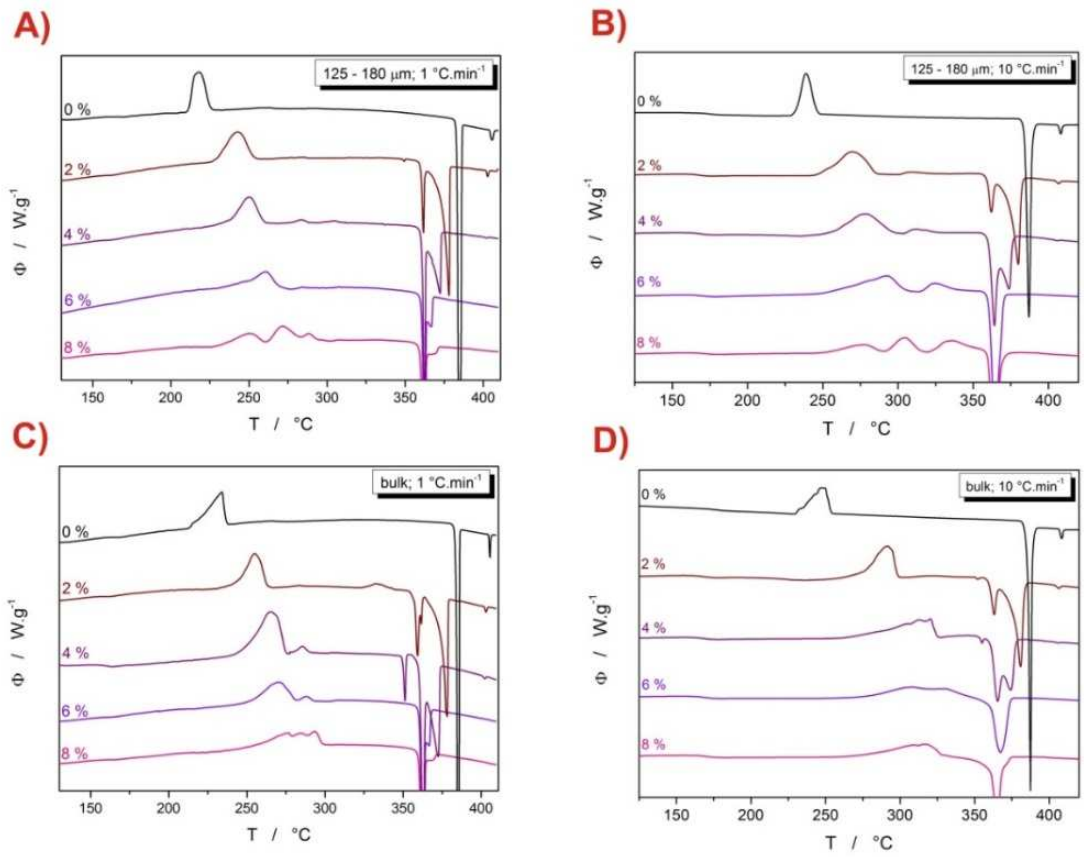

Figure 17: Example DSC curves obtained for applied heating rates 1 and 10 °C.min^{-1} and the 125-180 μm powders (graphs A and B) and bulk samples (graphs C and D) of the studied $Ge_{21}Se_xTe_{79-x}$ glasses. Each curve is marked according to the Se at. % content. Exothermic effects evolve in the "upwards" direction.

It can be concluded, that the occurrence of selenium leads to inhibition of both crystallization mechanisms (Te surface precipitation and volume-located GeTe crystallization). Selenium integrates into GeTe network and, as well, into Te-chains; that can be the reason for the obvious separation of crystallization peaks with increasing amount of selenium in Ge-Te matrix. As can be seen in Fig. 28B, where the dependence of crystallization onset on composition is displayed (the blue-labeled points correspond to Se-doped glass), the rising Se content does not influence the position of the initial surface Te precipitation (it means within the compositional line of the Se-doped glasses; the thermal properties of pure $GeTe_4$ glass are greatly improved by the addition of selenium into the matrix). However, the crystallization of GeTe is extensively influenced. This phenomenom can be caused by the arising restraint (undertaken by presence of Se) of GeTe units interconnections (Se incorporates directly into GeTe network).

The characterization of crystallization behavior can be realized by means of kinetic analysis including the determination of each of all parameters occurring in the universal kinetic DSC equation (7); this means the evaluation of apparent activation energy E_A, crystallization enthalpy ΔH and lastly the most suitable kinetic model $f(\alpha)$, which can be used for the description of crystallization behavior of the studied material. The methods how to obtain these parameters have been defined in Chapter 4. With using the Kissinger method [87] the apparent activation energy of crystallization was determined and the obtained E_A values can be found in Fig. 27A. As can be seen, the significant decrease in the E_A values representing the compositions with added selenium in comparison with pure $Ge_{21}Te_{79}$ system is observable. This change in E_A is caused by the first addition of selenium into pure GeTe matrix, which is accompanied by the change of the main crystal growth mechanism. While in case of $GeTe_4$ glass, only the surface crystallization was found (see **Paper III**) and the accelerating influence of mechanically induced defects on the primary crystallization process was confirmed, the Se-doped glass shows the two types of crystallization mechanisms, namely the surface Te precipitation and some volume-located crystals form (see Fig. 18); the addition of Se leads to a change in crystallization mechanism. These findings are also in good correspondence with the study focused on the influence of the Se ↔ Te substitution on crystallization mechanisms (**Paper VI**), where it was also shown, that the smaller number of large crystallites occurs with the addition of Se into $GeTe_4$ matrix. These crystallites exhibit a three-dimensional growth.

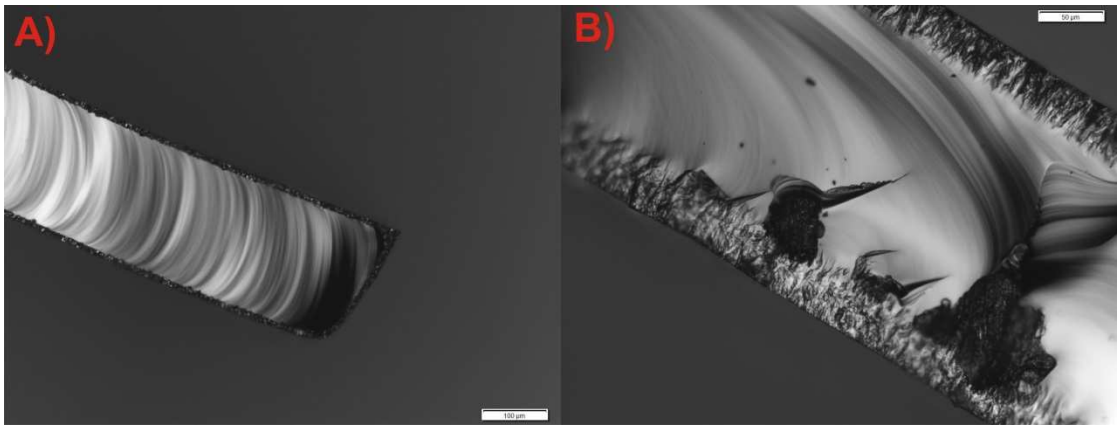

Figure 18: Selected infrared micrographs corresponding to the cross-section views of the partially DSC-crystallized pure $GeTe_4$ (A) and $Ge_{20}Se_2Te_{78}$ (B) materials.

The occurrence of two types of crystallization mechanisms was confirmed also by a huge IR microscopy study (**Paper XVI**), which was also used, for the first time, to directly confirm the crystallization originating from the mechanically induced defects. The partially-crystallized (in DSC) samples were prepared; the selected grains were carefully cracked and observed by IR microscope. Each piece of tested grains contained a large number of small crystallites, the presence of which confirmed the predicated defects-based crystallization. Also a large number of fragments were on their surfaces covered by a crystalline layer.

It was found that the fine alteration in amount of Ge in Ge-Te matrix ($Ge_{20}Te_{80}$ – **Paper I** vs. $Ge_{21}Te_{79}$ – **Paper II**) has not been critical, has not had any marked influence on thermal behavior and the results have been mostly similar, thus allowing making the same conclusions and the crucial influence on thermal behavior of the Se-doped glasses has been caused by the added amount of selenium.

The study dealing with the influence of particle size on crystallization processes of chosen $Ge_{20}Se_4Te_{76}$ glassy composition and the combined dilatometric and calorimetric study of kinetic processes occurring in this $Ge_{20}Se_4Te_{76}$ bulk glass can be found in **Paper IV** and **Paper V**. The question, why just this certain composition, will be answered later in Chapter 5.3. In **Paper IV** the full-scale kinetic analysis of prepared $Ge_{20}Se_4Te_{76}$ glass in dependence on particle size was performed in order to reveal the degree of reliance on experimental conditions (sample form, applied heating rate). Eight following particle size fractions: 0 – 20; 20 – 50; 50 – 125; 125 – 180; 180 – 250; 250 – 300; 300 – 500 μm and bulk sample with assigned averaged particle size equal to 1 mm, and ten following applied heating rates (0,5; 1; 2; 3; 5; 7; 10; 15; 20; 30 °C.min^{-1}) were tested. This approach was chosen due to the promising usability in potential real-life applications (such as far-IR optics) and consequently due to the need for the detailed knowledge of the ongoing process in the given material. The $Ge_{20}Se_4Te_{76}$ glass crystallization behavior was found largely dependent on experimental conditions, which is crucial for the next processing of glassy material, when the individual processing steps must be critically controlled to avoid the undesirable crystallization. The two well resolved crystallization peaks occurred for fine powders, with increasing particle size these peaks started to overlap and exhibited an apparent JMA kinetics (see Fig. 19C). The Fig. 19A depicts the deconvoluted complex crystallization peak obtained for fine powder fraction and high applied heating rate. The two differentiated crystallization peaks are signed by the two dashed lines, the circles correspond to experimental DSC data and solid line denotes the overall fit. The deconvolution procedure was performed by means of Fraser-Suzuki (FS) function (Eq. 21). The significantly higher activation energies observed

for the finest powders could be explained on the basis of the influence of mechanically induced defects on crystallization behavior. The existence of a larger energy barrier that needs to be overcome in order for the sample to crystallize is probable.

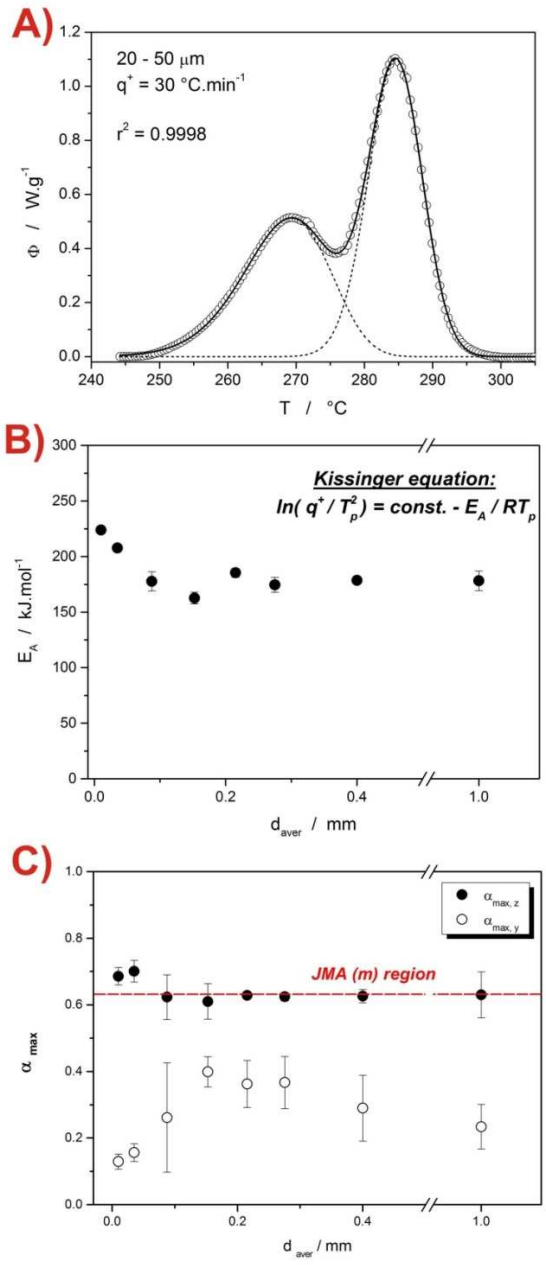

Figure 19: A) Example of deconvoluted complex crystallization peak for the powder fraction with particle size 20–50 μm of the $Ge_{20}Se_4Te_{76}$ glass;

B) The particle-size dependence of E_A values determined by the Kissinger method;

C) The dependence of the maxima of characteristic functions y(α), z(α) on the averaged particle size.

As the values of activation energy decrease with coarser fractions, the two kinetic peaks converge and cannot be distinguished from one another. Hence, the reliable deconvolution could not be performed for the coarser powder fractions. In Table 3, the estimated values of kinetic parameters for both deconvoluted crystallization peaks representing the finest powder fractions are summarized. The kinetic analysis of deconvoluted DSC data provided the similar trends in values of kinetic parameters for both fractions, which points to the uniformity of crystallization mechanisms.

Table 3: Summary of average values of parameters for both peaks of the deconvoluted fractions with particle size 0 - 20 μm and 20 - 50 μm.

particle size / parameters	0–20 μm		20–50 μm	
	1st peak	2nd peak	1st peak	2nd peak
ΔH, J.g^{-1}	18.2 ± 1.1	20.3 ± 2.2	21.5 ± 4.5	17.2 ± 3.7
E_A, kJ.mol^{-1}	235 ± 0.8	223.8 ± 1.7	202.5 ± 1.1	206.4 ± 0.43
$\alpha_{max,\ z}$	0.570 ± 0.037	0.461 ± 0.061	0.529 ± 0.083	0.480 ± 0.056
$\alpha_{max,\ y}$	0.267 ± 0.044	0.355 ± 0.054	0.282 ± 0.071	0.373 ± 0.056
M	0.41 ± 0.06	0.56 ± 0.08	0.43 ± 0.06	0.59 ± 0.08
N	1.14 ± 0.14	1.04 ± 0.2	1.17 ± 0.35	1 ± 0.17

However, it was also found, if the large as-prepared samples with minimum mechanical defects will be used and the applied heating rate will be 10 °C.min^{-1} (corresponding to the standard heating rate for most instruments and their calibration), the kinetic processes will be unified and the change with experimental conditions has a descending character.

The combination of dilatometric and calorimetric approaches used for the study of kinetic processes in $Ge_{20}Se_4Te_{76}$ glass is shown in **Paper V**. The crystallization behavior was examined by means of DSC and TMA. The combination of these two techniques offers an interesting sight into ongoing processes in materials in further detail, because the DSC experiments do not give the appropriate information about processes connected with softening of glassy material and viscous flow effects, which play an important role in the overall crystallization process. Also these processes largely influence the stability of glassy materials

and their potential usage (more in Chapter 5.3). Due to these motives, the correlation between these two techniques was searched for and a good agreement was found. Therefore, the crystallization kinetics was described by usage of DSC and also by usage of TMA data, whereas regarding the TMA data the T_p value (corresponding to the maxima of crystallization DSC peak) was replaced by the T_{ic}. The initial crystallization temperature T_{ic} obtained from the crystallization TMA measurements corresponds to an intersection of extrapolations from the inflexion point and final stabilized sample height. As was shown in Refs. [125-127], the dependence of T_{ic} on temperature follows on the Arrhenian kinetic assumptions, thus this parameter can be used for the kinetic analysis of crystallization. The evaluated apparent activation energies of $Ge_{20}Se_4Te_{76}$ crystallization obtained from the DSC and TMA data were very close, which was fairly startling due to the fact, that the E_A values provided by TMA used to be higher than the E_A values provided by DSC, because the DSC measurements give values corresponding to the overall crystallization process, while the E_A values determined by means of TMA usually correspond to the initial state of crystallization process. This fact can be explained on the basis of significantly higher amount of crystallites, which is needed for the formation of firm crystalline network and consequently for stopping the strong viscous flow in the $Ge_{20}Se_4Te_{76}$ glass.

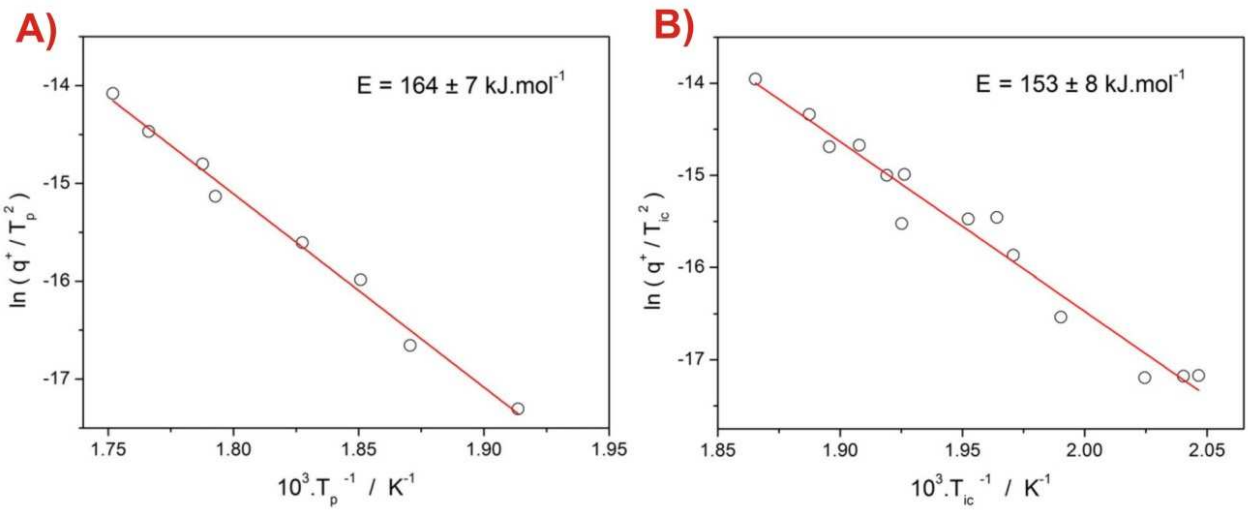

Figure 20: Kissinger plots constructed for the set of crystallization DSC (A) and TMA (B) measurements performed for the $Ge_{20}Te_{76}Se_4$ bulk glass.

To conclude the problematics of crystallization kinetic behavior of studied Se-doped GeTe glass, it must be noted that this material follows the JMA/AC kinetics. The characteristic z(α) and y(α) functions were utilized in order to determine the appropriate

kinetic model f(α). The appropriate kinetic model can then be chosen upon the value of degree of conversion α corresponding to the maximum of this function. Normally, the crystallization processes occurring in chalcogenide materials used to be described by means of JMA (m) and AC(M,N) models.

As can be seen in Fig. 21A, the basic requirement of JMA (m) model ($\alpha_{max,\ z}$ equals to 0.62 – 0.64; this value is indicated by red dashed line in Fig. 21A) is fulfilled for most measurements performed at different heating rates and the most of kinetic data could be described by JMA (m) model, except the borderline experimental conditions (the lowest and the highest applied heating rates). In this case, the more flexible AC(M,N) model was used for description of the crystallization kinetics.

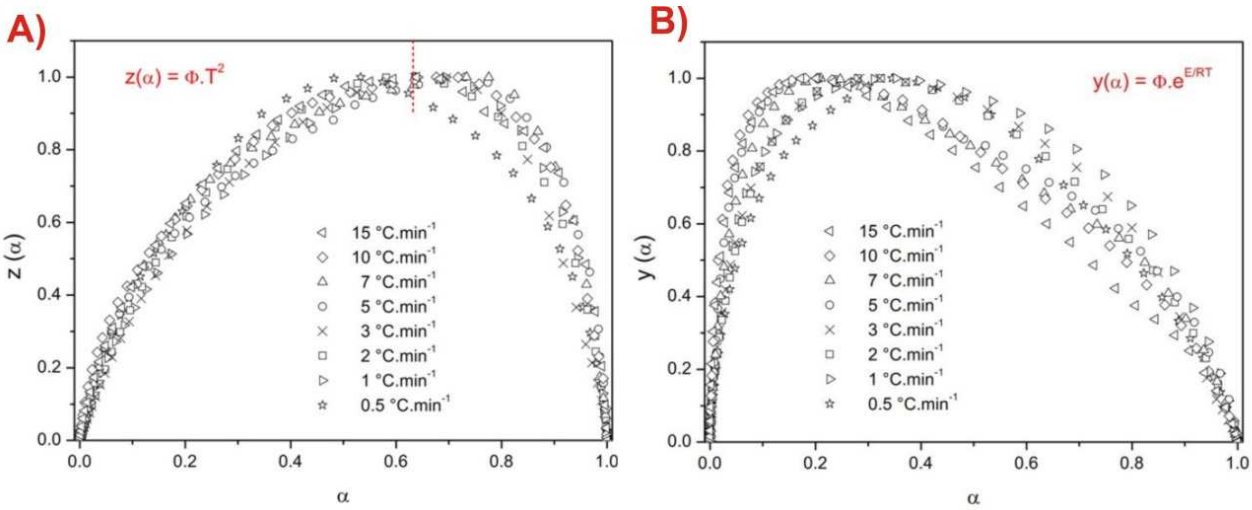

Figure 21: An illustration of set of characteristic functions z(α) (A) and y(α) (B) calculated for the set of crystallization DSC measurements performed for $Ge_{21}Se_4Te_{75}$.

The values of maxima of y(α) function (see Fig. 21B) serve for the determination of the parameters (m, M, N) of the previously found kinetic models (based on Equations 14, 16 and 17). The parameter m reflects the information about the dimensionality of formed crystallites. It was determined (based on the Eq. 14) that the crystallites formed as a 3-dimensional crystals under the lower heating rates, while as the applied heating rate increased, the crystal dimensionality decreased (to ~ 2) and the planar/surface crystals were formed. The change of crystal growth dimensionality occurs with increasing heating rate. Lastly, the value of preexponential factor A was determined ($A \sim 1.1 \cdot 10^{15}$) and the crystallization peaks could be described by the most suitable kinetic model.

5.1.2 Ge-Ga-Te system

The other promising materials for far-infrared optics applications can be the Ga-doped $GeTe_4$ glasses. As was mentioned above, the great advantage of choice of gallium as a dopant lies in the fact, that the presence of gallium in fully telluride matrix does not influence so much the width of transmittance window (can reach up to 28 μm [30]), therefore the Ga-doped $GeTe_4$ systems can introduce the good compromise between the thermal stability and optical properties of resulting glass. The understanding to the thermal and crystallization processes ongoing in various e.g. chalcogenides can be crucial not only for the processing of glassy material for the optical application purposes (such as fiber-drawing, molding), but the other possibilities how to utilize these materials exist. One of the feasible ways represents the glass-ceramics application area. The preparation of glass-ceramics with improved mechanical properties (determined by the crystalline phase fraction and its quality) requires the precise knowledge of thermal behavior of the given involved material, for example the Ga-doped glass. [30,37,43,45,49-51] This doctoral thesis includes several studies (**Papers VII – X**) focused on a detailed characterization of thermal, structural and kinetic behavior of $(GeTe_4)_x(GaTe_3)_{100-x}$ (x = 40; 50; 60; 67; 75; 86; 100 %) chalcogenide systems due to the limited knowledge about the thermo-kinetic and structural properties of this system.

Paper VII works with the crystallization behavior of $(GeTe_4)_x(GaTe_3)_{100-x}$ (x = 40; 50; 60; 67; 75; 86; 100 %) glasses in dependence on particle size in order to reveal the processes connected with a function of gallium as a stabilizing factor of $GeTe_4$ glass against undesirable devitrification and also to account of different ways how to obtain the Ga-doped glass with the best possible properties. In Fig. 22A, the DSC curves obtained for $(GeTe_4)_x(GaTe_3)_{100-x}$ (x = 40; 50; 60; 67; 75; 86; 100 %) systems for chosen experimental conditions are displayed. The impact of the Ga addition is obvious, the uniform single peak representing the pure $GeTe_4$ splits into two crystallization sub-peaks, which can be best noticed for the powder fractions. The important observable fact is that the crystallization onset remains invariable, whereas the second crystallization peak shifts to higher temperatures as the $GaTe_3$ content increases. The relative invariability of crystallization onset with composition can be explained as the fact that low amounts of gallium is needed to the saturation of centers intended for Te precipitation. So, it can be stated that gallium functions not only as a stabilizing factor of GeTe network, but also influences the precipitation of tellurium by preferentially occupying the crystallization centers primarily intended for the tellurium precipitation. It is worthy of notice, that the evolution of the shape

of melting peaks (see Fig. 22A) points out to the existence of eutectic (at ca. 357 °C); the exact eutectic composition appears to be close to $(GeTe_4)_{67}(GaTe_3)_{33}$.

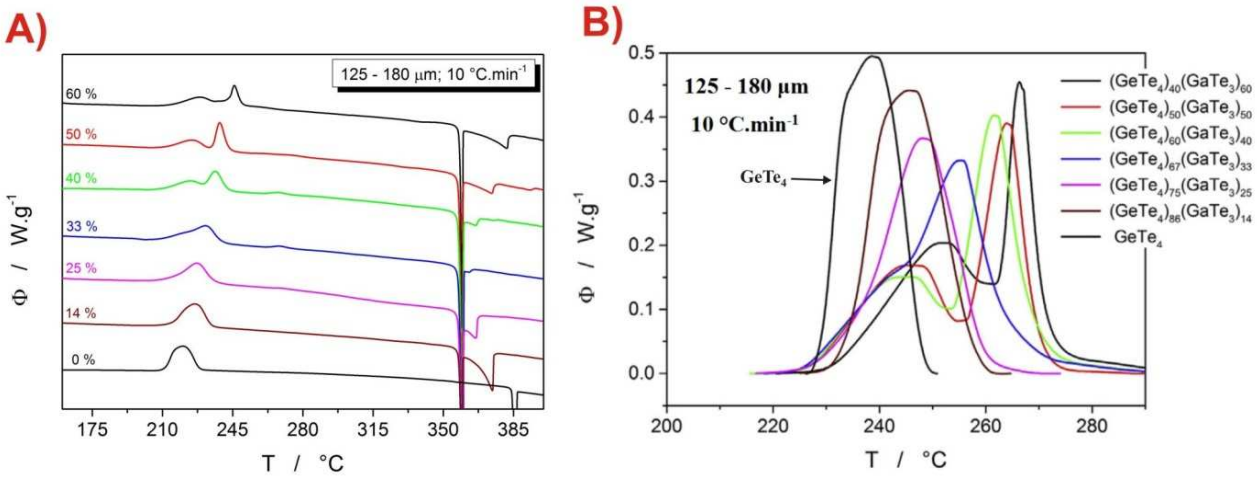

Figure 22: A) Example DSC curves obtained for applied heating rate 10°C.min^{-1} and the 125-180 µm powders of the studied $(GeTe_4)_x(GaTe_3)_{100-x}$ glasses. Each curve is marked according to the $GaTe_3$ at. % content. Exothermic effects evolve in the "upwards" direction.

B) Zoomed crystallization effects obtained for 125 - 180 µm powders heated at 10 °C.min^{-1}.

The akin crystalline phases as for Ge-Se-Te system (**Papers I, II, IV, V, VI**) were identified (hexagonal tellurium and rhombohedral GeTe – see Table 4) with using XRD analysis, which indicates that the similar crystallization mechanisms are involved in Ge-Ga-Te system as well as in Ge-Se-Te system. The XRD analysis of $(GeTe_4)_x(GaTe_3)_{100-x}$ crystallization products, besides the hexagonal tellurium and rhombohedral GeTe, offered the other crystalline phases, which were identified under certain experimental conditions. For example, at high applied heating rates some non-equilibrium crystalline phases arose for the 40/60 composition (tetragonal Ga_2Te_5), which are kinetically preferred and thus stabilized. Also the hexagonal Ga_2Te_5 phase form was found, however its strongest diffraction lines overlapped with those corresponding to Te. The presence of hexagonal Ga_2Te_5 has manifested itself as some weaker diffraction lines.

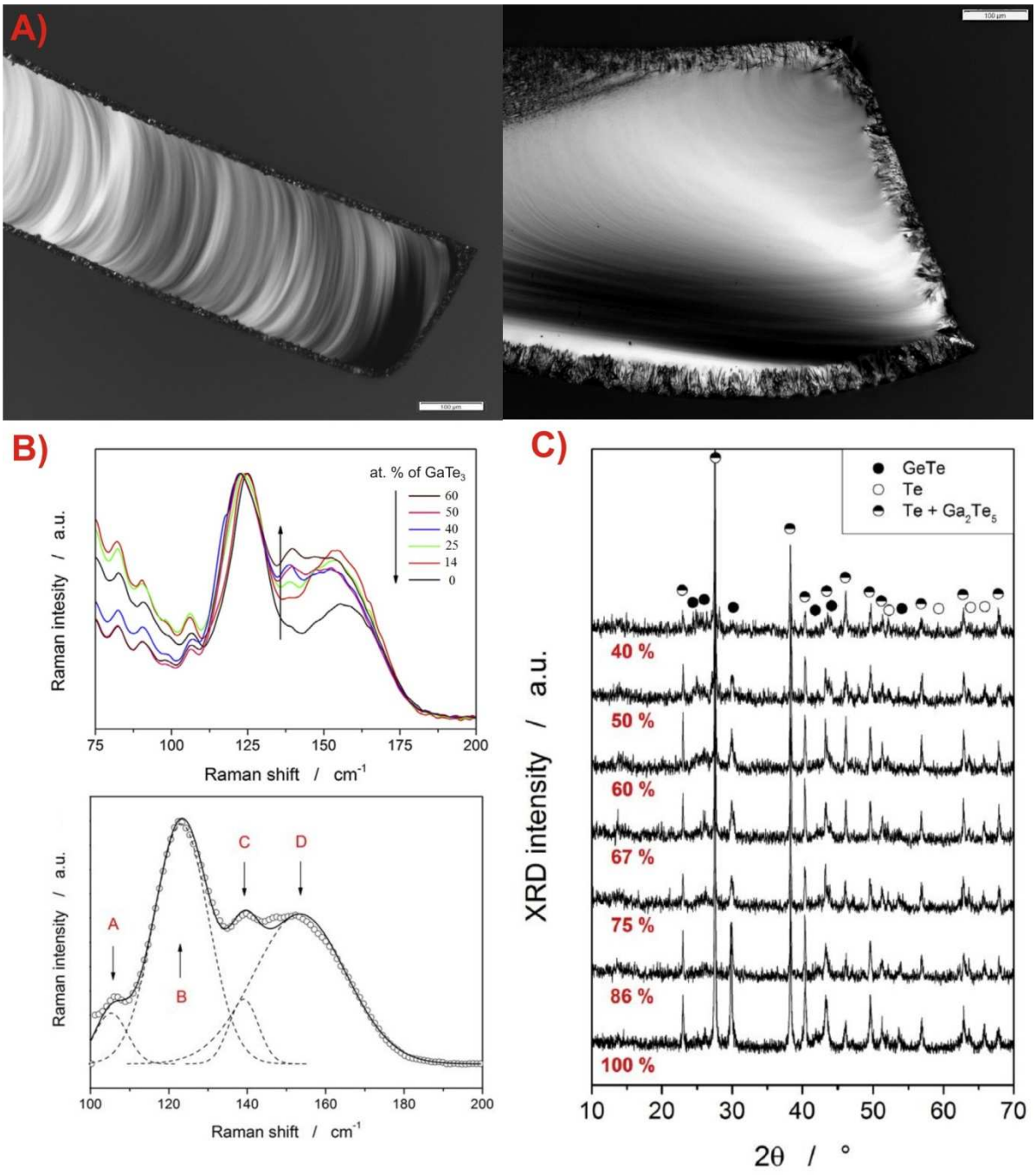

Figure 23: A) Infrared micrographs corresponding to the cross-section views of the partially DSC-crystallized pure $GeTe_4$ (the left-side micrograph) and $(GeTe_4)_{60}(GaTe_3)_{40}$ (the right-side micrograph) materials.

B) Raman spectra obtained for all investigated $(GeTe_4)_x(GaTe_3)_{100-x}$ glassy compositions (top) and Raman spectrum of chosen middle-positioned $(GeTe_4)_{50}(GaTe_3)_{50}$ glassy composition (below); dashed lines corresponding to the deconvoluted Gauss profile peaks, solid line corresponding to the overall fit, the circles corresponding to the experimental DSC data.

C) XRD records of crystallized $(GeTe_4)_x(GaTe_3)_{100-x}$ materials.

The first and very important difference in the crystallization mechanism and role of gallium (as dopant) in $GeTe_4$ matrix compared to Se-doped glasses emerges from the findings based on XRD analysis to which the partially-crystallized (heated to the maximum of the first peak) selected compositions (rich in gallium) were subjected. The presence of Ga_2Te_5 phase was confirmed already during this first crystallization peak (besides the Te phase), and this is completely different behavior in contrary to previously mentioned Ge-Se-Te (**Papers I**, **II**, **IV**, **V**, **VI**) and afterwards discussed Ge-I-Te (**Papers XI**, **XII**) systems, where the crystal growth of the GeSeTe and GeI phases is centered in the second crystallization mechanism, while in the partially-crystallized products (heated to the maximum of the first peak) only the hexagonal tellurium was present. This phenomenon can be explained on the basis of the previous structural study [50], that Ga atoms do not incorporate into the GeTe network and bond only to tellurium; as the Te precipitation begins, the Ga_2Te_5 phase forms too. These conclusions can be supported also by the results from IR microscopy (see Fig. 23A), where lower number of nuclei (for the higher amounts of Ga) can be seen in contrary to the pure surface growth.

The Raman spectroscopy provided the information about structural arrangements in $(GeTe_4)_x(GaTe_3)_{100-x}$ systems. The impact of gallium on structural arrangements in Ge-Ga-Te system could not be assigned so simply. The illustrated Raman spectra in Fig. 23B denote that the present Ga content in $GeTe_4$ matrix induces the partial segregation of tellurium, which manifests as a larger signal corresponding to the Te chains (label C: 140 cm^{-1}). The presence of Ga content in $GeTe_4$ matrix probably leads to some strengthening of the $GeTe_4$ network, which manifests as a higher signal of the edge-shared tetrahedra (label D: 154 cm^{-1}). The most pronounced peak (label B: 125 cm^{-1}) was found to be representing the symmetric stretching mode of corner-sharing Te-rich $GeTe_4 - {}_nGe_n$ (n = 0, 1, 2) tetrahedra and the subtle peak (label A: 106 cm^{-1}) was found to be corresponding to the corner-sharing GeTe4 (n = 0) tetrahedral. [132-138]

Papers VII – X also deal with the description of crystallization kinetics of $(GeTe_4)_x(GaTe_3)_{100-x}$ (x = 40; 50; 60; 67; 75; 86; 100 %) system. The multivariate kinetics analysis (MKA) was applied on DSC data to do the complete enumeration of the universal kinetic DSC equation (Eq. 7) for each dataset in order to describe the complex crystallization processes. The MKA optimization offers a testing of the standard available 21 models and their possible mutual dependences (e.g. parallel, competing, consecutive, reversible, etc. reactions) and on this basis the combination of two independent crystallization sub-processes were found (based on the best correlation coefficient) to be following the JMA (m) and

AC(M,N) kinetics. The JMA (m) model describes well the first (low-temperature) crystallization process, the AC(M,N) describes the second (high-temperature) crystallization process. The first process corresponds to the Te-precipitation and formation of hexagonal Ga_2Te_5 phase; the following second process represents the formation of rhombohedral GeTe and remaining Ga_2Te_5 phase. Naturally, the MKA method provides values of all of involved kinetic parameters; for example see Figs. 24B and 27A. The E_A values correspond to the three chosen particle size and each of all studied compositions. The crystallization process was found to be complex (see Fig. 24A). As is apparent, the E_A values representing the second crystallization sub-process are lower. This finding can be interesting for the following applications, such as glass-ceramics in regard to possible better checking of crystal growth. If the difference between E_A values of both sub-processes is larger, the system can be better controlled via application of different heating rates. This offers an advantage through enlarged portfolio of controlled crystal growth options in e.g. glass-ceramics applications. The Fig. 24C provides the compositional and particle size dependences of kinetic parameters obtained from MKA. The uniformity of most trends is obvious, which can ensure the reliable predictions of crystal growth for e.g. glass-ceramics applications.

In Fig 27A, the estimated E_A values for bulk samples can be seen (the chosen E_A values corresponding to the dominant crystallization process). The relative consistent trend is observable, which plays an important role in e.g. glass-ceramics or infrared optics application areas, where the crystal growth needs to be controlled. The studies of crystallization kinetics of these systems in dependence on particle size were performed due to the confirmation of the influence of mechanically induced defects on crystallization behavior. It was found in **Papers VII**, **IX** and **X** that the presence of mechanically induced defects amplifies the initial precipitation of Te and the first formation of Ga_2Te_5 phase (the magnitude of the first crystallization peak increases) with increasing $GaTe_3$ content and decreasing particle size. The study included in **Paper IX**, focused on the effect of powder coarseness on crystallization kinetics of $Ge_{11}Ga_{11}Te_{78}$ glass (middle-positioned composition inside the studied pseudo-binary line), briefly supports these findings. The values of apparent activation energy were found to have a descending character with particle size for both sub-processes, which also points out on the growth from mechanically induced defects.

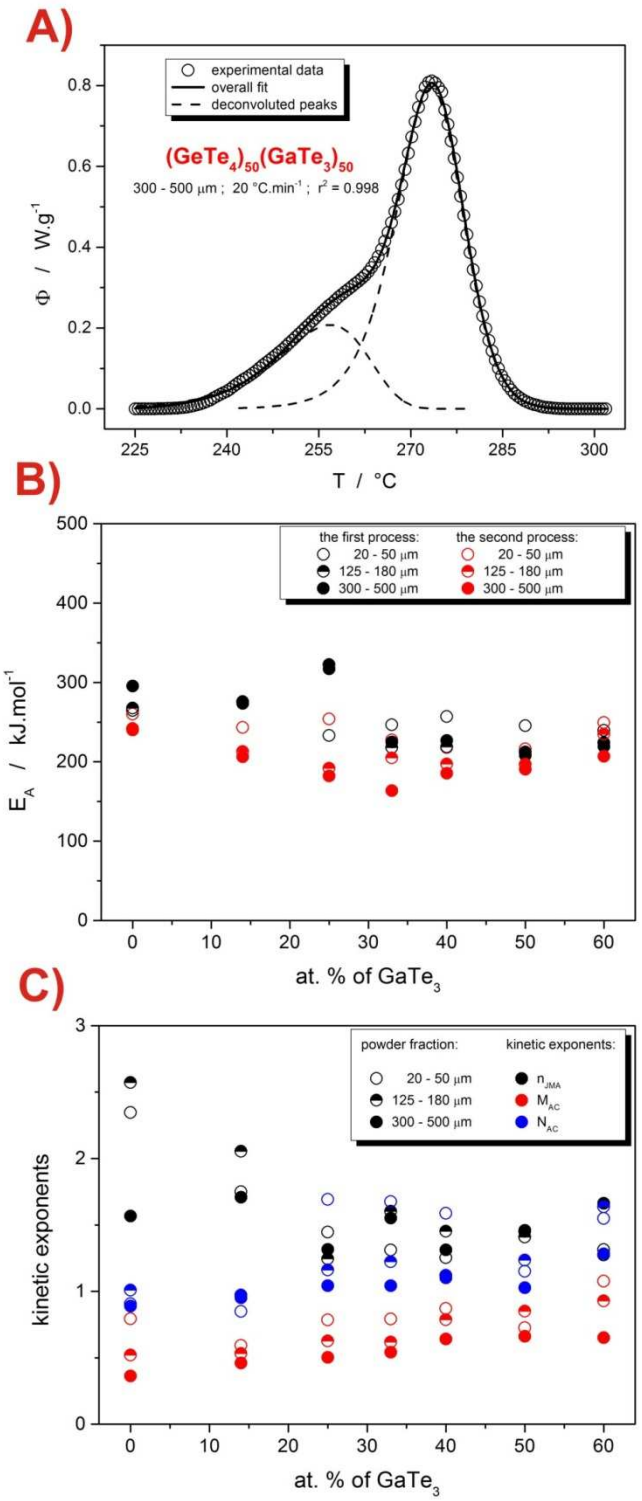

Figure 24: A) Example of deconvoluted DSC curve (corresponding to $(GeTe_4)_{50}(GaTe_3)_{50}$) by means of MKA.

B) Compositional and particle size dependence of E_A obtained from MKA for both deconvoluted crystallization processes.

C) Compositional and particle size dependence of kinetic parameters of JMA (m) and AC(M,N) models obtained from MKA.

The $Ge_{11}Ga_{11}Te_{78}$ glass was also subjected to the combined thermal analysis (**Paper X**), which was performed by means of DSC and TMA as for the case of Se-doped glasses, the same presumptions were approved. The results from MKA analysis were in a perfect agreement with those from TMA, only the relatively large errors associated with the evaluations of e.g. E_A from TMA measurements can be observed. This effect is probably caused by the worse reproducibility of determination of initial crystallization temperature, however the similar trend occurs. The results from thermal, structural and kinetic study of this glassy composition correlate very well with those quoted above.

5.1.3 Ge-I-Te system

The doping of $GeTe_4$ glass by iodine introduces the third (and last option presented in this doctoral thesis) possible way how to stabilize the fully telluride matrix against crystallization and improve the thermal properties of this glassy material with respect to the potential applicability in area of any practical usage. The function of iodine as stabilizing factor lies firstly in its terminating role in the three-dimensional GeTe network, and secondly, the iodine atoms are capable to trap the electrons from tellurium. [45,49,52-56]

In the following section of this thesis, the results originating from the detailed study dealing with the thermal and structural characterization of the $Ge_{20}I_xTe_{80-x}$ (x = 2; 5; 8; 12; 15 %) system, included in **Papers XI** and **XII**, will be introduced. **Paper XI** works with the study of whole investigated compositional line of $Ge_{20}I_xTe_{80-x}$ (x = 2; 5; 8; 12; 15 %) system with emphasis put on the comparison of the crystallization behavior and its kinetic description among the selected compositions with regard to predicative potential and quantification of the effect of mechanical induced defects on the crystallization (and also relaxation) behavior. **Paper XII** deals with one selected composition, namely the $Ge_{20}I_5Te_{75}$ glass, where the influence of experimental conditions (wide range of applied heating rates, particle size fractions) was extensively tested in order to kinetically and structurally describe the crystallization (and relaxation) behavior in detail.

The selected DSC curves (heating rate of 10 °C.min^{-1}; powdered samples with particle size 125 - 180 μm) are for the $Ge_{20}I_xTe_{80-x}$ (x = 2; 5; 8; 12; 15 %) system shown in Fig. 25A. The position of T_g changes minimally as the iodine content increases and this applies also for Se- and Ga-doped $GeTe_4$ systems (see Fig. 28A).

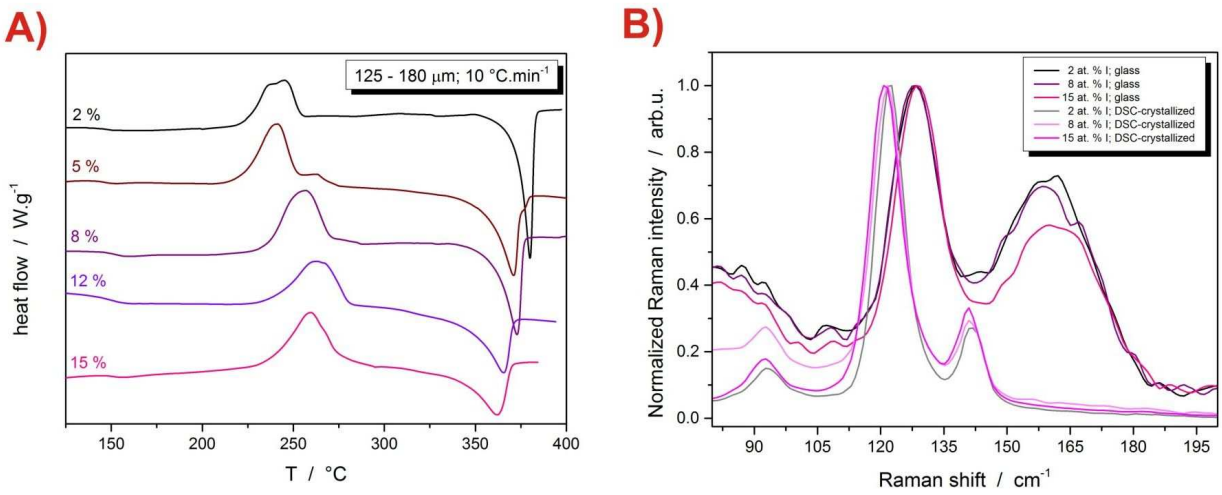

Figure 25: A) Example DSC curves obtained for applied heating rate 10°C.min^{-1} and the 125-180 μm powders of the studied $Ge_{20}I_xTe_{80-x}$ glasses. Each curve is marked according to the I at. % content. Exothermic effects evolve in the "upwards" direction.

B) Raman spectra of the selected glassy and DSC-crystallized $Ge_{20}Te_{80-x}I_x$ materials.

On the other hand, the behavior of crystallization peaks is more diverse. The crystallization process shows a certain degree of complexity (as for the Se- and Ga-doped systems), the occurring crystallization mechanisms overlap or compete against each other. From the overall shift of melting peaks with iodine content it can be inferred that the iodine incorporates into Ge-Te-I crystalline matrix at least to some degree, and as an impurity. The structural information achieved by means of XRD analysis revealed (see Table 4) that the hexagonal tellurium, rhombohedral GeTe and minor amounts of cubic GeI_4 form during the crystallization process in case of all investigated compositions. The Raman spectroscopy analysis (Fig. 25B) was applied on freshly fractured bulk glasses and DSC-crystallized powders and structural units occurring in investigated system were identified (see Table 5). The impact of increasing amount of iodine in glassy matrix manifested probably in decreasing trend of intensity of vibrations of edge-sharing $GeTe_4$ (or Ge-rich) tetrahedra or vibrations of short, amorphous, distorted tellurium chains [132-138].

With using the IR microscopy applied on partially-crystallized bulk samples, the crystallization mechanisms and morphology of formed crystalline phases can be investigated. The similar crystallization mechanisms as (rather) for Se-doped systems were uncovered. The formation of surface layer corresponds to the first crystallization peak,

namely the initial precipitation of tellurium and quite soon complete layer is formed. With further increase of temperature, the main crystallization mechanism (the growth of GeTe phase) manifests and volume-located crystallites start to form, however at high iodine contents the volume-located crystals formed by initiation from the surface layer, which means that some crystalline canals arose or the effect of mechanically induced defects manifested (see Fig. 26). The presence of iodine in $GeTe_4$ matrix leads to a slowdown of the volume-located GeTe and GeI_4 crystal growth (the eminent shift of the bulk crystallization to higher temperatures with rising applied heating rate).

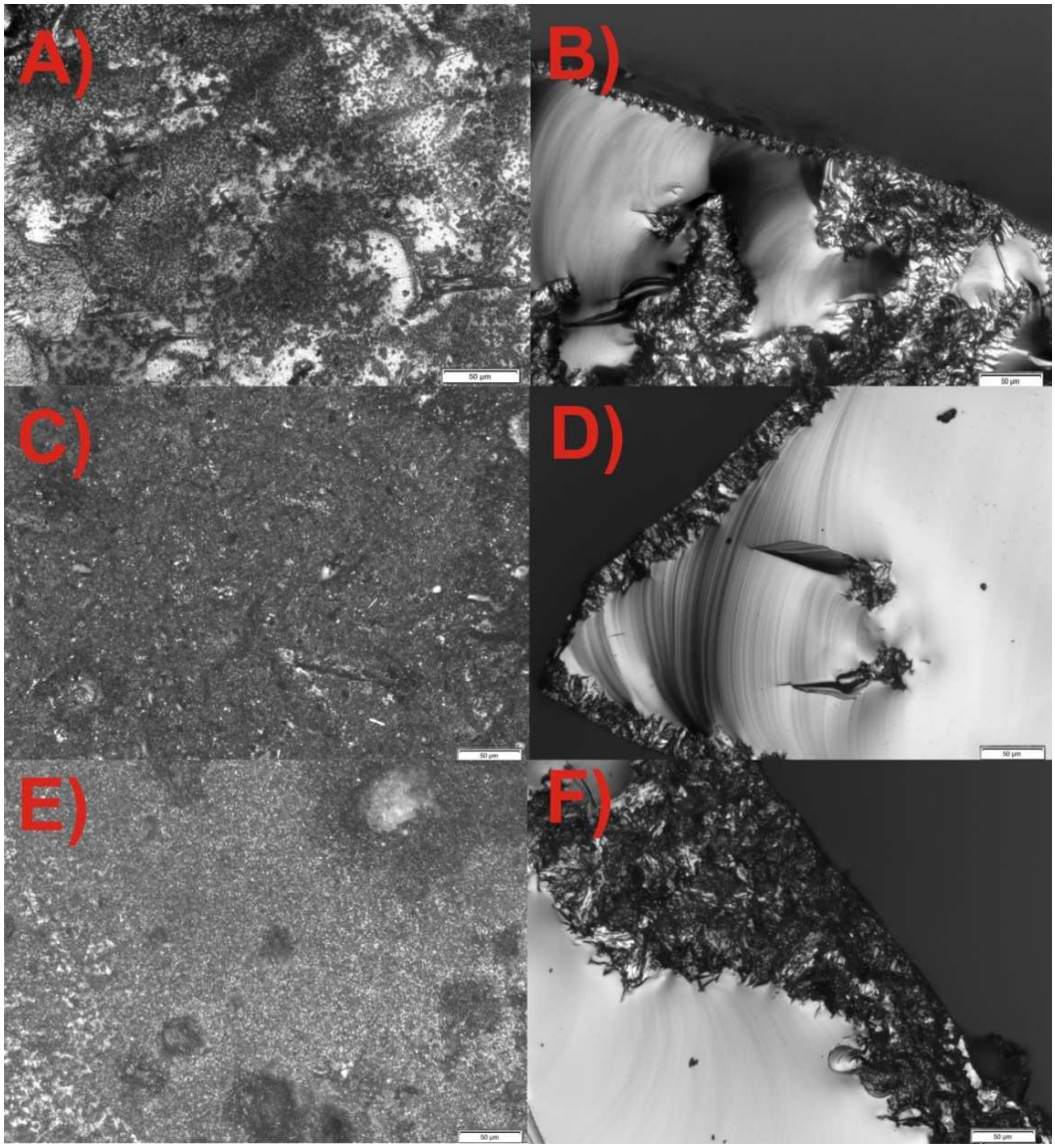

Figure 26: Infrared micrographs corresponding to the surface and cross-section views of the partially DSC-crystallized $Ge_{20}I_2Te_{78}$ (A, B), $Ge_{20}I_8Te_{72}$ (C, D) and $Ge_{20}I_{12}Te_{68}$ (E,F) materials (the scale is 50 µm).

The typical kinetic behavior of crystallization process was observed, which means that the shift of crystallization to higher temperatures with higher heating rates and increasing particle size occurs. After standard mathematic deconvolution procedure (more about this method in the following chapter) the dominant volume-located crystal growth in case of bulk samples was exposed (as was expected). In case of powdered samples, the surface and volume crystal growth appeared to be comparable. The subsequent kinetic analysis was realized by the determination of all parameters of the universal DSC kinetic equation (Eq. 7). It was found, that the E_A values were significantly influenced by experimental conditions and any trend cannot be assigned (see Fig. 27A). This indicates a large variability of initial phase of crystallization with applied experimental conditions and accelerating impact of the presence of mechanically induced defects. The flexible AC(M,N) model was found as the best choice in order to kinetic characterization of the crystallization DSC data.

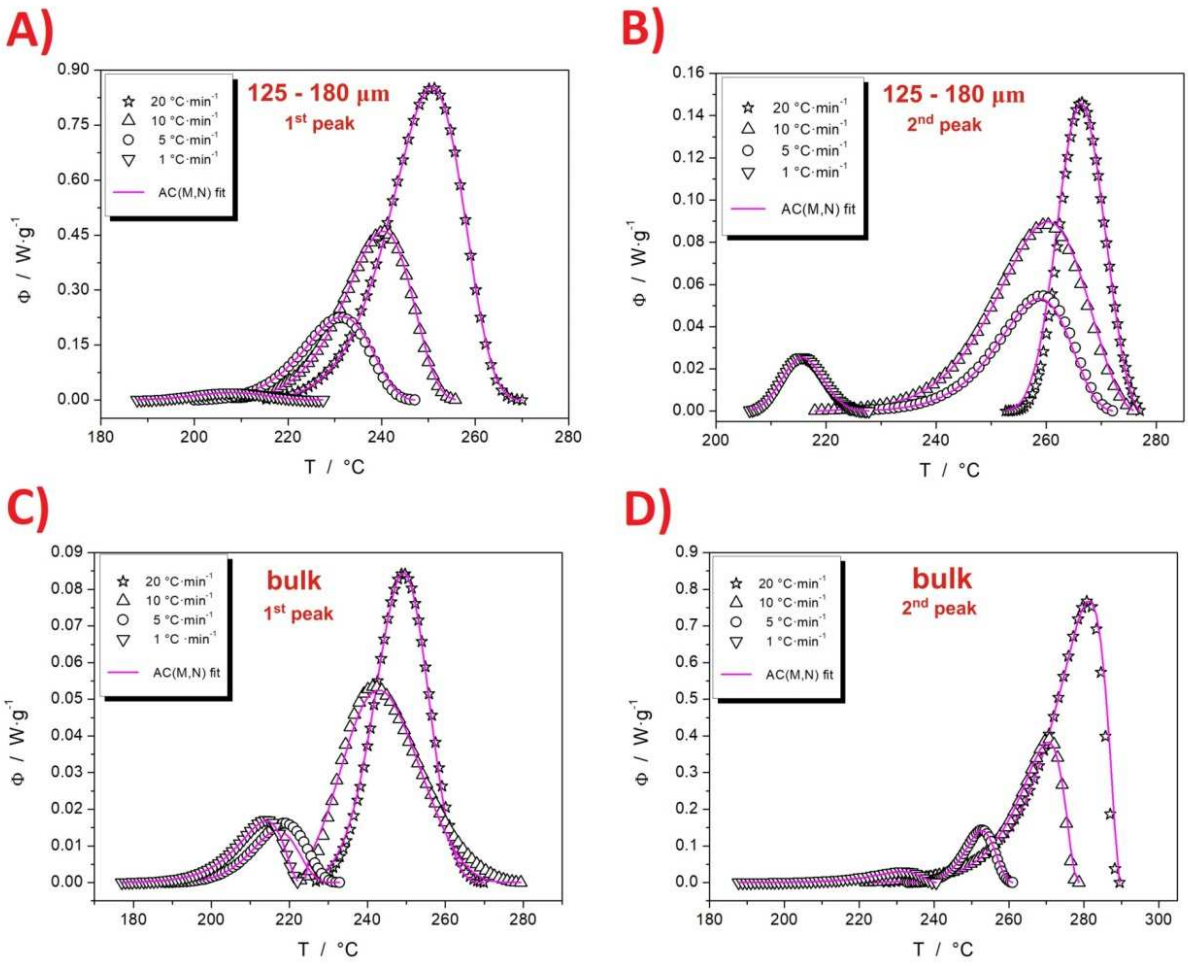

Figure 26: The sets of non-isothermal DSC deconvoluted crystallization peaks obtained for powdered and bulk samples of $Ge_{20}I_5Te_{75}$ composition. The fit by the AC(M,N) model is represented by the lines.

5.1.4 The structural relaxation behavior of doped Ge-Te systems

In the presented studies (**Papers I**, **II**, **IV**, **V**, **VIII**, **X – XII**) the relaxation behavior of doped $GeTe_4$ glasses was characterized by means of relaxation kinetics. This is a valuable tool how to complete the thermal, kinetic and structural knowledge about investigated systems. However, in this doctoral thesis, the description of the relaxation behavior is not a key topic and serves rather as a complementary subject to the thermal (mainly crystallization) and structural assessments of the inquired chalcogenide systems. The relaxation kinetic processes in the given systems were described by using the TNM [11,111,112] model. This phenomenological model belongs to the commonly used ways how to reveal the relaxation behavior of the various materials. Its basis and mathematic description was introduced above in Chapter 4.4, where this model was expressed by the set of mathematic equations (Eqs. 22 and 23). The relaxation behavior can be characterized using the parameter called the apparent activation energy of structural relaxation Δh^*, the evolution of which with various studied composition can be found in Fig. 27B. As can be seen, the initial addition of selenium slightly contributes to a decrease of the Δh^* values in case of the Se-doped $GeTe_4$ glass, which can indicate the coincidental incorporation of selenium into the $GeTe_{4-n}Ge_n$ tetrahedra. These processes probably correspond to the corner-/edge-shared tetrahedra ratio change, which means that the small amount of GeTe bonds would have to be broken to the change of conformation will be reached. It was pointed out (**Paper V**), that the main portion of relaxation movements is carried by the $GeTe_4$ tetrahedra. These conclusions were supported by data from Raman spectroscopy (see Table 5) and can be summarized as follows. The addition of selenium into GeTe matrix does not influence the position of T_g so much and the main portion of relaxation movements is carried by the $GeTe_4$ tetrahedra.

As was concluded in **Papers VIII and X**, the Ga atoms connects with the Te electronic lone pairs and do not interact with GeTe covalent network. That is a great difference as distinct from the previously reported results representing the Se-doped $GeTe_4$ glasses (**Papers I**, **II**, **IV**, **V**), where it was also established that the main portion of relaxation movements is undertaken by $GeTe_4$ tetrahedra. In contrary, in the case of Ga-doped $GeTe_4$ systems, the next dissimilarity arises, namely the presence of Ga-Te units influences the processes of relaxation movements in Ga-doped $GeTe_4$ glasses. It was found, that the Ga-Te units function as somehow diluting elements of the Ge-Te tetrahedral network, which leads to formation of small, partially sequestered $GeTe_4$ tetrahedral groups. These groups are

separated by Te-chains and dimmers terminated by Ga. The decrease of available relaxation movements ensues from this dilution effect of Ga.

On the basis of structural relaxation study of $Ge_{20}I_xTe_{80-x}$ (x = 2; 5; 8; 12; 15 %) system (**Papers XI** and **XII**) it was found that the iodine solely connects with germanium, therefore the structure is formed by the $GeTe_4$ and $GeTe_{4-x}I_x$ tetrahedra, which are linked by Te-Te bonds, that implies the iodine atom terminates the tetrahedral interconnections. This can be the explanation of lower values of Δh^* due to the less interconnection of matrix, which results in a lower amount of bonds needing to be transformed. In consequence of these effects of iodine on $GeTe_4$ matrix, the lower interconnectivity in glassy matrix is present (in comparison with pure $GeTe_4$) and in this case perhaps the larger structural units have to be moved to spread the relaxation movement. With respect to results from Raman spectroscopy, which do not indicate any major differences between the low I-doping (2 at. % of I) and higher I-doping (8 at. % of I), can be supposed that the surplus Ge is more capable to bond with iodine (forming the GeI_4 tetrahedra; the addition of iodine was at the expense of tellurium) and the terminating role of iodine is therefore narrowed. Also, a part of iodine appeared to be not covalently bonded in the Ge-Te-(I) matrix. The spontaneous condensation on the walls of vessels, in which the prepared glassy or crystallized samples were stored, occurred. However, the experimental characteristics (DSC records, Raman spectra) did not change after 3 months of storage.

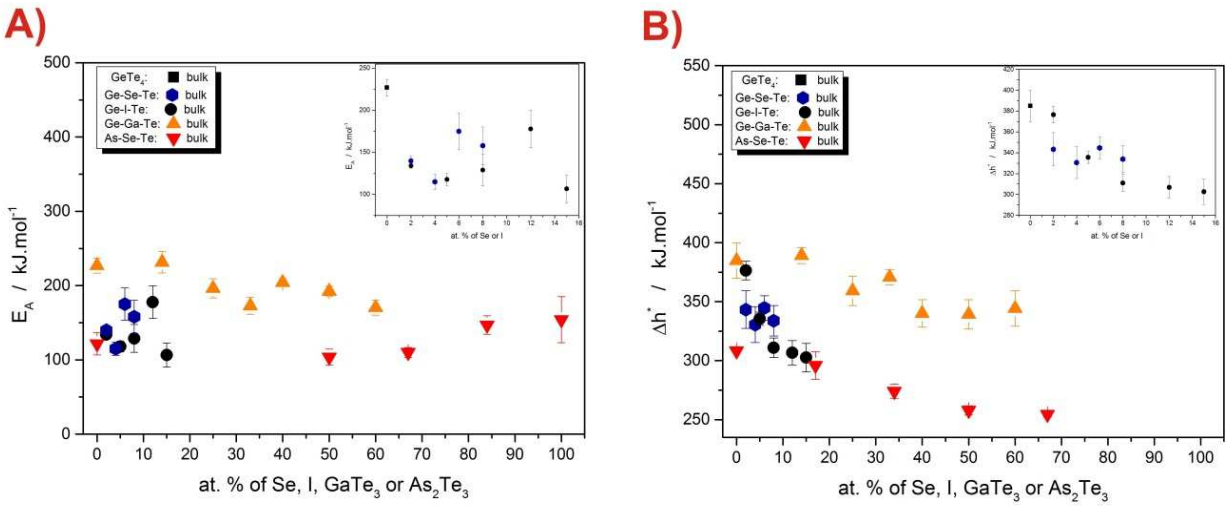

Figure 27: Compositional dependence of crystallization (A) and relaxation (B) activation energies for all investigated systems in form of bulk samples; the inset illustrates the zoomed area corresponding to the compositions with 0 - 15 at. % Se or I.

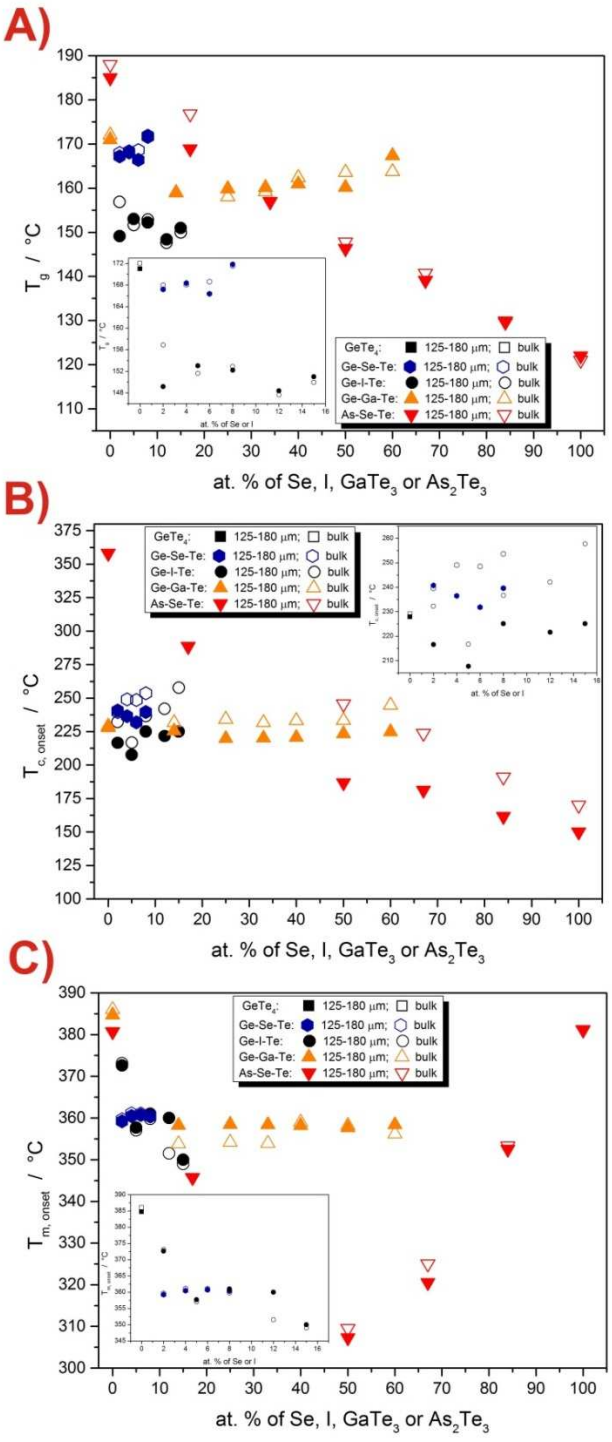

Figure 28: The of evaluated characteristic temperatures of all of studied systems for powder with particle size 125 - 180 µm and bulk samples; the glass-transition temperatures determined as half-height midpoints, the crystallization and melting temperatures as extrapolated onsets.

5.1.5 As-Se-Te system

An alternative to the investigated doped-$GeTe_4$ glasses is the As-Se-Te glass, where the As-Se content is added to As-Te fully telluride matrix in order to improve the thermal properties. It is believed, that As-Se-Te glasses can be comparable with doped-$GeTe_4$ glasses and the thorough knowledge of crystallization, relaxation and structural behavior is crucial for the next processing of glassy material. The As_2Se_3 binary system is well-known as an excellent glass-former and its addition to As_2Te_3 results in great improvement of thermal properties of glass. [31,34,38,40,43-45,49,58-63] Therefore, for the first time, thermal and structural behavior of As-Se-Te glasses was investigated in detail in the present thesis.

Paper XIII deals with the thermo-structural characterization of $(As_2Se_3)_{100-x}(As_2Te_3)_x$ glasses along the whole compositional line, whereas **Paper XIV** is focused on the thermal characterization of middle-positioned composition on the promising pseudo-binary line, namely the $(As_2Se_3)_{50}(As_2Te_3)_{50}$ system.

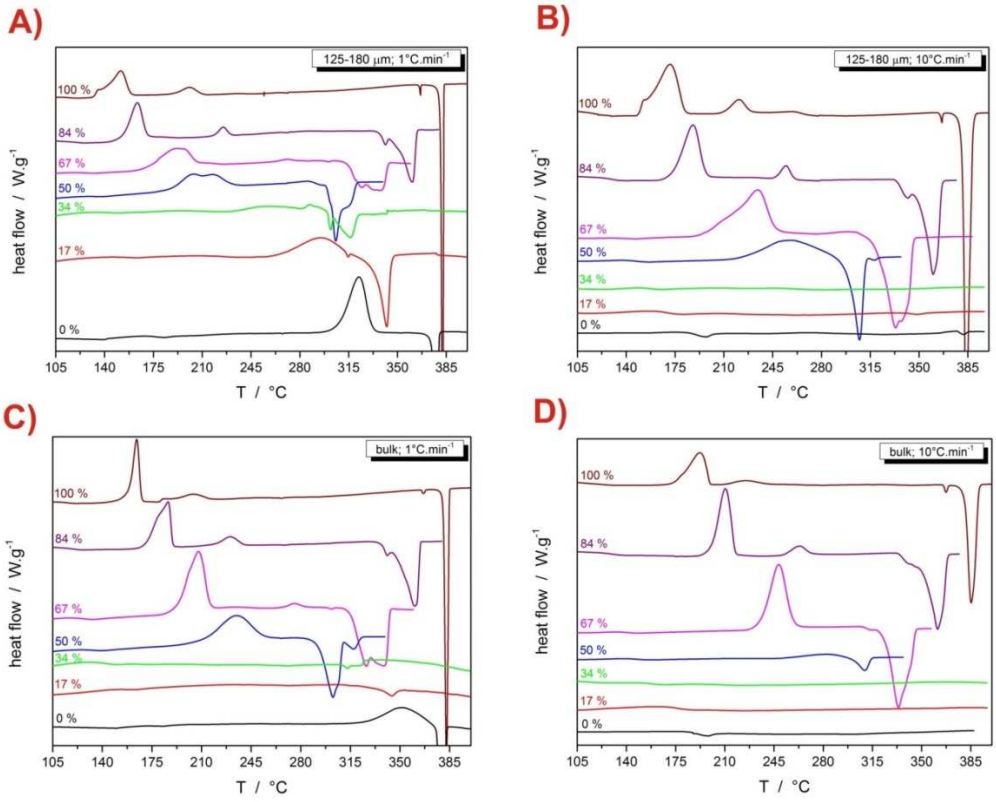

Figure 29: Example DSC curves obtained for applied heating rates 1 and 10°C.min^{-1} and the 125-180 µm powders (graphs A and B) and bulk samples (graphs C and D) of the studied $(As_2Se_3)_{100-x}(As_2Te_3)_x$ glasses. Each curve is marked according to the As_2Te_3 at. % content. Exothermic effects evolve in the "upwards" direction.

In Fig. 29, the DSC curves representing all of seven studied compositions of $(As_2Se_3)_{100-x}(As_2Te_3)_x$ (x = 0; 17; 34; 50; 67; 84; 100 %) chalcogenide system for the selected sample forms and applied heating rates are depicted. The first thermal effect, the glass transition, occurring on DSC curve, shows a shift to higher temperatures with increasing As_2Se_3 content; the behavior of the glass transition associated with structural relaxation phenomena will be shortly discussed below. The second observable thermal effect on DSC curve is the crystallization peak. In case of investigated system, the temperature shift towards higher temperatures with rising amount of As_2Se_3 units is evident, which is a good correspondence with the strong resistance of As_2Se_3 glasses against crystallization.

Typically, the XRD analysis was used (see Table 4) for identification of created crystallization products and some complications with a definition of structure arose. It was found, that monoclinic As_2Te_3 and As_2Se_3 units form (the pure As_2Te_3 and As2Se3 compositions), also the neighboring compositions (with 17 and 84 at. % of As_2Te_3) manifest the similar crystalline phases (only with slight shift of diffraction lines). However, the intermediate compositions (34, 50, 67 at. % of As_2Te_3) showed that completely different crystalline phases emerge. With using the temperature-resolved XRD analysis it was revealed that at the beginning of crystallization process the cubic $As_{50}Se_{25}Te_{25}$ forms, however the re-crystallization of this phase into more stable monoclinic As-Se-Te probably took place very quickly.

From the results provided by Raman spectroscopy it can be read that the significant changes in structure with addition of tellurium manifest up to 50 at. % of As_2Te_3. Above this percentage, the representation of As_2Te_3 the structure changes minimally with addition of tellurium. The assignment of structural arrangements in investigated glassy systems can be carried out on the basis of deconvolution of obtained Raman spectra (via Gauss function). The identified structural units occurring in investigated system can be found in Table 5.

The IR microscopy analysis was performed in order to better recognize the crystallization mechanisms and morphology of formed crystalline phases (see the example of IR micrograph of As-Se-Te system in Fig. 31). The presence of two morphologically different crystallites was observed. The spherulites, which form predominantly in case of compositions with increasing amount of As_2Se_3, and needle-shapes crystals characteristic for As_2Te_3-rich compositions.

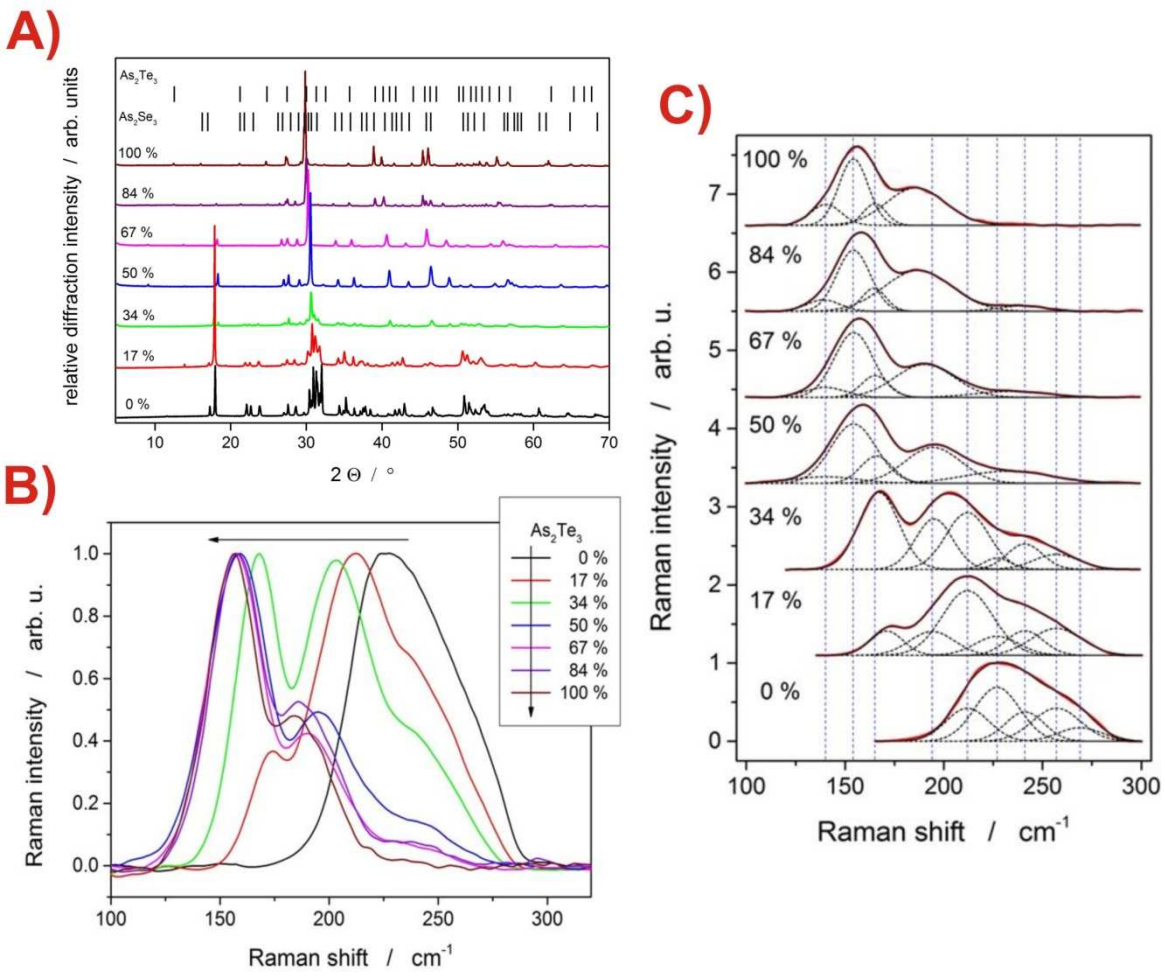

Figure 30: A) The diffraction patterns obtained from XRD analysis of all of investigated DSC-crystallized $(As_2Se_3)_{100-x}(As_2Te_3)_x$ compositions.

B) The Raman spectra for glassy $(As_2Se_3)_{100-x}(As_2Te_3)_x$ compositions; the arrows show the evolution of Raman spectra with composition.

C) The illustration of deconvolution of Raman spectra from Figure 30B.

All the samples crystallize on surface with subsequent inward crystal growth. This type of crystallization was also observed for previously studied $GeTe_4$ glasses and it can be supposed that the presence of surface crystallization mechanism is associated with rising amount of tellurium in the structure. For the 50/50 composition (**Paper XIV**), the structural study (XRD analysis, Raman spectroscopy, IR microscopy) proved the complicated structural arrangement. The physical dispositions of As_2Se_3 and As_2Te_3 phases permit to interchange each other in the structure. The $As_2Se_3 \leftrightarrow As_2Te_3$ substitution exists. The difficulties of unambiguous determination of crystallization morphology occurring in $(As_2Se_3)_{100-x}(As_2Te_3)_x$ system produce also the random incorporation of Te in the structure. No strict

structural morphology exists. This can explain the observed complexity of the crystallization processes.

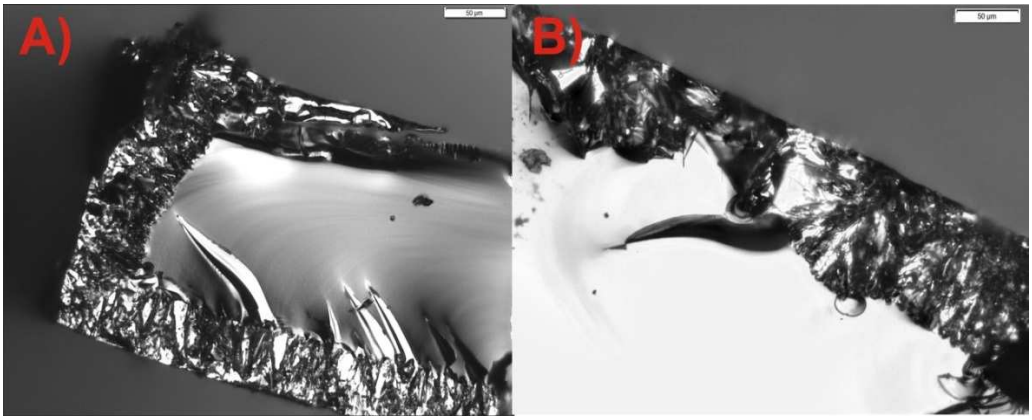

Figure 31: Infrared micrographs corresponding to the cross-section views of the partially DSC-crystallized As_2Te_3 (A) and $(As_2Se_3)_{50}(As_2Te_3)_{50}$ (B) materials.

The two crystallization sub-processes correspond to the development of morphologically different crystalline phases – the needle-shaped vs. spherulitic crystallites. The crystallization complexity occurs also in case of pure As_2Te_3, it can then correspond to the initial formation of cubic AsTe phase (the first peak), which recrystallizes into stable monoclinic As_2Te_3, and the second crystallization process then corresponds to the recrystallization of remaining cubic AsTe phase.

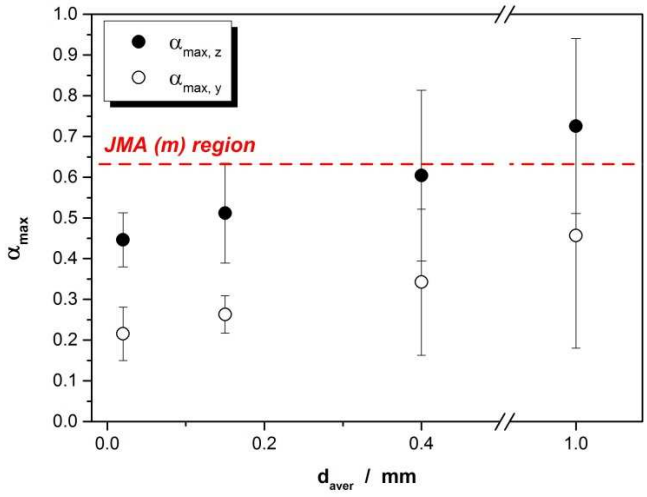

Figure 32: The dependence of the maxima of characteristic functions y(α), z(α) on the averaged particle size representing the $(As_2Se_3)_{50}(As_2Te_3)_{50}$ system.

The crystallization kinetic analysis of $(As_2Se_3)_{100-x}(As_2Te_3)_x$ (x = 0; 17; 34; 50; 67; 84; 100 %) chalcogenide system was realized on the basis of determination of the universal kinetic DSC equation (Eq. 7) similarly to the previously studied doped-$GeTe_4$ glasses. The large disinclination to crystallization was marked for As_2Se_3-rich side of studied compositional line; only the composition containing 34 at. % of As_2Te_3 slightly crystallizes under certain conditions (low heating rate, powdered sample). This composition seems to be very close to the eutectic point (see the complex shape and changes of melting peak profile with composition). On the basis of the possible presence of eutectic alloy (between 34 and 50 at. % of As_2Te_3) the extensive stability against crystallization can be clarified. In regard to the choice of the suitable kinetic model, the JMA (m) and AC(M,N) models were tested. As is apparent from Fig. 32, the only one (the coarsest one) of powder fractions is close to the JMA(m) model usability condition. For the best description of crystallization kinetics of $(As_2Se_3)_{100-x}(As_2Te_3)_x$ (x = 0; 17; 34; 50; 67; 84; 100 %) system the AC(M,N) model was selected (also due to its flexibility to experimental data). The significant influence of experimental conditions (sample form, applied heating rate) on crystallization kinetics was found, thus the individual steps of potential processing of this glassy system must be critically controlled.

The relaxation processes in $(As_2Se_3)_{100-x}(As_2Te_3)_x$ (x = 0; 17; 34; 50; 67; 84; 100 %) glass were described in terms of TNM model. It must be noticed that for compositions containing more than 67 at. % of As_2Te_3 the signals were very weak and scattered, so that the acquisition of reliable information was not possible. The decreasing trend in values of apparent activation energy of structural relaxation Δh^* (see Fig. 27B) of As_2Se_3-rich part of investigated compositional line appeared to be bound towards the Δh^* value equal to 258 $kJ.mol^{-1}$ (in the As_2Te_3-rich part). The significant decrease in T_g values was also marked. As was said, the Raman spectra revealed the minor changes in structure occurring in compositions containing more than 50 at. % of As_2Te_3 with the further addition of As_2Te_3. The rest of selenium was found to be primarily bound in the combined $AsTe(Se)_3$ pyramids and only part of selenium goes to form the pure $AsSe_3$ pyramids, which is in good correspondence with the compositional evolution of Δh^* values and T_g. As the As_2Se_3 content decreases, the Δh^* values also decrease due to the weaker As-Te bonds in contrary to As-Se bonds in $AsSe_3$ pyramids, therefore the energy needed to structural arrangements is also smaller. The replacement of fully selenide pyramidal units ($AsSe_3$) by mixed $AsTe(Se)_3$ pyramids causes the cessation of the Δh^* value decrease at lower As_2Se_3 amounts due to the

dependence of these pyramids on distortion of the weaker As-Te bonds. The energy of relaxation movements does not depend on selenium content.

Table 4: The summary of identified crystalline phases by means of XRD analysis for all investigated systems.

Composition	Crystalline phases	
$Ge_{20}Se_xTe_{80-x}$		
$Ge_{20}Se_2Te_{78}$	hexagonal Te rhombohedral GeTe unidentified GeTeSe phase	+ $GeSe_2$ (300 – 500 μm; 0.5 °C.min^{-1})
$Ge_{20}Se_4Te_{76}$		
$Ge_{20}Se_6Te_{74}$		
$Ge_{20}Se_8Te_{72}$		
$Ge_{21}Se_xTe_{79-x}$		
$Ge_{21}Se_2Te_{77}$	hexagonal Te rhombohedral GeTe	
$Ge_{21}Se_4Te_{75}$		
$Ge_{21}Se_6Te_{73}$		
$Ge_{21}Se_8Te_{71}$		
$(GeTe_4)_x(GaTe_3)_{100-x}$		
$(GeTe_4)_{40}(GaTe_3)_{60}$	hexagonal Te + Ga_2Te_5 rhombohedral GeTe	tetragonal Ga_2Te_5
$(GeTe_4)_{50}(GaTe_3)_{50}$		
$(GeTe_4)_{60}(GaTe_3)_{40}$		
$(GeTe_4)_{67}(GaTe_3)_{33}$		
$(GeTe_4)_{75}(GaTe_3)_{25}$		
$(GeTe_4)_{86}(GaTe_3)_{14}$		
$Ge_{20}I_xTe_{80-x}$		
$Ge_{20}I_2Te_{78}$	hexagonal Te rhombohedral GeTe cubic GeI_4	
$Ge_{20}I_5Te_{75}$		
$Ge_{20}I_8Te_{72}$		
$Ge_{20}I_{12}Te_{68}$		
$Ge_{20}I_{15}Te_{65}$		
$(As_2Se_3)_{100-x}(As_2Te_3)_x$		
$(As_2Se_3)_{17}(As_2Te_3)_{83}$	monoclinic As_2Se_3 monoclinic As_2Te_3	
$(As_2Se_3)_{34}(As_2Te_3)_{66}$		+ cubic $As_{50}Se_{25}Te_{25}$
$(As_2Se_3)_{50}(As_2Te_3)_{50}$		
$(As_2Se_3)_{67}(As_2Te_3)_{33}$		
$(As_2Se_3)_{84}(As_2Te_3)_{16}$		

Table 5: The summary of identified structural units occurring in all of investigated glassy systems by means of Raman spectroscopy.

Composition	Structural units
$Ge_{20}Se_xTe_{80-x}$	corner-sharing Te-rich $GeTe_{4-n}Ge_n$ (n = 0; 1; 2) tetrahedra edge-sharing $GeTe_4$ (or Ge-rich) tetrahedra short, amorphous, distorted Te-chains pure Te structures
$Ge_{20}Se_2Te_{78}$	
$Ge_{20}Se_4Te_{76}$	
$Ge_{20}Se_6Te_{74}$	
$Ge_{20}Se_8Te_{72}$	
$Ge_{21}Se_xTe_{79-x}$	
$Ge_{21}Se_2Te_{77}$	
$Ge_{21}Se_4Te_{75}$	
$Ge_{21}Se_6Te_{73}$	
$Ge_{21}Se_8Te_{71}$	
$(GeTe_4)_x(GaTe_3)_{100-x}$	
$(GeTe_4)_{40}(GaTe_3)_{60}$	
$(GeTe_4)_{50}(GaTe_3)_{50}$	
$(GeTe_4)_{60}(GaTe_3)_{40}$	
$(GeTe_4)_{67}(GaTe_3)_{33}$	
$(GeTe_4)_{75}(GaTe_3)_{25}$	
$(GeTe_4)_{86}(GaTe_3)_{14}$	
$Ge_{20}I_xTe_{80-x}$	
$Ge_{20}I_2Te_{78}$	
$Ge_{20}I_5Te_{75}$	
$Ge_{20}I_8Te_{72}$	
$Ge_{20}I_{12}Te_{68}$	
$Ge_{20}I_{15}Te_{65}$	
$(As_2Se_3)_{100-x}(As_2Te_3)_x$	
$(As_2Se_3)_{17}(As_2Te_3)_{83}$	Se-As-Te chains As_2Te_3, $AsTe_3$, $AsSe_3$ units Se-Se chains short, amorphous, distorted Te-chains pure Te structures
$(As_2Se_3)_{34}(As_2Te_3)_{66}$	
$(As_2Se_3)_{50}(As_2Te_3)_{50}$	
$(As_2Se_3)_{67}(As_2Te_3)_{33}$	
$(As_2Se_3)_{84}(As_2Te_3)_{16}$	

5.2 PAPER DISCUSSION – Part II

In this section, the complex kinetics manifesting in case of crystallization of glasses and the ways how to solve this phenomenon will be introduced. As was said, the crystallization process of tellurium-based glasses often shows a certain degree of complexity, which means that the individual crystallization peaks overlap and at least two kinetic mechanisms proceed simultaneously. The most of solid-state processes are complex, the revelation lies in an application of different experimental conditions (e.g. heating rate). In practice, the thermoanalytical records can show either only partial overlap or a pseudo-single peak behavior.

In general, there are three approaches how to treat such complex kinetics. The first approach offers such a way of the methods suggested primarily for single-process kinetic analysis applied on whole complex data-set and the following interpretation of changes and distortions of the obtained data. Usage of isoconversional methods for determination of activation energy (e.g. KAS [89] method) can serve as an example. The second approach uses the procedures of mathematic deconvolution of the complex kinetic signal using some suitable mathematic functions. After that, each set of these peaks is separately evaluated by means of normal single-process analysis. As a suitable mathematic function was found the Fraser-Suzuki (FS) [107-110] function, which was thoroughly tested in the past and it was confirmed that the FS function can describe all kinetics readily occurring for the solid-state reactions. [107-110] The FS function is expressed via the Eq. (21) in the Chapter 4.3 and offers a reliable description of crystallization complexity observed for non-isothermal data. In case of isothermally obtained data, the Avrami [93-95,128] dogma can serve for the isothermally obtained complex data. The third approach includes a full reaction scheme containing all the kinetic equations and their determination proceeds by means of non-linear optimization for all involved sub-processes simultaneously. This is called kinetic deconvolution. The multivariate kinetic analysis (MKA) was found as a the most suitable procedure, it represents a curve-fitting routine in terms of full-scale complex kinetics and model-free results (E_A and A) obtained for overall signal are used as input parameters [85,99-103]. All these methodologies are established and work very well.

However, if the kinetic behavior of the involved sub-processes changes with the experimental conditions (temperature, heating rate), these phenomena can be presented by the change of intensity of involved sub-processes likewise the increase or decrease

of the enthalpy ΔH in case of DSC measurements; or kinetic mechanism can change for the given sub-process or simply the activation energy of each sub-process can be temperature or heating rate dependent. The above-mentioned facts are summarized in **Paper XV**, which is focused on solution of crystallization kinetics complexity of glassy materials. It was found that the change of crystallization kinetics of particular sub-processes with temperature or heating rate is real and can occur for complex glassy matrices as well as for single-element glasses (chalcogenide Ge-Ga-Te glass vs. selenium glass vs. vanadium-doped ZrO_2 catalyst vs. $Y_3Al_5O_{12}$ microspheres). The kinetics variability can be often only matter of the extent of applied experimental conditions. The conclusions resulting from **Paper XV** can be interpreted as follows. The crystallization of the germanium-gallium-tellurium far-infrared glass can serve as the example of the examined systems. After the multivariate kinetic analysis was applied on tested data, it was found, that the kinetic parameters change in dependence on the range of considered heating rates, which means that the kinetics depends on heating rate.

Table 6: The summary of kinetic parameters obtained via MKA for the $(GeTe_4)_{50}(GaTe_3)_{50}$ material (different sets with given ranges of applied heating rates). The errors associated with these evaluations were lower than 0.02 for A, 0.2 for E_A, 0.02 for m_{JMA} and M and 0.01 for N parameter.

q^+ range / parameters	0.5 - 2 °C.min^{-1}	7 - 30 °C.min^{-1}	0.5 - 30 °C.min^{-1}
log (A_1 / s^{-1})	18.06	17.00	18.60
$E_{A\,1}$, kJ.mol^{-1}	199.45	188.02	203.86
m_{JMA}	1.68	1.49	1.44
log (A_2 / s^{-1})	22.32	17.55	17.70
$E_{A\,2}$, kJ.mol^{-1}	237.42	192.52	194.22
N	1.55	1.20	1.18
M	0.92	0.83	0.81

Another example of presence of crystallization complexity can be found in **Paper XVI**, which deals with topic of crystal growth from mechanically induced defects. The pure $GeTe_4$ glass was studied by means of DSC and IR microscopy. The typical crystallization complex behavior was observed and the two sub-processes were revealed for all eight tested particle size fractions (0-20; 20-50; 50-125; 125-180; 180-250; 250-300; 300-500 μm and bulk sample). The mathematic deconvolution procedure via the Fraser-Suzuki function was applied on crystallization data and the two present crystallization mechanisms was described by JMA (m) and AC(M,N) models.

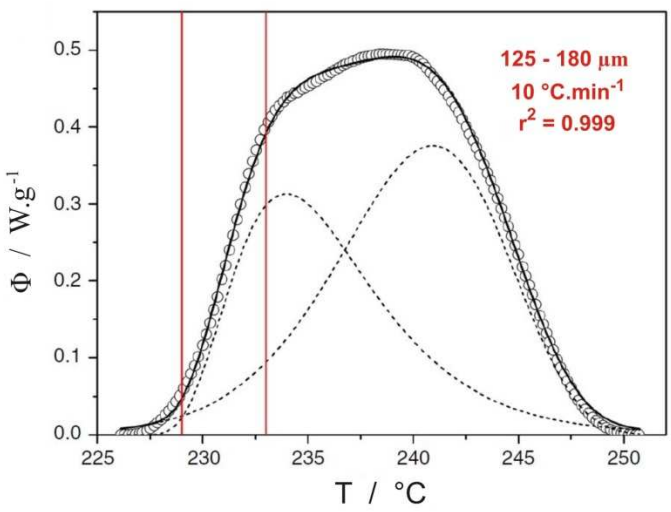

Figure 33: The deconvoluted DSC curve corresponding to the pure $GeTe_4$ powdered material; the dashed lines - the deconvoluted crystallization peaks, solid line - the overall fit, the experimental data - circles.
The vertical red lines represent the limits of temperature needed to the partial crystallization to revelation of crystal growth originating from mechanically induced defects.

The partially-crystallized samples (in DSC) were prepared by two ways - the $GeTe_4$ powder was heated to 229 and 233 °C (see the vertical red lines in Fig. 33). The lower temperature (229 °C) corresponds to the state, when both crystallization sub-processes manifest only moderately, whereas at the higher temperature (233 °C) the manifestation of the crystal growth following the AC(M,N) kinetics becomes more noticeable. The selected grains were then carefully cracked and observed by IR microscope. Each piece of tested grains contained a large number of small crystallites, which presence confirmed the predicated

defects-based crystallization. Also a large number of fragments were on their surfaces covered by a crystalline layer.

The both deconvolution procedures (mathematic and kinetic) provided suitable and consistent results (see **Papers I – IV**, **VI – XVI**). The examples of selected deconvoluted DSC curves representing all of investigated systems (Se-, Ga-, I-doped $GeTe_4$ and As-Se-Te glasses), which this presented doctoral thesis includes, are illustrated in Fig. 34. The number of curves, on which the deconvolution procedures were applied (within the framework on this doctoral thesis) exceeds one thousand, excepting the Ge-Ga-Te system (MKA was applied), the mathematic deconvolution was applied on all of investigated data.

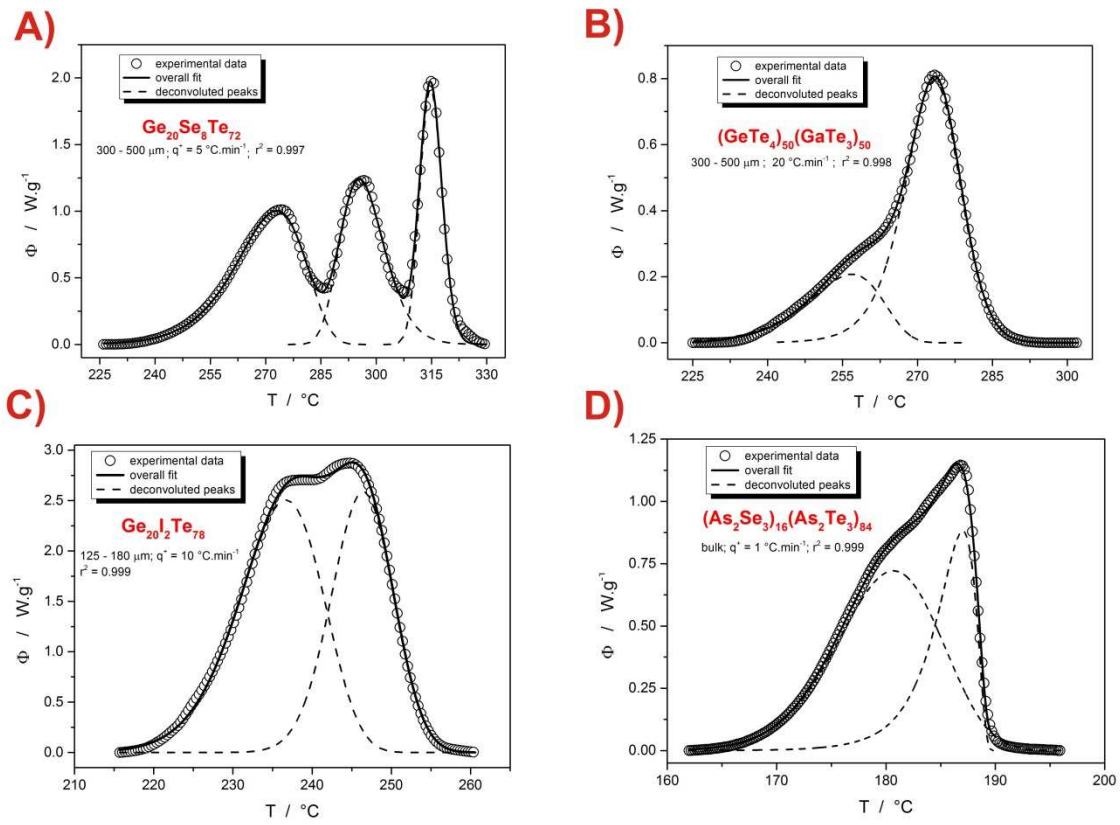

Figure 34: The examples of deconvoluted DSC curves representing the studied systems: A) $Ge_{20}Se_8Te_{72}$ system; B) $(GeTe_4)_{50}(GaTe_3)_{50}$ system; C) $Ge_{20}I_2Te_{78}$ system; D) $(As_2Se_3)_{16}(As_2Te_3)_{84}$ system.

The usage of MKA method is easy and fast and introduces an effective method at distinguishing of subtle changes and trends in evolution of kinetic parameters. However, this method requires the more-or-less constant values of E_A across the whole explored range of experimental conditions. This condition was fulfilled only for the explored

$(GeTe_4)_x(GaTe_3)_{100-x}$ (x = 40; 50; 60; 67; 75; 86; 100 %) system (**Papers VII – X**). In contrary, the mathematic deconvolution procedure, which is followed by kinetic analysis of each of determined single processes, can be comparatively difficult and time consuming (**Papers I – IV**, **VI**, **XI – XIV**, **XVI**). Nevertheless, this method represents a valuable tool for deconvolution purposes, when the kinetic deconvolution cannot be performed - for example in case, when data exhibit great changes of E_A values with experimental conditions. If the potential mutual inter-dependences of the fundamental sub-processes exist, the mathematic deconvolution is not able to properly account for this phenomenon (in comparison with MKA). For the physically meaningful interpretations there is only the way of the deconvolution of each separate curve followed by displaying various trends in dependence on the temperature or heating rate ranges. The main purpose of this branch of this doctoral thesis was to draw an attention to this problematic and, hopefully, start off a research leading to some advancements or at least some activity regarding this issue.

5.3 PAPER DISCUSSION – Part III

The third section of this doctoral thesis will be focused on detailed characterization of thermal behavior of investigated glassy systems with regard to the assessment of glass ability and glass stability of the examined materials. This field of the characterization of glassy matters belongs to a very important area due to the appraisal of the potential usability of studied chalcogenide tellurium-based glassy systems in far-IR optics or glass-ceramics application areas. The various well-known glass-stability (GS) criteria are used for the consideration, whether the given material is able to form a stable glass. It has been pointed out above that the most suitable criterion (for chalcogenide materials) was found to be the Hruby criterion (see Ref. [29]), which unfortunately strongly depends on experimental conditions. The thermal stability of glassy systems can be considered also by using the so-called ΔT criterion ($\Delta T = T_c - T_g$) [30-32], which takes into account only the difference between the glass transition temperature T_g and the crystallization temperature T_c. However, this temperature difference has still remained crucial, the wider the difference $T_c - T_g$, the more stable the glass is. Nonetheless, the mentioned GS criteria work only with the characteristic temperatures and do not take into account the other facts, which fundamentally influence the resulting thermal stability of glass. Therefore, a new approach has been recently suggested [33]. The combination of crystallization temperature value (obtained from DSC crystallization measurements) and the information about glass-softening and viscous flow effects (obtained from TMA crystallization measurements) is applied. The glass-softening and viscous flow effects become more apparent and important in the crucial temperature region between the glass transition temperature and crystallization.

The direct correlation of thermo-kinetic and thermo-mechanical properties of Se- and Ga-doped GeTe systems is one of the contents of this doctoral thesis. The Papers **II**, **V**, **VIII** and **X** deal with the combined DSC and TMA study, which can provide an information about the true nature of the crystal growth process limiting the fiber-drawing procedures. The emphasis is put on getting as much information as possible from the combined DSC and TMA measurements, and also on the estimation of the influence of glass transition and crystallization kinetics on glass stability and potential kinetic predictions regarding the formation of far-IR optical elements and glass-ceramics.

Papers II and **V**, for the first time, introduce the possibility to combine the DSC and TMA techniques with regard to obtaining the detailed information about ongoing processes

connected with crystallization (which restrict the glass preparation and processing) for the whole compositional line of $Ge_{21}Se_xTe_{79-x}$ (for x up to 8 at. % of selenium) glasses (**Paper II**) and one selected composition, namely the $Ge_{20}Se_4Te_{76}$ glass (**Paper V**). The crystallization process and its kinetics of $Ge_{21}Se_xTe_{79-x}$ and $Ge_{20}Se_xTe_{80-x}$ glasses was found (and described in Chapter 5.1.1) to be largely influenced by the added amount of Se. The addition of selenium increased a tendency for the gradual separation of initial tellurium precipitation and subsequent volume-located growth of GeTe crystalline phases. The selenium was found to be an inhibitor of crystallization process. The above-mentioned conclusions are based on DSC data. In **Papers II** and **V** can be also found the results from crystallization measurements performed by TMA. An illustration of results obtained from both thermo-analytical techniques (DSC, TMA) representing the selected compositions offers the Fig. 35, where the A-part corresponds to the pure $Ge_{21}Te_{79}$ without any addition of Se; the B-part then corresponds to the addition of 4 at. % of selenium.

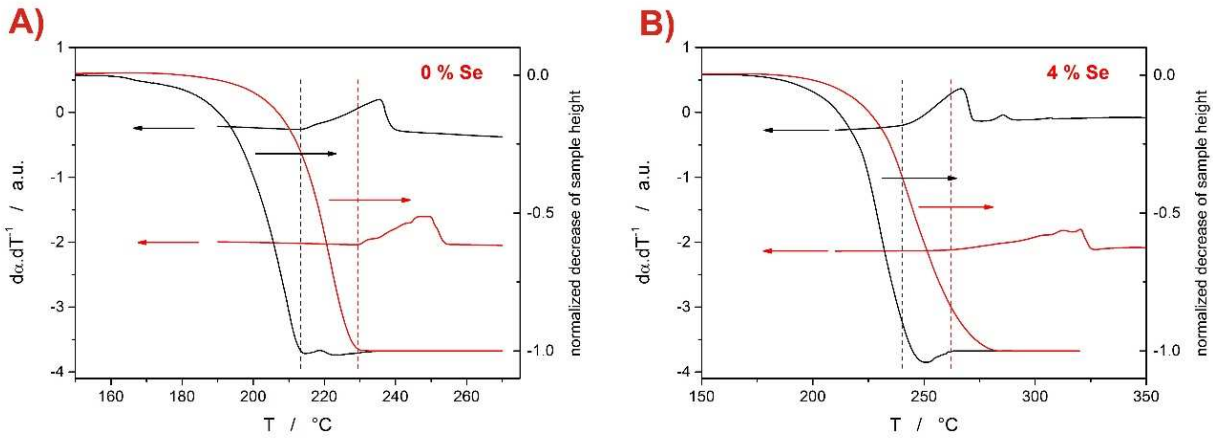

Figure 35: Comparison of DSC and TMA measurements for bulk samples of $Ge_{21}Te_{79}$ (A) and $Ge_{21}Se_4Te_{75}$ (B) compositions and applied heating rates 1 (black curves) and 10 (red curves) °C.min^{-1}.

In Fig. 35 the two vertical dashed lines (black and red) can be seen, marking the crystallization onsets for the DSC bulk samples. As can be seen, the marked crystallization onsets (DSC) well correspond to the cessation point of the sample height decrease in case of $Ge_{21}Te_{79}$ composition (0 at. % of Se). It is apparent that the initial tellurium precipitation stops the sample creep (similar behavior exhibited also the $GeTe_4$ material – **Paper III**) and the strong surface layer of minuscule tellurium crystals formed. This is also in a good agreement with the results from IR microscopy (see Fig. 18). In Chapter

5.1.1 it was also reported, that the addition of Se led to a significant change of crystallization mechanism. Selenium causes the inhibition of both crystallization mechanisms and the minuscule Te crystallites are substituted by larger crystallites, which grow inwards separately from a lower amount of surface nuclei. If the DSC and TMA measurements representing the composition with 4 at. % of Se will be compared, the larger amount of crystalline phase is required to cessation of viscous flow. This is caused by a demand of formation of larger crystallites (needed for creation of interconnected crystalline network) due to the lower amount of surface crystallization centers.

The crystallization and relaxation kinetics can be characterized by usage of DSC and also by usage of TMA data, whereas regarding the TMA data the T_p value (corresponding to the maxima of crystallization DSC peak) was replaced by the T_{ic}. The Fig. 36 offers a comparison of E_A and Δh^* values of all studied $Ge_{21}Se_xTe_{79-x}$ compositions obtained from DSC (black-labeled points) and TMA (red-labeled points) measurements. The E_A values determined with using the TMA crystallization data are considerably higher than those from DSC data. This phenomenon can be interpreted on basis of previously reported results [63,126] and can be ascribed to the larger sensitivity of TMA method to the first stages of crystallization. The Δh^* values obtained from DSC and TMA show better correspondence, which can validate the current Δh^* evaluations from the DSC and TMA data. Similar findings were obtained also for $Ge_{20}Se_4Te_{76}$ (**Paper V**). The conclusions concerned with crystallization and relaxation kinetics of $Ge_{21}Se_xTe_{79-x}$ (for x up to 8 at. % of selenium) and $Ge_{20}Se_xTe_{80-x}$ (for x up to 8 at. % of selenium) glasses were introduced in Chapter 5.1.1.

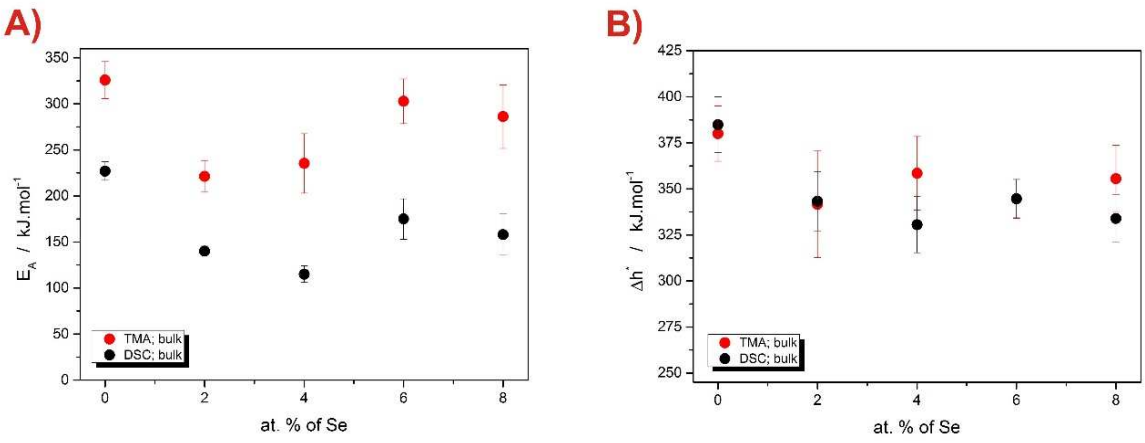

Figure 36: The comparison of E_A (A) and Δh^* (B) values of studied $Ge_{21}Se_xTe_{79-x}$ (for x up to 8 at. % of Se) glasses determined on basis of DSC (black points) and TMA (red points) experiments.

Papers VIII and **X** deal with the combined DSC and TMA crystallization study of Ga-doped $GeTe_4$ systems. **Paper VIII** works with whole compositional line, i.e. $(GeTe_4)_x(GaTe_3)_{100-x}$ (x = 40; 50; 60; 67; 75; 86; 100 %) systems; in **Paper X** the combined thermo-kinetic and thermo-mechanical characterization of selected $Ge_{11}Ga_{11}Te_{78}$ (it corresponds to $(GeTe_4)_{50}(GaTe_3)_{50}$ composition) glass can be then found, which is middle-positioned composition on the promising $GeTe_4$-$GaTe_3$ pseudo-binary line. The Fig. 37 illustrates the obtained DSC and TMA crystallization curves for the selected Ge-Ga-Te compositions, where the black and red curves correspond to the data representing the two applied heating rates (1 and 10 °C.min^{-1}) and the vertical dashed lines then represent the actual (not extrapolated) onsets of the DSC crystallization peaks.

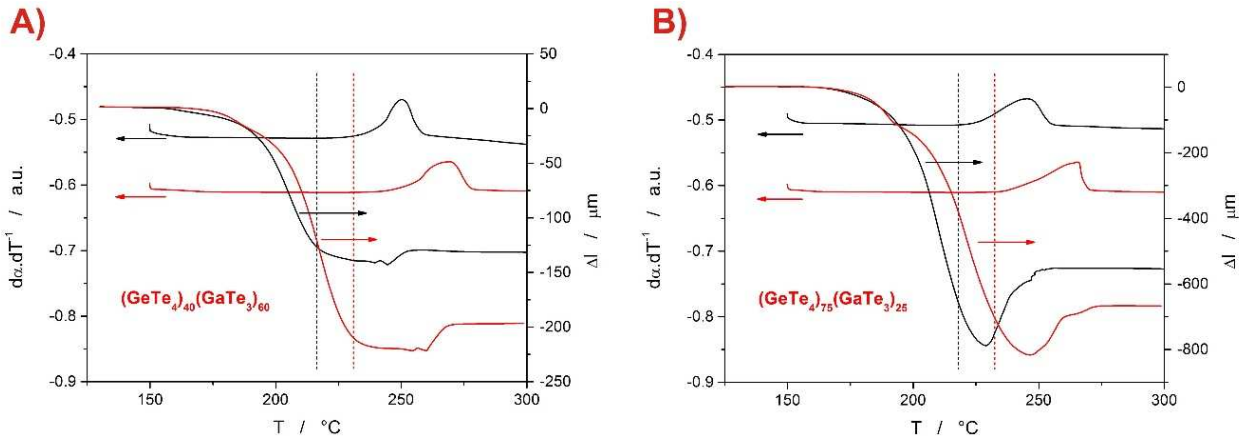

Figure 37: The comparison of DSC and TMA measurements for bulk samples of $(GeTe_4)_{40}(GaTe_3)_{60}$ (A) and $(GeTe_4)_{75}(GaTe_3)_{25}$ (B) compositions and applied heating rates 1 (black curves) and 10 (red curves) °C.min^{-1}.

The typical sample height decrease above T_g due to the rising viscous flow with increasing temperature and constant compressing force applied by TMA is apparent. The moment that crystallization occurs, the decrease of sample height stops, because the crystalline network starts to form and hinders the sample from further flow. As is evident from the comparison of DSC and TMA crystallization measurements, the cessation of TMA curve corresponds to the formation of first crystallites (the Te-precipitation). The similar findings were observed also for Se-doped GeTe glasses (**Papers II** and **V**).

The apparent activation energy of crystallization E_A was determined for all studied systems (see Fig. 38) on basis of both measuring methods (DSC, TMA). The results provided by both techniques well agree together. Certain dispensation can be observed for pure $GeTe_4$.

In this case, it seems that the crystallization is speeded up by applied force during TMA measurement. This statement was confirmed using the infrared microscopy procedure, the fine tellurium crystals appeared, when the first softening of the sample passed. The presence of early crystal formation then can influence the E_A evaluations.

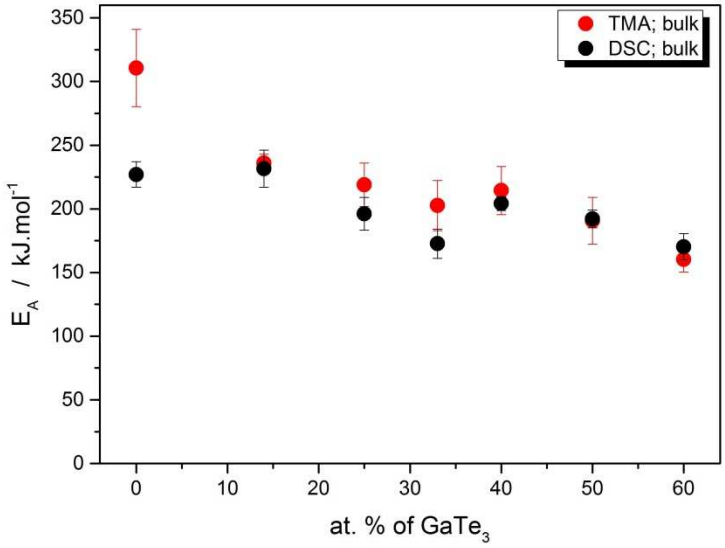

Figure 38: The comparison of E_A values of studied $(GeTe_4)_x(GaTe_3)_{100-x}$ (x = 40; 50; 60; 67; 75; 86; 100 %) glasses determined on basis of DSC (black points) and TMA (red points) experiments.

The characterization of overall thermal behavior of glassy materials and the consequent determination of glass stability play an important role in scientific practice due to the ability to predict the thermal behavior of given glassy system for its potential processing. The noticeable effort has been dedicated to the search of the most suitable GS criteria in regard to the potential real-life applications of the given glassy material. In the presented doctoral thesis the Hruby [23] criterion, the recently developed K_S [129-131] criterion and the next new-developed criteria called workability window and new viscous-flow-related parameter [33] (**Paper VIII**) will be discussed with regard to studied systems by reason they were used to determination of glass stability of all investigated glassy systems included in this thesis. The mentioned K_H and K_S criteria belong to the group of GS criteria, which are based on characteristic temperatures (T_g. T_c, T_m) and their relations. These criteria are widely used and their evaluation is very simple. Unfortunately, their outcomes are rather

abstract and usually used for comparison purposes. In order to enhance this important approach, the utilization of the combined DSC and TMA crystallization data is suggested.

The Fig. 39 offers a summary of results provided by means of K_S and K_H criteria for all investigated systems. In case of $Ge_{20}Se_xTe_{80-x}$ and $Ge_{21}Se_xTe_{79-x}$ systems (**Papers I, II, IV**), the recently developed K_S criterion was applied to evaluation of glass stability. The data in Fig. 39 show that the glass stability of bulk materials (relevant for real-life applications) rises with the addition of selenium into GeTe matrix and get at a standstill above ~ 4 at. % of Se.

The glass stability of $Ge_{21}Se_xTe_{79-x}$ system seems to be slightly better than that of $Ge_{20}Se_xTe_{80-x}$ system but not as much as was expected. The slightly higher amount of Ge, which was in case of Ge-Se-Te far-IR glasses used mainly to optimize the glass stability, did not have much impact on glass stability. However, the $Ge_{21}Se_xTe_{79-x}$ system was found as more suitable (in comparison with $Ge_{20}Se_xTe_{80-x}$) for the potential processing; the higher amount of germanium in the structure leads to slow-down of crystallization but without the influence on the position of crystallization onsets. With regard to the actual utilization of Ge-Se-Te glasses in the far-IR optics applications, it is needed to make a compromise between the width of the transmittance window, which a little narrows with Se addition, and the glass stability, which increases with addition of selenium. The compositions with selenium content $\geq$ 4 at. % were found to be favorable considering the glass stability and the potential manufacture (fiber-drawing, shaping) of the glassy material. This conclusion can be also confirmed by the results from TMA analysis (see Fig. 35). In case of the composition with 4 at. % of Se, the workability window (Eq. 25), which is defined as a temperature range between the first softening of the sample and first occurrence of crystallites, was 75 – 80 °C wide. As the selenium content increased, the workability window narrowed and for the composition with 8 at. % of selenium was 60 – 65 °C wide. These effects point to facts, that the glass-softening, viscous flow effects and occurrence of first crystallites determine the glass-stability of given materials and the correlation of DSC and TMA data can help with consideration of stability and processability of glassy materials. The $Ge_{21}Se_4Te_{75}$ glass was found as the most suitable for the further processing and applicability as a far-IR optical fibers and mold-formed optic elements.

The Hruby criterion was used for determination of glass stability of Ge-I-Te (**Papers XI**, **XII**), As-Se-Te (**Papers XIII**, **XIV**) and Ge-Ga-Te (**Papers VII**, **VIII**) systems. The thermal stability of $Ge_{20}I_xTe_{80-x}$ (x = 2; 5; 8; 12; 15 %) assessed on the basis of Hruby criterion was found to be fairly variable with respect to the composition and experimental

conditions. The K_H values range from 0.5 to 2.5. While the glass transition temperatures and melting temperatures are invariant with regard to the sample form and heating rate, the crystallization of $Ge_{20}I_xTe_{80-x}$ glasses is largely influenced by experimental conditions. This causes the large variability of glass stability. The consideration of the influence of experimental conditions on thermal (and glass) stability of given systems is crucial. In this instance, if the bulk samples and low heating rates will be taken, the macroscopic IR optics applications (such as molded lenses) with utilization of $Ge_{20}I_xTe_{80-x}$ glasses are possible. Unfortunately from this point of view, the Se- and Ga-doped GeTe glasses are more suitable for far- IR optics applications due to the unpredictable surface precipitation of tellurium and complicated glass synthesis of I-doped $GeTe_4$ glasses. Nonetheless, the $Ge_{20}I_2Te_{78}$ glassy composition seems to be suitable for the far-IR optics ceramics and glass-ceramics due to the most pronounced transition from the pure surface to the volume-located crystal growth with the initial iodine addition.

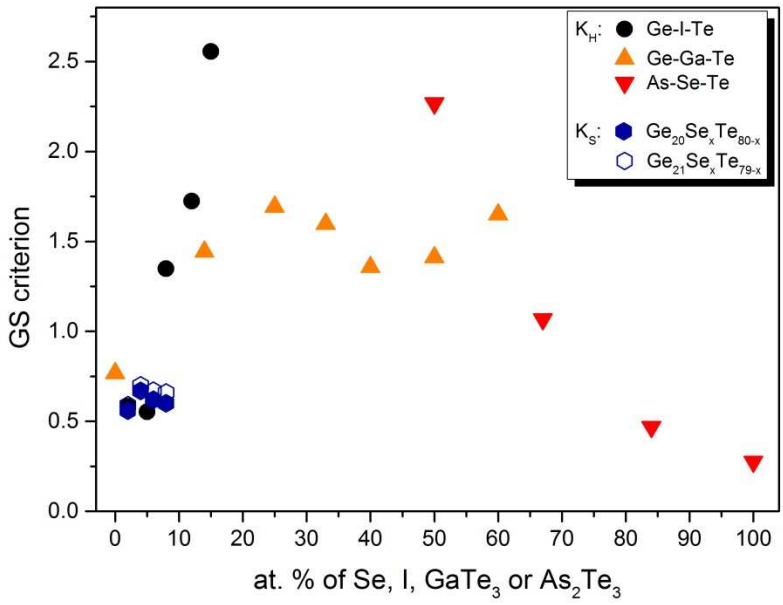

Figure 39: The compositional dependence of the evaluated GS criteria of all investigated systems for bulk samples and selected heating rate (10 °C.min^{-1}).

In case of the investigated $(As_2Se_3)_{100-x}(As_2Te_3)_x$ glassy system (**Papers XIII**, **XIV**), the eutectic-based character was observed. The position of eutectic is probably between 34 and 50 at. % As_2Te_3, this is claimed on basis of the evolution and position of the melting peaks and sub-peaks. As can be seen in Fig. 39, the glass stability for $(As_2Se_3)_{100-x}(As_2Te_3)_x$ system decreases as the As_2Te_3 content increases. The absence of crystallization process in

case of 0, 17 and 34 at. % of As_2Te_3 indicates the strong glass stability, but the utilization of classic glass stability criteria (based on characteristic temperatures) fails. However, the rising glass stability with rising amount of As_2Se_3 was expected due to the fact, that the binary As_2Se_3 is well-known excellent glass-former [31,34,38,40,43-45,49,58-63] and also due to the presence of eutectic alloy between 34 and 50 at. % As_2Te_3.

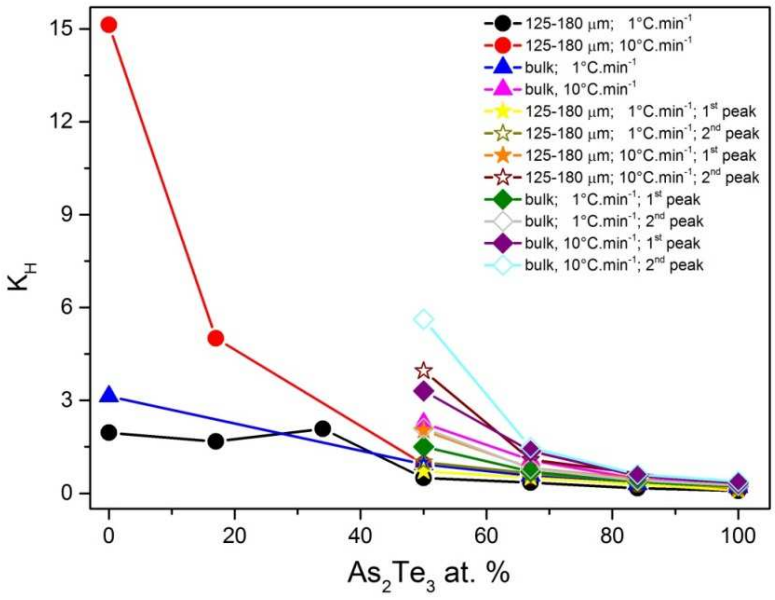

Fig. 40: The compositional dependence of the values of Hruby criterion calculated for the deconvoluted data and for the data, when only a single crystallization peak occurred on the DSC curve (or when the overall DSC response for the complex crystallization peak was evaluated), the corresponding results are without peak number denotation.

The compositions with 50 at. % of As_2Te_3 (and more) exhibit the inclination towards crystallization, which becomes stronger and more apparent with increasing amount of As_2Te_3. For these compositions, the evaluation of glass stability by means of Hruby criterion is possible. The complexity and variation of crystallization behavior with applied experimental conditions significantly affect the reliability of determination of GS criteria. As was noted, the T_g slightly shifts and T_m is invariable with experimental conditions, the crystallization strongly depends on applied heating rate and examined sample form, which is reflected in K_H values. The great differences in K_H values observed for the same material may denote the potential unreliability of these glasses as good glass-formers and indicate that the conditions of potential processing of this glassy system must be strictly controlled.

Considering the advantage of present system, the combination of an excellent glass-former As_2Se_3 and a novel telluride glass As_2Te_3 with wide transmittance window operating in far-IR region offers a chance to choose the compromise between the glass stability and width of transparency window. With respect to revealed thermal properties of $(As_2Se_3)_{100-x}(As_2Te_3)_x$ system, the $(As_2Se_3)_{66}(As_2Te_3)_{34}$ composition seems to be most suitable for far-IR optics applications.

The Hruby criterion was applied also on $(GeTe_4)_x(GaTe_3)_{100-x}$ (x = 40; 50; 60; 67; 75; 86; 100 %) system (**Papers VII, VIII**) in order to evaluate the glass stability of investigated glasses. In Chapter 5.1, where the crystallization behavior of this system was discussed, it was found, that the crystallization onset (which determines the temperature corresponding to the first formation of crystallites) did not change with various amounts of gallium. This fact indicates the influence of T_g on resulting glass stability. As is shown in Figs. 39 and 41, on basis of results provided by Hruby criterion, the highest glass stability can be expected in case of compositions with low $GaTe_3$ content (i.e. 15 – 25 at. % of $GaTe_3$) and for the $(GeTe_4)_{40}(GaTe_3)_{60}$ compositions. Based on the findings from particle size study (**Paper VII**), it was found that the $(GeTe_4)_{86}(GaTe_3)_{14}$ glassy composition seems to be the most stable and impassive to the presence of structural defects and the most suitable for far-IR applications using the fully glassy materials. As far as the potential usage of this material for glass-ceramics purposes, the possible utilization of this glass (containing the low $GaTe_3$ content) is feasible due to the invariable formation of all present crystalline phases with experimental conditions, these compositions exhibited the most uniform behavior of crystallization processes. This allows the best control over the processes of crystal growth. It was also found, that the kinetics only slightly depends on applied heating rate, so that the processing of corresponding ceramics can be easier in this regard.

The Fig. 41 offers an illustration of the compositional dependence of three parameters, which can be used for the evaluation of glass stability and was applied on all investigated $(GeTe_4)_x(GaTe_3)_{100-x}$ systems. The usual way how to evaluate the glass stability of given glassy system represents the utilization of Hruby criterion (black points in Fig. 41). As was said, this GS criterion introduces the simple way to obtain certain information about glass stability. Its utilization in scientific practice is quite limited due to the nature of this GS criterion. The Hruby criterion is based only on characteristic temperatures, provides rather qualitative information about glass stability and used to be recommended only for comparison purposes.

With respect to this limitation, the newly developed parameters ([33], **Paper VIII**) based on the combined information provided by DSC and TMA can better serve for the GS evaluations than the commonly used Hruby criterion. The parameter called "workability window" (red points in Fig. 41) is formulated as a temperature range between the first sample height decrease arising from the viscous flow effects (TMA measurements) and the first occurrence of crystallites (DSC measurements – the true crystallization onset). The Equation 25 is an expression of workability window (w.w.) parameter:

$$w.w. = T_{onset,DSC} - T_{flow,TMA} \tag{25}$$

As is the workability window wider, the more suitable the glass is for the next processing (fiber-drawing, molding). The information about glass stability is more exact in contrary to the standard $T_c - T_g$ difference, where the information about the glass-softening and viscous flow effects is not included.

In Fig. 41, the next parameter occurs (the blue points). This "new parameter" was introduced as a supplementary parameter to w.w. parameter, which accounts also with the rapidity of viscous flow linked to the given temperature window. The Equation 26 expresses this "new parameter" associated with the proportional decrease of sample height during the TMA crystallization measurement.

$$new\ parameter = (l_{onset,DSC} - l_{min})/(l_{max} - l_{min}) \tag{26}$$

The $l_{onset,\ DSC}$ represents the sample height at $T_{onset,\ DSC}$, l_{max} and l_{min} represent the maximum and minimum sample height during the TMA crystallization measurement. The value of the "new parameter" then corresponds to the degree of the viscous flow, which can be achieved until a moment, when the first crystallites occur. The smaller the value of this parameter, the higher viscous flow can be reached without the danger of presence of crystallization.

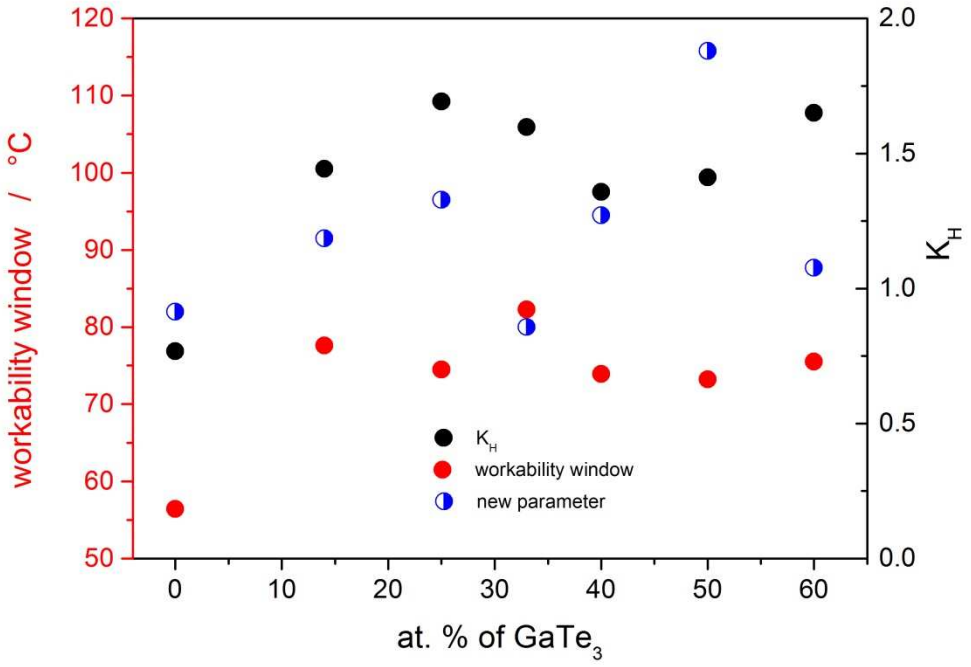

Figure 41: The compositional dependence of Hruby criterion, workability window and new-parameter for all studied $(GeTe_4)_x(GaTe_3)_{100-x}$ bulk glasses.

As was previously discussed, based on results provided by Hruby criterion, the compositions with 25 and 60 at. % of $GaTe_3$ seem to be the most stable. Nonetheless, if the next parameters (w.w. and new parameter) will be taken into account, it is apparent, that the width of workability window and the value of "new parameter" do not correspond to the K_H prediction. The better results of these new-introduced parameters are obtained for the $(GeTe_4)_{67}(GaTe_3)_{33}$ glass. This composition is also close to the eutectic, which confirms the conclusion, that the $(GeTe_4)_{67}(GaTe_3)_{33}$ composition is probably the most suitable for the far-IR optics applications with regard to the thermal stability. Thus, the Hruby criterion was found to be less suitable for the glass-stability predictions in comparison to the new-introduced parameters.

5.4 CONCLUSIONS

The first goal of presented doctoral thesis was the characterization of crystallization behavior of tellurium-based chalcogenide glasses, which belong to the promising materials with potential applicability in the far-infrared optics.

- The crystallization behavior of all investigated systems was characterized by means of DSC (and TMA in selected cases).
- The crystallization (and relaxation) kinetics was described by utilization of commonly used kinetic models in dependence on experimental conditions (sample form, particle size, heating rate) on account of the possibility to acquire the complete detailed information about ongoing processes. The good knowledge of crystallization (and relaxation) kinetics can help with the predictions of preparation and further processing of glassy materials due to possibility of monitoring the individual steps, experimental conditions of glass processing and the opportunity to predict the glassy material's behavior under various optional experimental conditions. The crystallization kinetics of all investigated systems (except the $(GeTe_4)_x(GaTe_3)_{100-x}$ system) was found to be strongly dependent on applied experimental conditions due to the presence of a slightly unpredictable surface precipitation of tellurium, which determines the potential usability of these materials in real-life applications. The improvement of glass thermal properties with doping of pure Ge-Te material by selenium, gallium, iodine or with the search of optimum ratio of As_2Se_3 and As_2Te_3 contents of As-Se-Te glasses was confirmed by an extensive study of crystallization (and relaxation) behavior of whole compositional lines of all investigated systems with respect to various tested experimental conditions.
- The crystallization (and relaxation) kinetic findings were interpreted and supported by the systematic detailed structural analysis, which was performed by means of XRD analysis, Raman spectroscopy and infrared microscopy with an effort to obtain the complete thermo-structural information about the studied systems.

With regard to the observed complexity of crystallization processes of all investigated systems, this phenomenon needed to be addressed. Therefore, the second aim of this doctoral thesis was a solution of crystallization complexity by means of two approaches, i.e. the mathematic deconvolution and kinetic deconvolution procedures.

- The procedure of mathematic deconvolution of the complex kinetic signal was performed by means of Fraser-Suzuki function as the most suitable function for the non-isothermally obtained calorimetric data.
- The procedure of kinetic deconvolution was performed by means of multivariate kinetic analysis (MKA). The multivariate kinetic analysis was found as the most suitable procedure representing a curve-fitting routine in terms of full-scale complex kinetics. However, this method has a certain limitation, which lies in requirement of the more-or-less constant E_A values across the whole explored range of experimental conditions. This condition was fulfilled only for the $(GeTe_4)_x(GaTe_3)_{100-x}$ system.
- Therefore, the mathematic deconvolution procedure was applied via the Fraser-Suzuki function on the remaining investigated systems. The number of DSC curves, on which the deconvolution procedures were applied (within the work on this doctoral thesis) exceeds one thousand. Excepting the $(GeTe_4)_x(GaTe_3)_{100-x}$ system, the mathematic deconvolution was applied on all of investigated data. The mathematic deconvolution was found to be able to successfully address the issue of the temperature-dependent crystallization kinetics.
- The main purpose of this branch of this doctoral thesis was to draw an attention to this problematic and, hopefully, start off a research leading to some advancements or at least some activity regarding this issue.

The third goal of the presented doctoral thesis represents the utilization of the combined information obtained from crystallization measurements performed by means of DSC and TMA, results from crystallization kinetic calculations and results from a classical procedure of evaluation of glass stability of all investigated systems in order to the assessment of the suitability of studied tellurium-based glasses for the potential usage in real-life applications, such as far-IR optics, glass-ceramics, ceramics, from the thermo-kinetic point of view.

- On the basis of revealed insufficiency of classical evaluation of glass stability via Hruby criterion to correctly determine the true thermal stability of glassy material, the new approach was suggested, which is based on the combination of two thermo-analytical techniques (DSC and TMA).
- The combination of DSC and TMA crystallization measurements then offers extended information about processes ongoing in glassy materials until the moment the crystallization occurs. This area between the first softening of glass and the occurrence of the first crystallites is greatly important for the processing of the glassy material (e.g. fiber-drawing, molding, shaping) and the detailed exploration (as much as possible) can help with revelation of the behavior of the processed glass and then the experimental conditions can be exactly adjusted.
- The improvement of predictions of glass stability was proposed via the new-developed parameters (workability window and new processability parameter), which introduce an easy, fast and more accurate way of determining and tailoring the thermo-mechanical properties of glassy materials. These parameters can then serve to an effective estimation of the materials' processability.

Applying the above-mentioned approaches, the Ge-Ga-Te system, namely the $(GeTe_4)_{67}(GaTe_3)_{33}$ glass was found to be the most suitable system (with respect to the thermal behavior) for the far-IR optics applications from all of the investigated systems. Also the Se-doped tellurium-based glasses were found to be suitable for the production of far-IR optic elements, namely the composition $Ge_{21}Se_4Te_{75}$. However, some limitations exist and more attention in processing of this glassy system must be paid. In case of Ge-I-Te system, the rather unpredictable surface tellurium precipitation and complicated glassy synthesis led to the Se- and Ga-doping being preferred. The most suitable glassy composition from As-Se-Te system for the far-IR optics purposes seems to be the $(As_2Se_3)_{66}(As_2Te_3)_{34}$ glass. However, this system also behaves slightly unpredictably with respect to applied experimental conditions; therefore the processing must be strictly controlled. Nonetheless, all of detected flaws can be an incentive for further deeper studies of these relatively new promising materials.

REFERENCES

[1] Ch. Lilyquist, Bulletin of the American Schools of Oriental Research **290/291**, 29-94 (1993).

[2] Glassmaking may have begun in Egypt, not Mesopotamia. www.sciencenews.org 2018 [cited 2018-10-15];
Available from: https://www.sciencenews.org/article/glassmaking-may-have-begun-egypt-not-mesopotamia.

[3] R. W. Douglas and S. Frank, in *A history of glassmaking*, edited by G. T. Foulis, Co. Ltd. London (2007).

[4] P. Houizot, C. Boussard-Pledel, A. J. Faber, L. K. Cheng, B. Bureau, P. A. Van Nijnatten, W. L. M. Gielesen, J. Pereira do Carmo and J. Lucas, Opt. Exp. **15**, 12529 (2007).

[5] M. Frumar, Chemie pevných látek I, ediční středisko UPa, Pardubice (1992).

[6] S. R. Elliot, *Physics of Amofphous Materials*, Longman London, 6 (1990).

[7] P. G. Debenedetti and F. H. Stillinger, Nat. **410**, 259 (2001).

[8] C. A. Angell, K. L. Ngai, G. B. McKenna. P. F. McMillan and S. W. Martin, App. Phys. Rev. **88**, 3113 (2000).

[9] G. O. Jones, *Glass*, Methuen & Co. Ltd. London (1956).

[10] G. W. Scherer, *Glass Formation and Relaxation*, in: Materials Science and Technology **9**, edited by J. Zarzycki, VCH Weinheim, 121 (1991).

[11] A. Q. Tool. J. Am. Ceram. Soc. **29**, 240 (1946).

[12] G. W. Scherer. *Relaxation in Glass and Composites*, edited by J. Wiley&Sons, Wiley, New York (1986).

[13] A. Kovacs, Fortschr. Hochpolym. Forsch. **3**, 394-507 (1963).

[14] J. M. Hutchinson, Prog. Polym. Sci **20**, 703-760 (1995).

[15] I. M. Hodge, J. Non-Cryst. Solids **169**, 211-266 (1994).

[16] G. Tamman, W. Hesse, Z. Anorg. Allg. Chem. **156**, 245 (1926).

[17] D. R. Uhlmann, B. Chalmers, Ind. Eng. Chem. **57**, 19 (1965).

[18] J. J. Hammel, J. Chem. Phys. **46**, 2234 (1967).

[19] D. R. Uhlmann, *Advances in Nucleation and Crystallization in Glasses*, edited by L. L. Hench and S. W. Freiman, American Ceramic Soc., Columbus **91** (1972).

[20] K. A. Jackson, D. R. Uhlmann and J. D. Hunt, J. Cryst. Growth **1,** 1 (1967).

[21] W. H. Zachariasen, J. Am. Chem. Soc. **54**, 3841 (1932).

[22] J. Zarzycki, *Special Methods of Obtaining glasses and Amorphous Materials* in: Materials Science and Technology **9**, edited by Jerzy Zarzycki, VCH Weinheim (1994).

[23] A. Hrubý, Czechoslov. J. Phys. B **22**, 1187 (1972).

[24] M. Saad and M. Poulain, Mater Sci Forum. **19**, 11 (1987).

[25] M. C. Weinberg, Phys. Chem. Glasses **35**, 119 (1994).

[26] Z. P. Lu and C. T. Liu, Acta Mater. **50**, 3501(2002).

[27] Z. Long, G. Xie, H.Wei, X. Su, J. Peng, P. Zhang and A. Inoue, Mater. Sci. Eng. **509A**, 23 (2009).

[28] P. Zhang, H. Wei, X. Wei, Z. Long and X. Su, J. Non-Cryst. Solids **355**, 2183 (2009).

[29] R. Svoboda and J. Málek, J. Non-Cryst. Solids **413** 39-45 (2015).

[30] S. Danto, P. Houizot, C. Boussard-Pledel, X. H. Zhang, F. Smektala and J. Lucas, Adv. Funct. Mater. **16**, 1847-1852 (2006).

[31] G. Wang, C. Li, Q. Nie, Z. Pan, M. Li, Y. Xu, H. Wang and D. Shi, J. Non-Cryst. Solids **463**, 80-84 (2017).

[32] C. Conseil, V. S. Shiryaev, S. Cui, C. Boussard-Pledel, J. Troles, A. P. Velmuzhov, A. M. Potapov, A. I. Suchkov, M. F. Churbanov and B. Bureau, J. Light. Technol. **31**, 1703-1707 (2013).

[33] R. Svoboda, D. Brandová, M. Chromčíková and M. Liška, J. Non-Cryst. Solids – in press.

[34] P. Lucas, M. A. Solis, D. L. Coq, C. Juncker, M. R. Riley and J. Collier, Sens Actuators B **119**, 355-362 (2006).

[35] S. Maurugeon, B. Bureau, C. Boussard-Plédel, A. J. Faber, X. H. Zhang, W. Geliesen and J. Lucas, J. Non-Cryst. Solids **355,** 2074–2078 (2009).

[36] P. Houizot, C. Boussard-Plédel, A. J. Faber, L. K. Cheng, B. Bureau, P. A. Van Nijnatten, Opt Exp. **15**, 12529-12538 (2007).

[37] A. Léger, Adv. Space Res. **25**, 2209 (2000).

[38] D. Le Coq, K. Michel, J. Keirsse, C. Boussard-Plédel, G. Fonteneau, B. Bureau, J.-M. Le Quéré, O. Sire and J. Lucas, Comptes Rendus Chimie **5**, 907-913 (2002).

[39] J. A. Moon and D. T. Schaafsma, Fiber Integrated Opt. **19**, 201–210 (2000).

[40] G. Tao, H. Ebendorff-Heidepriem, A. M. Stolyarov, S. Danto, J. V. Badding, Y. Fink, J. Ballato and A. F. Abouraddy, Adv. Opt. Photon. **7**, 379-458 (2015).

[41] I. Chung and M. G. Kanatzidis, Chem. Mat. **26**, 849-869 (2014).

[42] S. Maurugeon, B. Bureau, C. Boussard-Plédel, A. J. Faber, P. Lucas, X. H. Zhang and J. Lucas, Opt Mater **33**, 660-663 (2011).

[43] S. Cui, R. Chahal, C. Boussard-Plédel, V. Nazabal, J. L. Doualan, J. Troles, J. Lucas and B. Bureau, Molecules **18**, 5373-5388 (2013).

[44] S. Maurugeon, C. Boussard-Pledel, J. Troles, A. J. Faber, P. Lucas, X. H. Zhang, J. Lucas and B. Bureau, J. Light. Technol. **28**, 3358-3363 (2010).

[45] B. Bureau, S. Danto, H. L. Ma, C. Boussard-Plédel, X. H. Zhang and J. Lucas, Solid State Sci. **10**, 427-433 (2008).

[46] A. Giridhar, S. Mahadevan and A. K. Singh, J. Non-Cryst. Solids **103**, 73-78 (1988).

[47] S. Bordas, M. T. Clavaguera-Mora and V. Balek, Thermochim. Acta **93**, 263-266 (1985).

[48] S. Cui, C. Boussard-Plédel, J. Troles and B. Bureau, Opt. Mater. Express **6**, 971-978 (2016).

[49] B. Bureau, C. Boussard-Pledel, P. Lucas, X. Zhang and J. Lucas, Molecules **14**, 4337-4350 (2009).

[50] P. Jóvári, I. Kaban, B. Bureau, A. Wilhelm, P. Lucas, B. Beuneu and D. A. Zajac, J. Phys. Cond. Matt. **22**, 404207 (2010).

[51] P. Petkov, V. Ilcheva, T. Petkova and P. Ilchev, AIP Conference Proceedings **1203**, 932-937 (2010).

[52] G. X. Wang, Q. H. Nie, M. Barj, X. S. Wang, S. X. Dai, X. A. Shen, T. F. Xu and X. H. Zhang, J. Phys. Chem. Sol. **72**, 5-9 (2011).

[53] C. Jiang, C. Cheng, Q. D. Zhu, X. S. Wang, Q. H. Nie, S. X. Dai, G. M. Tao, M. M. Zhu, F. X. Liao, P. Q. Zhang, X. Shen, T. F. Xu, P. Q. Zhang, Z. J. Liu and X. H. Zhang, Appl. Phys. Mater. **120**, 127-135 (2015).

[54] A. Feltz, H. J. Büttner, F. J. Lippmann and W. Maul, J. Non-Cryst. Solids **8-10**, 64-71 (1972).

[55] M. Mitkova and P. Boolchand, J. Non-Cryst. Solids **240**, 1-21 (1998).

[56] A. A. Wilhelm, C. Boussard-Plédel, Q. Coulombier, J. Lucas, B. Bureau and P. Lucas, Adv. Mat. **19**, 3796-3800 (2007).

[57] G. Wang, Q. Nie, X. Wang, S. Dai, T. Xu, X. Shen and X. Zhang, Phys. B **405**, 4424-4428 (2010).

[58] D. W. Henderson and D. G. Ast, J. Non-Cryst. Solids **64**, 43-70 (1984).

[59] J. Málek, Macromolecules **31**, 8312-8322 (1998).

[60] J. Málek and J. Shánělová, J. Non-Cryst. Solids **351**, 3458-3467 (2005).

[61] E. Černošková, Z. Černošek, J. Holubová and M. Frumar, J. Non-Cryst. Solids **284**, 73-78 (2001).

[62] R. Svoboda and J. Málek, Thermochim. Acta **579**, 56-63 (2014).

[63] Z. Zmrhalová, P. Pilný, R. Svoboda, J. Shánělová and J. Málek, J. All. Compd. **655**, 220-228 (2016).

[64] M. A. Popescu, *Non-Crystalline Chalcogenicides*, Springer Netherlands (2001).

[65] G. Delaizir, M. Dussauze, V. Nazabal, P. Lecante, M. Dollé, P. Rozier, E.I. Kamitsos, P. Jovari and B. Bureau, J. All. Compd. **509**, 831-836 (2011).

[66] L. Calvez, E. Lavanant, A. Novikova, C. Goncalves, B. Bureau, V. Nazabal, T. Jouan and X. H. Zhang, J. Non-Cryst. Solids **480**, 28-33 (2018).

[67] V. S. Shiryaev, J. L. Adam, X. H. Zhang and M. F. Churbanov, Solid State Sci. **7**, 209-215 (2005).

[68] S. Hocdé, C. Boussard-Plédel, G. Fonteneau, D. L. Coq, H. L. Ma and J. Lucas, J. Non-Cryst. Solids **274**, 17-22 (2000).

[69] M. F. Kotkata, H. H. Labib and S. A. Rahman, J. Therm. Anal. **34**, 93-98 (1988).

[70] P. Lucas, G. J. Coleman, S. Jiang, T. Luo, Z. Yang, Opt Mat. **47**, 530-536 (2015).

[71] E. A. Anashkina, V. S. Shiryaev, G. E. Snopatin, S. V. Muraviev and A. V. Kim, J. Non-Cryst. Solids **480**, 38-42 (2018).

[72] V. S. Shiryaev and M. F. Churbanov, J. Non-Cryst. Solids **377**, 225-230 (2013).

[73] Differential Scanning Calorimetry: First and Second Order Transitions in Polymers. www.colby.edu 2018 [cited 2018-11-12];
Available from: http://www.colby.edu/chemistry/PChem/lab/DiffScanningCal.pdf.

[74] Differential Scanning Calorimetry. www.princeton.edu 2018 [cited 2018-11-12]; Available from:
http://www.princeton.edu/~achaney/tmve/wiki100k/docs/Differential_scanning_calorimetry.html.

[75] M. J. Richardson, Polymer Testing **4**, 101-115 (1984).

[76] J. Málek, Habilitační práce (1996).

[77] M. E. Brown, *Introduction to Thermal Analysis: Techniques and Applications*, Kluwer Academic Publishers (2001). ISBN 1-4020-0472-9.

[78] P. Šulcová and L. Beneš, Experimentální metody v anorganické technologii, Univerzita Pardubice, Pardubice (2002).

[79] J. Šesták, Měření termofyzikálních vlastností pevných látek, Academia, Praha (1982).

[80] E. H. Fontana, Ceramic Bulletin, 594 (1970).

[81] J. Wang, Materials Letters **31**, 99 (1997).

[82] R. Polanský, *Teoretické a praktické aspekty termomechanické analýzy*, Západočeská Univerzita v Plzni (2008).

[83] P. Holba, J. Šesták. Heat inertia and its role in thermal analysis. J. Therm. Anal. Calorim. 119 (2015) 1453-1458.

[84] J. Málek, Thermochim. Acta **355**, 239 (2000).

[85] S. Vyazovkin, A. K. Burnham, J. M. Criado, L. A. Pérez-Maqueda, C. Popescu and N. Sbirrazzuoli, Thermochim. Acta **520**, 1-19 (2011).

[86] R. Svoboda and J. Málek, Thermochim. Acta **526**, 237-251 (2011).

[87] H. E. Kissinger, Anal. Chem. **29**, 1702 (1957).

[88] H. L Friedman, J. Polym. Sci. **C6**, 302 (1986).

[89] M. J. Starink, Thermochim. Acta **404**, 163-176 (2003).

[90] J. Málek and V. Smrčka, Thermochim. Acta **186**, 153-169 (1991).

[91] A. Khawam and D. R. Flanagan, J. Phys. Chem. B **110**, 17315-17328 (2006).

[92] J. Málek, Thermochim. Acta **200**, 257-269 (1992).

[93] M. Avrami, J. Chem. Phys. **7**, 1103–1112 (1939).

[94] M. Avrami, J. Chem. Phys. **7**, 212-224 (1940).

[95] M. Avrami, J. Chem. Phys. **7**, 177-184 (1941).

[96] J. Šesták, *Thermophysical Properties of Solids, Their Measurements and Theoretical Analysis*, Elsevier, Amsterdam (1984).

[97] J. Málek, Thermochim. Acta **138**, 337-346 (1989).

[98] J. Málek, J. M. Criado, J. Šesták and J. Militký, Thermochim. Acta **153**, 429-432 (1989).

[99] M. E. Brown, M. Maciejewski, S. Vyazovkin, R. Nomen, J. Sempere, A. Burnham, J. Opfermann, R. Strey, H. L. Anderson, A. Kemmler, R. Keuleers, J. Janssens, H. O. Desseyn, C. R. Li, T. B. Tang, B. Roduit, J. Málek and T. Mitsuhashi, Thermochim. Acta **355**, 125-143 (2000).

[100] S. Vyazovkin and C. A. Wight, Thermochim. Acta **340–341**, 53-68 (1999).

[101] L. A. Perez-Maqueda, J. M. Criado, F. J. Gotor and J. Málek, J. Phys. Chem. A **106**, 2862-2868 (2002).

[102] L. A. Perez-Maqueda, J. M. Criado and P. E. Sanchez-Jimenez, J. Phys. Chem. A **110**, 12456-12462 (2006).

[103] J. Opfermann, J. Therm. Anal. Calorim. **60**, 641-658 (2000).

[104] C. Wagner, J. Vazquez, P. Villares and R. Jimenezgaray, Mater. Lett. **18**, 280 (1994).

[105] S. Bernard, K. Fiaty, D. Cornu, P. Miele and P. Laurent. J. Phys. Chem. B **110**, 9048 (2006).

[106] W. Weibull, J. Appl. Mech. **18**, 293 (1951).

[107] A. Perejon, P. E. Sanchez-Jimenez, J. M. Criado and L. A. Perez-Maqueda, J. Phys. Chem. B **115**, 1780-1791 (2011).

[108] R. Svoboda and J. Málek, J. Therm. Anal. Calorim. **111**, 1045-1056 (2013).

[109] R. D. B. Fraser and E. Suzuki, Anal. Chem. **38**, 1770 (1966).

[110] R. D. B. Fraser and E. Suzuki, Anal. Chem. **41**, 37 (1969).

[111] O. S. Narayanaswamy, J. Am. Ceram. Soc. **54**, 491-498 (1971).

[112] C. T. Moynihan, A. J. Easteal, M. A. Bolt and J. Tucker, J. Am. Ceram. Soc. **59**, 12-16 (1976).

[113] G. Williams and D. C. Walts, Trans. Faraday Soc. **66**, 80 (1970).

[114] S. M. Rekhson, A. V. Bulaeva and O. V. Mazurin, Izv. Akad. Nauk. SSR **7**, 714 (1971).

[115] M. A. DeBolt, A. J. Easteal, R. B. Macedo and C. T. Moynihan, J. Am. Ceram. Soc. **59**, 16 (1979).

[116] I. M. Hodge and A. R. Berens, Macromolecules **15**, 762 (1982).

[117] I. M. Hodge and A. R. Berens, Macromolecules **18**, 1980 (1985).

[118] J. M. Hutchinson. Prog. Polym. Sci. **20**, 703 (1995).

[119] R. Svoboda and J. Málek, J. Non-Cryst. Solids **378**, 186-195 (2013).

[120] A. J. Kovacs, J. J. Aklonis, J. M. Hutchinson and A. R. Ramos, J. Polym. Sci B **17**, 1097 (1979).

[121] R. E. Robertson, R. Simha and J. G. Curro, Macromolecules **17**, 911 (1989).

[122] K. L. Ngai, Comments on Solid State Physics **9**, 127 (1979).

[123] P. K. Gupta, J. Non-Cryst. Solids **102**, 25 (1988).

[124] P. B. Macedo and T. A. Litovitz, J. Chem. Phys. **42**, 245 (1965).

[125] J. Málek, Z. Zmrhalová, J. Barták and P. Honcová, Thermochim. Acta **511**, 67 (2010).

[126] Z. Zmrhalová, J. Málek, D. Švadlák and J. Barták, Phys. Status Solidi C **8**, 3127 (2011).

[127] J. Málek, Z. Zmrhalová and P. Honcová, J. Therm. Anal. Calorim. **105**, 565-567 (2011).

[128] W.A. Johnson and K.F. Mehl, Trans. Am. Inst. Min. (Metall) Eng. **135**, 416-442 (1939).

[129] R. Svoboda and J. Málek, J. Chem. Phys. **141**, 224507 (2014).

[130] R. Svoboda and J. Málek, J. All. Compd. **627**, 287-298 (2015).

[131] R. Svoboda, M. Kincl and J. Málek, J. All. Compd. **644**, 40-46 (2015).

[132] R. De Bastiani, E. Carria, S. Gibilisco, et. al. Phys. Rev. B **80**, 245205 (2009).

[133] O. Uemura, N. Hayasaka, S. Tokairin, T. Usuki, J. Non-Cryst. Solids **205-207**, 189-193 (1996).

[134] M. Upadhyay, S. Murugavel, M. Anbarasu, T.R. Ravindran, J. Appl. Phys. **110**, 083711-083716 (2011).

[135] M.H. Brodsky, R.J. Gambino, J.E. Smith, Y. Yacoby, Phys. St. Sol. B **52**, 609-614 (1972).

[136] E.M. Vinod, K.S. Sangunni, Thin Solid Films **550**, 569-574 (2014).

[137] A.V. Kolobov, P. Fons, J. Tominaga, et. al., J. Phys. Cond. Matt. **16**, 5103 (2004).

[138] S.S. Garje, M.C. Copsey, M. Afzaal, et. al., J. Mater. Chem. **16**, 4542 (2006).